ÉCOLE DE TECHNOLOGIE SUPERIEURE
UNIVERSITÉ DU QUÉBEC

THESIS PRESENTED TO
ÉCOLE DE TECHNOLOGIE SUPERIEURE

IN PARTIAL FULFILLMENT OF THE REQUIREMENTS FOR
THE DEGREE OF DOCTOR OF PHILOSOPHY
Ph.D.

BY
Amin KARBASSI

PERFORMANCE-BASED SEISMIC VULNERABILITY EVALUATION OF EXISTING BUILDINGS IN OLD SECTORS OF QUEBEC

MONTREAL, JULY 20, 2010

THIS THESIS HAS BEEN EVALUATED

BY THE FOLLOWING BOARD OF EXAMINERS

Prof. Marie-José Nollet, Thesis Supervisor
Département de génie de la construction à l'École de technologie supérieure

Prof. Omar Chaallal, Internal Examiner
Département de génie de la construction à l'École de technologie supérieure

Prof. Patrick Terriault, President of the Board of Examiners
Département de génie mécanique à l'École de technologie supérieure

Prof. Luc Chouinard, External Examiner
McGill University – Department of Civil Engineering and Applied Mechanics

THIS THESIS WAS PRESENTED AND DEFENDED

BEFORE A BOARD OF EXAMINERS AND PUBLIC

June 15, 2010

AT ÉCOLE DE TECHNOLOGIE SUPÉRIEURE

To the survivors of the earthquake in
Bam City, who have been always
the great examples
of HOPE and INSPIRATION for me.

ACKNOWLEDGMENTS

Here I get to this part of my thesis which comes at the beginning of the document, though it is really written as one of the last parts! This is probably because I wanted to make sure to remember everyone on the long list of names who not only gave me a hand in conducting this research work but also helped me to be where I am now. However, now I realize that if like movie credits, I want to mention everyone's name, I will end up having several pages for this part. Emotions can also be involved as I am writing this page on the 5th anniversary of leaving home to come to Canada to pursue my PhD studies. Time passes fast, doesn't it!

Getting to know Marie-José in the CSCE conference in 2002 was one of the greatest chances I have had in my academic life. Who knew that she would become my research supervisor three years later when I felt confident enough with my French language to come to École de technologie supérieure. Marie-José, I am really thankful for your academic advices, support, and kindness through all these 5 years which has made me think of you not only as my research supervisor but also as one of my best friends: how many supervisors in the world would come all the way down to their student's apartment just after he arrives in town, on a Sunday afternoon, to make sure he has the necessary house stuff!

The days away so far from home would have not passed easy if I did not feel that I had the absolute emotional support of my family, whenever I needed it. Dad and Mom, although I will never be able to pay you back for what you have done for me, I want you to know that I am sincerely grateful for it. My brother Arsha and his wife Niloofar, though you still owe me a visit here, your remote support has been endless, and I am really thankful for that.

Finally, the word HOME has always been something unique for me. However, after living in the lovely city which they call it MONTREAL, I have come to this belief that home is any place where one can find peace and endless friendships, somewhere like Montreal! Whom can I thank for that?

PERFORMANCE-BASED SEISMIC VULNERABILITY EVALUATION OF EXISTING BUILDINGS IN OLD SECTORS OF QUEBEC

Amin KARBASSI

ABSTRACT

To perform a seismic vulnerability evaluation for the existing buildings in old sectors of Quebec, two major tools at two different levels are missing: first, in the context of the seismic vulnerability assessment of a group of buildings, an updated rapid visual screening method which complies with the Uniform Hazard Spectra presented in the 2005 version of the *National Building Code of Canada* (NBCC) does not exist; and second, in the context of loss estimation studies, capacity and fragility curves which are developed based on the specific building typologies present in those sectors are required. In this research work, in the first place, a building classification for the existing buildings in old sectors of Quebec considering the masonry as the main construction material is proposed. Later, an updated rapid visual screening method—in the form of vulnerability indices for different typologies and cities in Quebec—which is adapted to the Uniform Hazard Spectra in NBCC 2005 is proposed. The structural vulnerability indices (SVI) are calculated through the application of the improved nonlinear static analysis procedure in FEMA 440 *Improvement of nonlinear static seismic analysis procedures* for three levels of seismic hazard. A set of index modifiers are also presented for the building height, irregularities, and the design and construction year. To deal with the second problem, on the other hand, a performance-based seismic vulnerability evaluation method is applied to examine the structural performance of two buildings—a 6-storey industrial masonry building and a 5-storey concrete frame with masonry infill walls, as two of the building classes constructed vastly in old sectors in Quebec—at multiple seismic demand levels. The results of such an assessment are used to develop dynamic capacity and fragility curves for the target buildings. The Applied Element Method is used here as an alternative to FE-based methods to conduct a thorough 4-step performance-based seismic vulnerability evaluation. To this end, the Incremental Dynamic Analyses (IDA) for the buildings are carried out using various sets of synthetic and real ground motions representing three M and R categories. Consequently, the fragility curves are developed for the three structural performance levels—Immediate Occupancy, Life Safety, and Collapse Prevention. Finally, the mean annual frequencies of exceeding those performance levels are calculated by combining the data from the calculated fragility curves and those from the region's hazard curves. The proposed method is shown to be useful to conduct seismic vulnerability evaluations in regions for which little observed damage data exists.

Keywords: Applied Element Method, Masonry, Incremental Dynamic Analysis, Rapid Visual Screening, Performance-Based Seismic Evaluation

ÉVALUATION DE LA VULNÉRABILITÉ SISMIQUE BASÉE SUR LA PERFORMANCE POUR DES BÂTIMENTS EXISTANTS DANS LES ANCIENS QUARTIERS DU QUEBEC

Amin KARBASSI

RESUMÉ

Actuellement, il manque deux outils importants et cela à deux niveaux différents pour l'évaluation de la vulnérabilité sismique des bâtiments existants dans les anciens quartiers du Québec. Premièrement, dans le cadre de l'évaluation de la vulnérabilité sismique d'un groupe de bâtiments, il n'y a pas de méthode d'attribution de pointage qui soit conforme aux spectres d'aléa uniforme de l'édition 2005 du *Code national du bâtiment du Canada* (CNBC). Deuxièmement, pour compléter des analyses d'estimation des dommages il est nécessaire de développer des courbes de capacité et de fragilité pour les typologies spécifiques de bâtiments qu'on retrouve dans les anciens quartiers. Dans ce travail de recherche, on propose d'abord une classification typologique des bâtiments existants des anciens quartiers du Québec considérant la maçonnerie comme matériau de construction principal. Par la suite, on propose une nouvelle procédure d'évaluation rapide sur la base d'indices de vulnérabilité sismique pour les différentes typologies et villes du Québec. Un niveau de sismicité (faible, modéré ou élevé) est attribué à chaque ville selon les valeurs d'accélération spectrale de l'édition 2005 du *Code national du bâtiment du Canada*. Pour chaque niveau de sismicité, des indices de la vulnérabilité sismique structurale (IVS) et des modificateurs (ceux-ci considèrent la hauteur du bâtiment, les irrégularités, et les années de conception et de construction) sont calculés à partir de la procédure d'analyse statique non-linéaire améliorée du FEMA 440 « *Improvement of nonlinear static seismic analysis procedures* ». Pour répondre à la deuxième problématique, une méthodologie basée sur les niveaux de performance est appliquée afin d'étudier la vulnérabilité sismique de deux bâtiments à de multiples niveaux de demande sismique. Deux classes de bâtiment présentes en grande proportion dans les anciens quartiers du Québec sont considérées, soient un bâtiment industriel en maçonnerie non armée de 6 étages et un cadre en béton armé avec des remplissages en maçonnerie non armée de 5 étages. Les résultats de cette évaluation sont utilisés pour développer les courbes de capacité dynamique et les courbes de fragilité de ces bâtiments. La méthode des éléments appliqués (MEA) est utilisée ici, comme une alternative aux éléments finis, afin de faire une étude d'évaluation en quatre (4) étapes. À cette fin, une série d'analyses dynamiques incrémentales temporelles (IDA) est réalisée en utilisant des accélérogrammes synthétiques et réels représentant trois combinaisons amplitude-distance (M et R). Les courbes de fragilité sont développées pour trois niveaux de performance structurale (occupation immédiate, sécurité des occupants, et prévention de l'effondrement). La fréquence annuelle moyenne de dépassement de ces niveaux de performance est ensuite calculée en combinant les données des courbes de fragilité à celles des courbes d'aléa de la région. Une comparaison des courbes de fragilité développées dans ce travail de recherche

avec les courbes de fragilité de HAZUS est présentée et les différences et les similarités sont discutées. Il est démontré que la méthode proposée ici est efficace pour réaliser des évaluations de vulnérabilité sismique dans les régions pour lesquelles il existe peu de données sur les dommages observés.

Mots-clés: méthode des éléments appliqués, maçonnerie, analyse dynamique incrémentale temporelle, méthode d'attribution de pointage, niveaux de performance

TABLE OF CONTENTS

Page

LIST OF TABLES

Page

LIST OF FIGURES

Page

LIST OF ACRONYMS AND INITIALISMS

AEM	Applied Element Method
BSH	Basic Structural Hazard
ASCE	American Society of Civil Engineering
ATC	Applied Technology Council
[C]	Damping matrix
CIW	RC frame with unreinforced masonry infill walls
CP	Collapse Prevention
DM	Damage measure
E	Young's modulus
E_b	Brick Young's modulus
E_D	Energy dissipated by damping
E_m	Mortar Young's modulus
E_{So}	Maximum strain energy
FC	Fragility curve
FEM	Finite Element Method
FEMA	Federal Emergency Management Agency
$\Delta f(t)$	Incremental applied load vector
g	Ground acceleration
G	Shear modulus
G_b	Brick shear modulus

G_m	Mortar shear modulus
HC	Hazard curve
IDA	Incremental Dynamic Analysis
IM	Intensity measure
IO	Immediate Occupancy
ISD	Inter-storey drift
[K]	Stiffness matrix
K_n	Normal stiffness
K_{Neq}	Equivalent normal stiffness
K_s	Shear stiffness
K_{Seq}	Equivalent shear stiffness
LS	Life Safety
[M]	Mass matrix
MAF	Mean annual frequency
MDOF	Multi-degree-of-freedom
MMI	Modified Mercalli intensity
NBCC	National Building Code Canada
NIBS	National Institute of Building Sciences
NRCC	National Research Council Canada
PBSE	Performance-based Seismic Evaluation
PGA	Peak ground acceleration
PRI	Priority retrofit index

R_G	Residual force vector
S_a	Spectral acceleration
S_d	Spectral displacement
SDOF	Single-degree-of-freedom
SI	Structural index
SPI	Seismic priority index
SVI	Structural vulnerability index
T_e	Effective period
T_{eq}	Equivalent period
T_i	Initial period
URMW	Unreinforced masonry with wood floors
USGS	United States Geological Survey
$[\Delta U]$	Incremental displacement vector
$[\Delta U']$	Incremental velocity vector
$[\Delta U'']$	Incremental acceleration vector
β	Standard deviation
β_{eq}	Equivalent damping
β_{eff}	Effective damping
Φ	Lognormal-cumulative distribution
μ	Median value
μ_1	Ductility factor

INTRODUCTION

In spite of all developments in the seismic design of new buildings in Canada in the recent years, it is important to know that the first detailed seismic provisions were not incorporated in the National Building Code of Canada until the 1950's. This means that there are several structures, built before that time, which are not designed to resist earthquake loads. Consequently, human and economic losses can be high among those building stocks as a result of an earthquake in the future. Therefore, the same amount of attention that is given to the seismic design of new buildings should be paid to loss estimation of existing structures. Significant damages to structures built without seismic load resisting provisions have been observed in different parts of the world. The recent devastating earthquake in Haiti, in January 2010, is a clear example (USGS/EERI 2010).

Although the occurrence rate of earthquakes in Quebec is lower in comparison with the earthquake frequency in Western Canada, the social and economical impacts of earthquakes on buildings that have been built before the existence of seismic regulations in the province cannot be neglected. The seismic zone of Charlevoix (located at a 100km distance from Quebec City) is the most active zone in the east part of Canada. Five earthquakes with the magnitude of six or more (in 1663, 1791, 1860, 1870, and 1925) have occurred in the region[1]. Moreover, in the 20th century, three significant earthquakes—The 1925 Charlevoix-Kamouraska (Magnitude 6.2), The 1935 Timiskaming (or Témiscaming) (Magnitude 6.2), and The 1944 Cornwall-Massena (Magnitude 5.6)—have occurred in the province.

Defining the problem

Based on a study of the approximate distribution of seismic risk among Canada's urban population due to the existing seismic hazard (probability of occurrence of an earthquake) (Adams et al. 2002) showed that Montreal and Quebec City are among the 6 most vulnerable

[1] http://earthquakescanada.nrcan.gc.ca/zones/eastcan-eng.php

cities in the country. In this study, Vancouver is stated to have the highest population at risk, Montreal is placed second, and Quebec City is positioned in the 6th place.

In regions highly populated and constructed, such as Montreal and Quebec City, the seismic risk can be high especially among old masonry buildings because of the combination of seismic hazard with the vulnerability of such a building class and the social and cultural values of those ancient structures.

Masonry is considered the most important construction material in the world as it has been used in public and residential building construction over the past hundred years. Although some specific features have been added to improve the seismic behavior of masonry buildings during the course of time, such as the confined masonry construction and tying the walls, masonry constructions remain, even nowadays, the most vulnerable part of existing building stocks.

To evaluate the seismic vulnerability of a building stock and perform a loss estimation study, several approaches are available. Most of those approaches rely on having a clear building classification for the area and developing the corresponding fragility curves for each class. These curves give the probability of exceeding a particular damage state given a level of seismic demand. It has been shown in previous studies that the available building classifications in North America does not include all types of unreinforced masonry buildings present in old sectors of Quebec (Lefebvre 2004).

Taking into account the nonlinear dynamic behaviour of structures is essential for developing precise fragility curves for existing buildings. However, the dynamic structural analysis of unreinforced masonry buildings faces several challenges: because of the brittle properties of brick units and mortar joints, the overall behaviour of masonry units is often considered linear; nevertheless, the masonry units are shown to have an explicit nonlinear behaviour in progressive collapse cases (Colliat et al. 2002). Consequently, fragility curves should reflect

this nonlinear behaviour. Nonetheless, the difficulties to represent the global dynamic behaviour of masonry structures in an accurate way, stated in the literature, questions the validity of the available fragility curves for masonry buildings, developed by static pushover analysis.

Objectives, applied methodology, and originality

The main objective of this research work is to develop a predicted-based seismic vulnerability evaluation method for buildings with masonry construction in old sectors of Quebec. The focus will be on two types of masonry buildings: (1) unreinforced brick masonry buildings with wood floors (URMW) which represent the structures in the old industrial sectors in Montreal and Quebec City at the beginning of the century, and (2) RC frames with unreinforced masonry infill walls (CIW) which used to be a very popular building type between 1930 and 1950 in Quebec. The main objective is achieved at two levels. First of all, a rapid visual screening method compatible with the regional seismic hazard of the province is developed, and second, the dynamic capacity and fragility curves for buildings with unreinforced brick masonry are established considering the nonlinear dynamic behaviour of the masonry.

To achieve the objective of this study, the following methodology is followed.

1. Reviewing the existing seismic vulnerability evaluation methods used in different part of the world.
2. Proposing a building classification that properly categorizes the existing ancient structures in Quebec, based on their structural characteristics and constructional materials.
3. Establishing a vulnerability scoring system or index calculation, compatible with the seismic demand in Quebec.

4. Calculating the "dynamic" capacity and fragility curves for the most frequently seen classes in old sectors in Quebec (masonry and concrete building with masonry infill walls).

The last step represents the main effort in this research thesis. The methodology used to calculate the dynamic capacity and fragility curves for the studied buildings consists of the most original contribution of this research work which is:

1. Applying the Applied Element Method to overcome the problems one would encounter when using a FE-based method in the dynamic analyses of masonry buildings. This method is based on dividing structural members into virtual elements connected through springs, and is used in this research work as an alternative to Finite Element Method (FEM) to model the progressive collapse in brick masonry in an adequate way.
2. Replacing the conventional dynamic analysis methodology by an Incremental Dynamic Analyses approach, when calculating the capacity and fragility curves because the later is shown to be an effective tool for thoroughly examining the structural performance of buildings under seismic loads (Christovasilis et al. 2009; Lagaros 2009).
3. Using the latest regional seismic demands for Quebec, presented in the 2005 edition of the *National building code of Canada* (NBCC) (NRCC 2005) in the form of spectral acceleration response values.

Organization of the thesis

Various seismic vulnerability evaluation methods which are currently in use in different parts of the world are reviewed in Chapter 1, and the essential elements for a suitable seismic vulnerability evaluation method in Quebec are identified and discussed. Based on such a literature review, a new building classification is proposed for the existing buildings in the old sectors of the province. Later on in Chapter 2, the procedure to develop a score assignment method which is adapted to the seismic demand in the province, for the seismic vulnerability evaluation of a group of buildings in old sectors of Quebec is explained.

Chapter 3 explains a performance-based seismic vulnerability evaluation to develop the dynamic capacity and fragility curves for two target buildings in this study. This section of the research work aims to overcome the lack of appropriate capacity and fragility curves, unavailable in the literature, for buildings with masonry construction in Quebec. The results obtained from such a methodology is presented in Chapter 4 for a typical unreinforced brick masonry building and a RC frame with unreinforced masonry infill walls, in Quebec, and a set of fragility curves are calculated for each building. In the context of loss estimation, the return period of exceeding the performance levels considered in this study is also calculated in the same Chapter. In Chapter 5, the results of the Incremental Dynamic Analyses are used to study the local dynamic behaviour of the buildings. Moreover, the fragility curves calculated in Chapter 4 are discussed in further details. Finally, the summary of the study along with recommendations for future works are presented in Chapter 6.

CHAPTER 1

LITERATURE REVIEW

1.1 Introduction

Different types of seismic vulnerability evaluation studies may be used depending on the nature of the problem at hand and the purpose of the study (Coburn and Spence 2002). These are:

1. Scenario studies, in which the effect of a single earthquake is calculated on a region (Fah et al. 2001). Major historic earthquakes are modeled to assess their effects on present-day portfolios to evaluate the resources that would be needed to withstand disasters such as those that occurred in the past, should similar ones occur in the future.
2. Probabilistic risk analysis, in which potential losses from different sources are calculated along with their probability of occurrence for an individual building, group of buildings, or for a region (Shaw et al. 2007). The latest can be performed when a clear building classification exists for the building stock. The results of such studies can be used to develop loss exceedance probability curves, which illustrate the level of loss that would be experienced with different return periods.
3. Potential loss studies, in which the effect of expected hazard levels across a region or country is mapped in order to show the locations of probable heavy losses to identify high-risk areas (Tantala et al. 2000).

One of the key elements in every study of this type is the assessment of the seismic vulnerability of the population of buildings under investigation. In this regard, a clear definition of the terms frequently used in those studies would be helpful for the reader.

1.2 Definition of Terms

1.2.1 Seismic Hazard

In seismic engineering, the term *Hazard* is defined as «the probability of occurrence of an earthquake with a certain severity, within a specific period of time, at a given location » (Coburn and Spence 2002). The earthquakes can be specified in term either of their source characteristics (e.g., magnitude) or their effect on a specific location (e.g., intensity or peak ground acceleration). In either case, the annual recurrence rates are usually used. The inverse of this term is called the average return period.

1.2.2 Seismic Vulnerability

Seismic Vulnerability is defined as the degree of exposure to loss (as the ratio of the expected loss to the maximum possible loss) for a given item at risk, ensuing from the occurrence of a specific level of seismic hazard. According to the characteristics of the element at risk, the measure of loss can be the casualty number, number of injuries or repair cost ratio. In a large population of buildings, this term may be defined as the proportion of buildings experiencing some particular level of damages.

1.2.3 Seismic Risk

This term refers to the potential economic, social and environmental consequences of an earthquake in terms of probable physical damages to properties, human losses, and injuries that may occur over a specific future time-period. The loss and physical damage elements are key points in the definition. In a region with a high seismic hazard in which there are no people or property that could be injured or damaged by an earthquake, the seismic risk is zero.

Based on the definition stated for each term, the seismic risk for a building (or a group of buildings) can be calculated as follows.

$$Seismic\ risk = Seismic\ hazard \times vulnerability \times value \tag{1.1}$$

The seismic risk in a region is defined as the probability of occurrence of an earthquake with a certain magnitude, times the probability of damage caused by that earthquake (seismic vulnerability) times the economical or social value of the building(s) at risk.

1.3 Fragility Curves

The fragility curve for a building presents the probability of exceeding a damage state D (e.g., Collapse Prevention level), given intensity measure IM (e.g., spectral acceleration or spectral displacement) Therefore, the fragility curve is presented in the form of a two-parameter lognormal distribution function as follows.

$$F(X) = P(d > D) = \Phi\left[\frac{\ln(X) - \mu}{\sigma}\right] \tag{1.2}$$

In Equation 1.2, Φ is the standard normal cumulative distribution function, X is the distributed intensity measure (e.g., S_a or S_d), and μ and σ are the median and standard deviation of the natural logarithm of the intensity measures, respectively. Figure 1.1 shows an example of the fragility curves for a masonry building in terms of its spectral displacement.

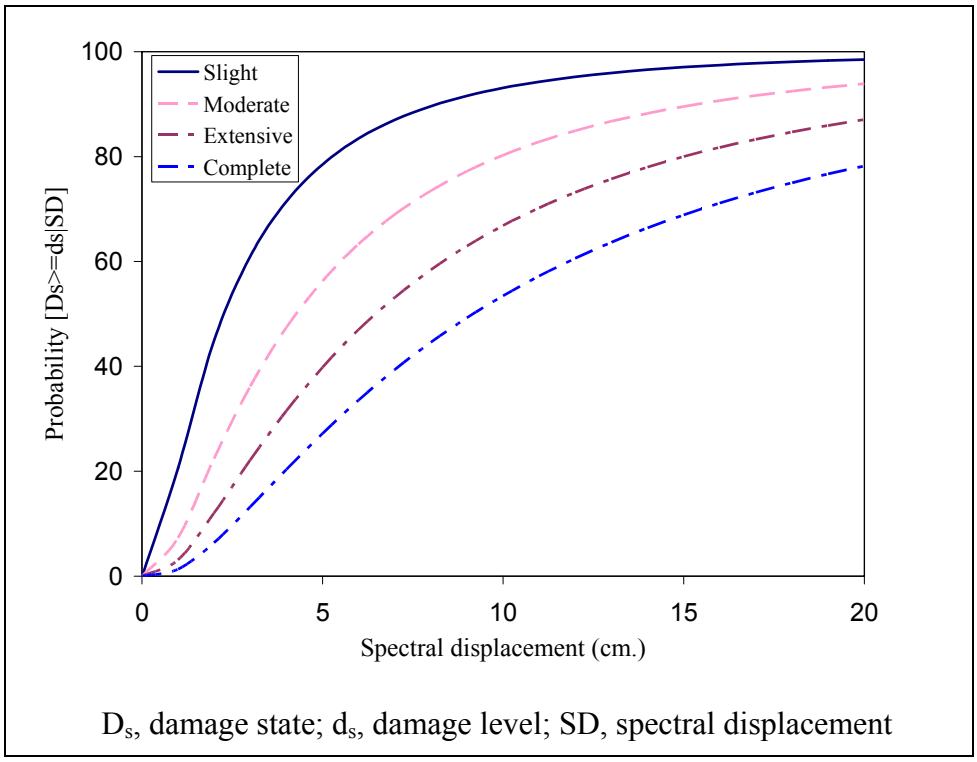

Figure 1.1 Example of fragility curves for unreinforced masonry buildings.

1.4 Seismic Vulnerability Assessment Methods

It is seen from Equation 1.1 that one of the key elements in every loss estimation study is the assessment of the seismic vulnerability of the building population under investigation. There are two principal methods used in the seismic vulnerability assessment of existing buildings, one of which is known as the observed vulnerability procedure and the other, as the predicted vulnerability method (Sandi 1982). The later is based on a combined use of analytical modelling and expert opinions.

The observed vulnerability assessment is based on the statistics of past earthquake damages. These can be accompanied by the opinion of experts and used to derive damage probability matrices (DPMs) which describe the probability that a building class is in a specific damage state for a given level of hazard. Such a procedure is suitable for non-engineered structures

whose earthquake resistance is difficult to calculate but for which, substantial statistical damage data exist.

In the absence of sufficient observed data, the *predicted* vulnerability assessment is applied to evaluate the seismic vulnerability of buildings. This method evaluates the expected performance of building classes based on calculations and design specifications. The assessment can be performed using either simple analytical models (D'Ayala et al. 1997) or detailed analysis procedures (Decanini et al. 2004), depending on the objective of the particular evaluation. Simple analytical models are applicable where the procedure's precision is not as important as its rapidity. Detailed analysis methods, generally used for the evaluation of individual building, are not suitable for earthquake scenario projects where a large number of buildings have to be evaluated. However, they can be used to generate fragility curves for typical buildings from which one can either perform a loss estimation analysis or develop scores that correlate potential structural deficiencies with structural characteristics for different building classes. This is the basis for a seismic vulnerability assessment method called the score assignment, which will be explained in further detail in the next chapter. In situations where there is a lack of sufficient observed earthquake damage data, such as in the province of Quebec, the predicted vulnerability technique, coupled with a score assignment procedure, can be a suitable method for the seismic vulnerability evaluation of a group of buildings. Figure 1.2 shows the different available methods to conduct a predicted-based seismic vulnerability assessment for existing buildings as a group or individually.

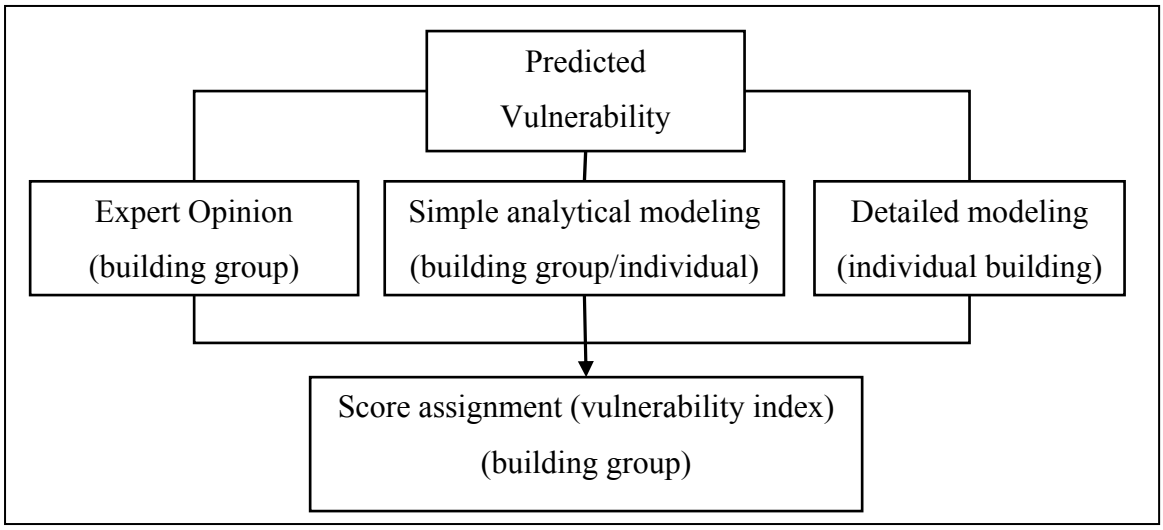

Figure 1.2 Existing methods for the predicted vulnerability assessment.

Table 1.1 summarizes a number of references studied in this chapter as part of the literature review, based on their assessment methodology. Each method is described in the following sections.

Table 1.1 Selected references classified based on the assessment methodology

	Observed Vulnerability	**Expert Opinions**	**Simple Analysis Models**	**Score Assignment**	**Detailed Analysis**
(NRC-IRC 1992)	---	---	---	√	---
(McCormack and Rad 1997)	---	√	---	√	---
(D'Ayala et al. 1997)	---	---	√	---	---
(Faccioli et al. 1999)	---	---	√	√	---
(Tantala et al. 2000)	---	√	---	---	---
(Onur 2001)	---	√	---	---	---
(D'Ayala and Speranza 2001)	√	---	√	---	---
(ATC 2002a)	---	---	---	√	---
(D'Ayala and Speranza 2002)	---	---	√	---	---
(Lang 2002)	---	---	√	---	---
(ASCE 2003)	---	---	---	---	√
(Rossetto and Elnashai 2003)	√	---	---	---	---
(Cohen et al. 2004)	---	---	---	---	√
(White et al. 2005)	---	---	---	√	---
(Valluzzi et al. 2005)	---	---	√	---	---
(LeBoeuf and Nollet 2006)	---	---	---	√	---
(Belmouden and Lestuzzi 2007)	---	---	---	---	√
(Calderini and Lagomarsino 2008)	---	---	---	---	√
(Christovasilis, Filiatrault et al. 2009)	---	---	---	---	√

1.4.1 Observed damage data

To define a relationship between earthquake damages and earthquake intensity, a substantial quantity of data is requires. Such equations are only valid for the original region or for areas with similar building population. However, if the calculated equation acknowledges the seismic resisting system of damaged buildings, seismic design practices in the region, and the building's characteristics such as height and the number of storeys, then the equation can be used in the seismic assessment of other buildings with similar structural characteristics but in a different region (Rossetto and Elnashai 2003). The reason lies in the fact that there are such structural uncertainties in deriving those equations that any differences in construction practices and detailing between different regions are overcome.

1.4.2 Expert opinions

The observed vulnerability assessment method is the basis for the ATC 13 report, *Earthquake damage evaluation data for California* (ATC 1985), which provides experts' damage estimations that can be used to evaluate the local, regional, and national economic impacts of earthquakes in California. The report essentially derives damage probability matrices for 78 different facility classes, 40 of which refer to buildings by asking 58 experts to estimate the expected level of damage that a specific structural class would undergo if subjected to a Modified Mercalli Intensity (MMI) from VI to XII. However, in addition to the uncertainties due to the variability in the buildings actual performance inherent in any estimation of damages, there are uncertainties related to opinions of the experts.

These damage probability matrices can not be easily calibrated or modified to incorporate new data and technological innovation (Porter et al. 2000) and it is difficult to extend the results to other building classes in other regions that have different construction practices, which include different construction details, building code requirements, construction materials, and workmanship quality.

Similar to ATC 13 methodology, damage probability matrices (DPM) have been developed for 31 building classes in British Columbia (Ventura et al. 2005). This study started with a

preliminary investigation of the seismic vulnerability of the general building stock in British Columbia using ATC-13 methodology as a benchmark, i.e., surveying local engineers. To this end, the building classes in ATC-13 were included in the survey and experts were asked to provide their opinions about the existence of each building class in British Columbia. The numbers of occurrences were categorized as low (0 to 10 occurrences), medium (10 to 50 occurrences), or high (more than 50 occurrences). Out of the 40 original building classes, 11 were chosen as the most prevalent in British Columbia. Following up on this initial work, a more comprehensive classification system including 31 building classes was developed to encompass the local building inventory.

1.4.3 Simple Analytical model

In the absence of observed damage data to generate vulnerability functions, other methods are required to assess the vulnerability of existing buildings. In assessing the vulnerability of a group of buildings, those methods should be able to analyse a large number of buildings in a short amount of time. To this end, analytical methods including simple models of buildings which require a few input parameters can be applied. To make the results reliable, those input parameters must be able to model the general seismic behaviour of the buildings.

Application in Europe

Examples of such a methodology are the seismic vulnerability assessments based on the identification of potential collapse mechanisms, expressed as the critical acceleration (D'Ayala et al. 1997; Faccioli et al. 1999). This method was applied in the seismic vulnerability assessment for a group of buildings in a historical center in the Umbria region in Italy (Valluzzi et al. 2005). A collapse coefficient equal to a/g (the mass multiplier able to led the building's elements (walls, floors, and roofs) to failure) was presented for each building class. Such a multiplier was calculated based on reaching the upper limit of the equilibrium conditions (for out-of-plane and in-plane mechanism) rather than the maximum strength of the materials.

Analytical models can be applied to define the capacity curves of buildings that typify given building classes. These curves are then combined with the seismic demand (Figure 1.3) to produce the fragility curves for each of the building classes according to damage states definitions. Within the scope of the seismic vulnerability evaluation of existing buildings, Lang (2002) presents a simple and effective evaluation method for masonry and concrete buildings derived from analytical models. The method considers the nonlinear deformation capacity of the buildings under study; however, it misses to consider the dynamic properties of the materials under seismic loads. Moreover, the method can be time-consuming for buildings with numerous openings.

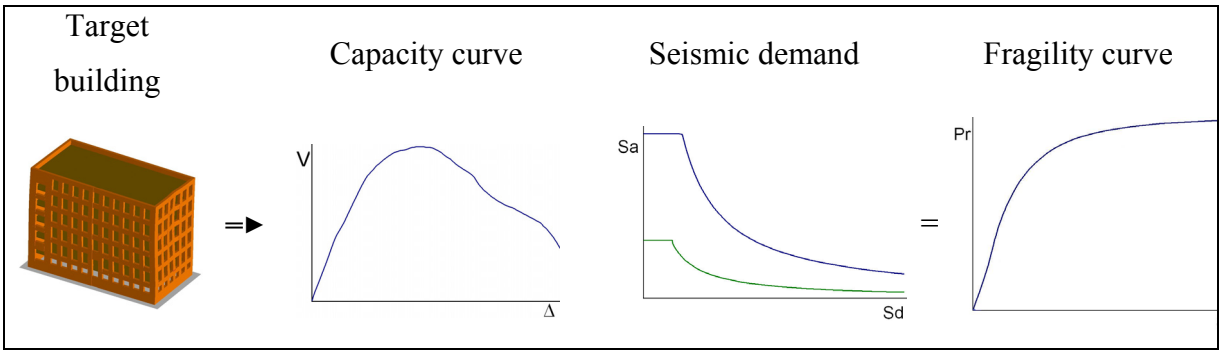

Figure 1.3 Basics of vulnerability assessment using analytical models.

1.4.4 Detailed analysis

A detailed analysis evaluation is necessary for potentially hazardous buildings which have been flagged in the rapid screening step of a multi-phase seismic assessment procedure. This method is not suitable for earthquake scenario projects where a large number of buildings have to be evaluated. However, the procedure can be used to improve the results of simple analytical methods. Detailed analyses are also helpful for developing fragility curves of buildings which typify a building class. The methodology can be divided into linear (static or dynamic) or non-linear categories (static or dynamic).

Linear static analysis

A linear procedure maintains the traditional use of a linear stress-strain relationship; however, to consider the nonlinear characteristics of a building's seismic response in such a procedure, adjustments to the building's deformations and material acceptance criteria are incorporated (ASCE 2000). In a linear static procedure, the building is modelled as an equivalent single-degree-of-freedom (SDOF) system with a linear elastic stiffness and an equivalent viscous damping. The seismic input is modelled by an equivalent lateral force with the objective to produce the same stresses and strains as the earthquake it represents. The equivalent lateral force is determined from the response spectrum (acceleration) of the fundamental vibration mode, multiplied by the building's mass. This corresponds to the typical formula to calculate the lateral force, in the seismic design codes.

$$V = \mathrm{m}.S_a.C \tag{1.3}$$

As shown in Equation 1.3, the second order effects such as stiffness degradation and force reduction due to anticipated inelastic behaviour are taken into account by the seismic coefficient *C*. This lateral force is then distributed over the height of the building and the corresponding internal forces and displacements are determined using linear elastic analysis. The results of linear procedures can be very inaccurate when applied to buildings with highly irregular structural systems, unless the building is capable of responding to the design earthquake(s) in a nearly elastic manner.

Linear dynamic analysis

Static procedures can be useful only when higher mode effects are not significant. This is generally true for short, regular buildings; otherwise, a dynamic procedure is required for buildings with irregularities (ASCE 2000). In the linear dynamic procedure, the building is modelled as a multi-degree-of-freedom (MDOF) system with a linear elastic stiffness matrix and an equivalent viscous damping matrix. The seismic input is modelled using either modal spectral analysis or time history analysis. In either case, the corresponding internal forces and

displacements are determined using linear elastic analysis. The advantage of a linear dynamic procedure with respect to a linear static one is that higher modes can be taken into consideration in the former. However, they are based on linear elastic response and hence, the applicability decreases in predicting the damage levels in the buildings in progressive collapse cases such as for masonry or concrete structures in an earthquake. Linear procedures are only applicable when the structure is expected to remain nearly elastic for the level of ground motions or when the design results in nearly uniform distribution of nonlinear response throughout the structure. However, from a performance point of view, greater inelastic demands are expected to be applied to the structure. Therefore, the uncertainty with linear procedures increases up to a point at which a high level of conservatism in demand assumptions and acceptability criteria is required to avoid unintended performance (ATC 2005). The procedures incorporating inelastic analysis can reduce such uncertainty and conservatism.

Nonlinear static analysis

In a nonlinear static procedure, the building is modeled as a SDOF structural system. The seismic ground motion, on the other hand, is represented by a demand parameter such as the spectral acceleration response. Subsequently, story drifts and component actions are related to the demand parameter through the pushover or capacity curves. Those capacity curves are generated by subjecting the structural model to one or more lateral load patterns (vectors) and then increasing the magnitude of the total load to generate a nonlinear inelastic force-deformation relationship for the structure at a global level. The load vector is usually an approximate representation of the relative accelerations associated with the first mode of vibration of the structure.

Two main applications of such a procedure are known as (i) the Coefficient Method of Displacement Modification presented in FEMA 356, *Pre-standard and Commentary for the Seismic Rehabilitation of Buildings* (ASCE 2000) and (ii) the Capacity-Spectrum Method of Equivalent Linearization presented in ATC 40, *Seismic Evaluation and Retrofit of Concrete*

Buildings (ATC 1996). In the Coefficient Method of Displacement Modification, the total maximum displacement of the SDOF system is estimated by multiplying the elastic response, based on the initial linear properties and damping, by a series of coefficients (C_0 through C_3). At the first step, an idealized force-deformation curve (pushover) relating the base shear to roof displacement should be produced (Figure 1.4). An effective period, T_{eff}, is generated from the initial period, T_i, by a graphical procedure to take into account some losses of stiffness in the transition from elastic to inelastic behaviour. The peak elastic spectral displacement is directly related to the spectral acceleration (obtained from the response spectrum) through Equation 1.4.

$$S_d = \frac{T_{eff.}^2}{4\pi^2} S_a(T_{eff.}) \tag{1.4}$$

The final displacement is calculated through Equation 1.5.

$$\delta_t = C_0.C_1.C_2.C_3.S_d \tag{1.5}$$

In this equation, C_0 is the shape factor, C_1 is the dynamic load factor, C_2 implements the effect of pinching in load-deformation relationship due to degradation in stiffness and strength, and C_3 applies the P-Δ effect. The values of each coefficient can be calculated from the corresponding table or equation presented in Chapter 3 of FEMA 356.

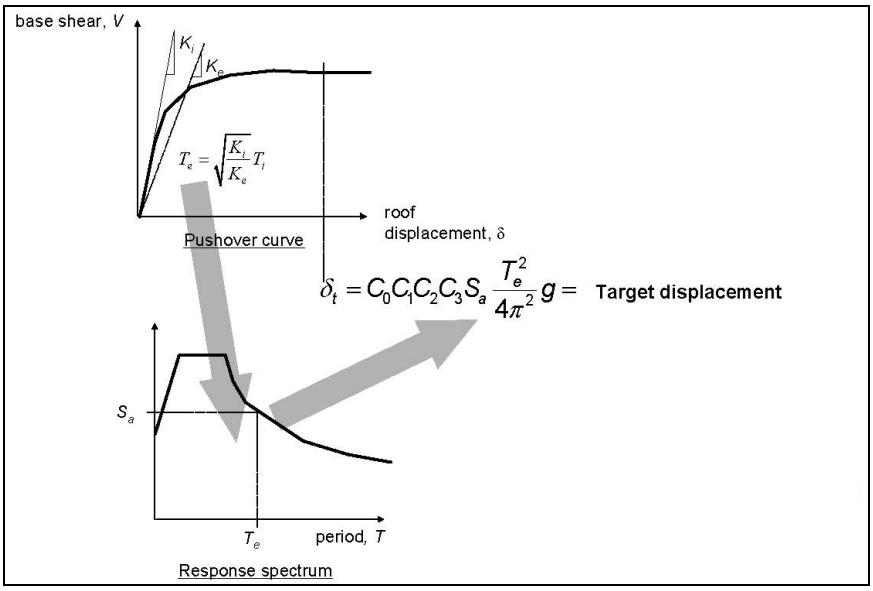

Figure 1.4 Coefficient method of displacement modification process.
Taken from ATC (2005)

The other method of the nonlinear static analysis, the Capacity-Spectrum Method of Equivalent Linearization, was first introduced by Freeman et al. (1975) as a rapid evaluation procedure in a pilot project for assessing the seismic vulnerability of buildings. The method assumes that the maximum total deformation (elastic and inelastic) of an SDOF system can be estimated from the elastic response of a system that has a larger period and greater damping than the original structure. The process begins with developing a force-deformation relationship (pushover curve) for the structure. To compare such a pushover curve with the seismic demand, as shown in Figure 1.5, the next step is to convert the force-formation capacity curve to an acceleration-displacement response spectrum.

In this format, period is represented as radial lines emanating from the origin. The equivalent period, $T_{eq,}$ is assumed to be the secant period at which the seismic ground motion demand, reduced for the equivalent damping, intersects with the capacity curve (Capacity Spectrum) at the performance point. It is also assumed that the equivalent damping of the system is associated with the full hysteresis loop area, as shown by the shaded area in Figure 1.5. As the equivalent period (T_{eq}) and damping areas (E_D) are both functions of the displacement, the solution to determine the maximum inelastic displacement is therefore iterative. This is

the basis of the simplified analysis methodology presented in ATC 40 to determine the displacement demand imposed on a building expected to deform inelastically.

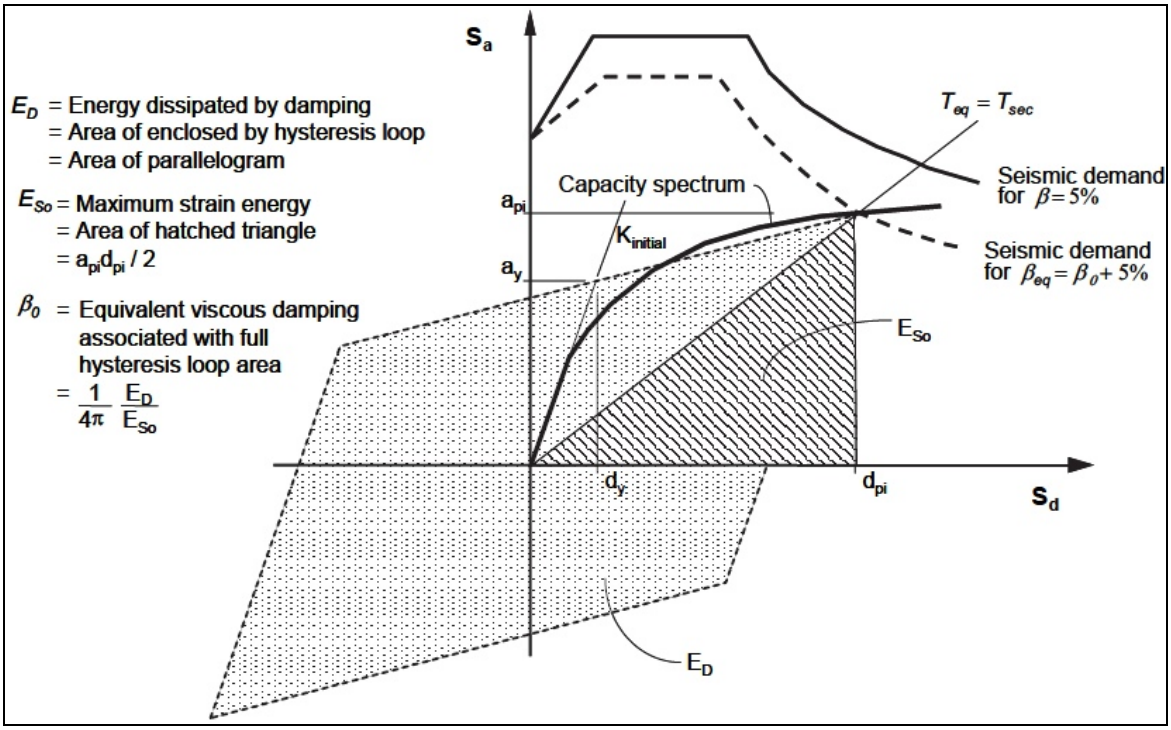

Figure 1.5 Graphical illustration of the Capacity-Spectrum Method.
Taken from ATC (2005)

Recent studies (Chopra and Goel 2000; ATC 2005; Powell 2006) indicate that the capacity spectrum method implemented in ATC 40 leads to very large overestimations of the maximum displacement for relatively short-period systems (i.e., periods shorter than about 0.5 s which relates to low and medium height buildings). Estimated maximum displacements in this period range can be, on average, more than twice as large as real maximum displacements. It is also shown that the procedure generally underestimates, by 30%, the maximum displacements of systems with periods greater than 0.5s. The results of an effort to improve the capacity spectrum method of ATC 40 are presented in FEMA 440, *Improvement of Nonlinear Static Seismic Analysis Procedures* (ATC 2005). The resulting suggestions focus on improved estimations of the equivalent period and damping. Similar to the current

ATC 40 procedure, the modified procedure's effective period and damping both depend on the ductility, and so an iterative or graphical technique is required to calculate the performance point. The improved procedure is similar in application, to the current ATC 40 capacity spectrum method, and is used in this research work (explained in more details in Chapter 2) to develop the scores for a modified index assignment procedure in Quebec.

The current nonlinear static procedures based on invariant loading vectors such as those recommended in FEMA 356 or ATC 40 are shown to possess inherent drawbacks in adequately representing the effects of varying dynamic characteristics during the inelastic response of structures (Kunnath and Kalkan 2005). Although some improved nonlinear static procedures have been developed over the past few years (such as those in FEMA 440), their validity for a variety of structural systems and a range of ground motion characteristic have yet to be demonstrated. The results of nonlinear time history analyses based on actual earthquake recordings serve as the only reliable benchmark solutions against which the NSP results can be compared.

Nonlinear dynamic analysis

In a nonlinear dynamic analysis, a detailed structural model is subjected to a ground-motion record to produce estimates of the components deformations for different degrees of freedom. The modal responses at those degrees of freedom are then combined using schemes such as the square-root-sum-of-squares. This method is the most sophisticated analysis procedure for developing fragility curves of buildings which typify a building class. Because the calculated responses are sensitive to the characteristics of the individual ground motion used as the seismic input, different ground motion records are required to obtain a good estimation of the building's responses. To this end, the Incremental Dynamic Analysis (IDA) has emerged as a potential tool for seismic evaluation because it applies a series of time history analyses.

Incremental Dynamic Analysis

An IDA involves subjecting a structural model to various ground motion records, each scaled to multiple levels of intensity up to the point at which a collapse limit state is reached (Vamvatsikos and Cornell 2002). Therefore, the IDA method is often described as a "dynamic" pushover procedure. The approach has the potential to demonstrate the variation of structural responses, as measured by a damage measure (DM, e.g., inter-storey drift), versus the ground motion intensity level, measured by an intensity measure (IM, e.g., peak ground acceleration or the first-mode spectral acceleration). The IDA procedure provides dynamic capacity curves for different ground motion levels. Although it is possible to utilize a single record for IDA, it is essential to consider variations in ground motion content when utilizing IDA in performance-based assessment. For this reason, the selection of ground motion records that takes into consideration site characteristics and source mechanisms is critical. This will be discussed in Chapter 2 where the IDA method is applied to develop the fragility curves for two building classes in Quebec.

1.4.5 Score assignment procedures

The score assignment procedure aims to identify seismically hazardous buildings by exposing structural deficiencies. Potential structural deficiencies and structural characteristics are correlated for different building classes using certain sets of scores that are usually calibrated by experts or analytical models. In most cases, these scores do not have a probabilistic meaning, and can just be used to prioritize buildings with respect to the probability of collapse.

Score assignment procedure in Canada

The rapid visual screening (RVS) method in Canada is described in the *Manual for Screening of Buildings for Seismic Investigation* (NRC-IRC 1992). As shown in Table 1.2, 15 building classes are introduced in this manual based on the construction material and the seismic

resistance system. The seismic screening procedure examines a building's seismicity, soil condition, structure type, structural irregularities, presence of non-structural hazards, usage, and occupancy to determine its seismic priority index (SPI). The SPI is the sum of a building's structural index (SI) and non-structural index (NSI), and it is a measure of the building's deviation from the National Building Code of Canada 1990 (NRCC 1990) seismic requirements. Buildings are then ranked according to their respective scores and divided into low-, medium-, or high-risk categories. An SPI higher than 20 is an indication that the building requires a detailed investigation. The 15 building types described in this procedure have been defined based on previous work done by the Applied Technology Council of California (ATC 1998), and are presented in Table 1.2.

The current rapid visual screening method in Canada is based on seismic requirements of NBCC 1990; therefore, the indices in this manual would not fully comply with NBCC 2005 (NRCC 2005) requirements. Some research works have been conducted (Karbassi and Nollet 2008; Turenne 2009) to adapt this screening method to the 2005 version of NBCC. The structural indices in the current Canadian manual do not provide any probabilistic interpretation, and were developed mainly by considering the different base-shear force calculation concepts described in different versions of the NBCC. Later in Chapter 2, we will develop an index assignment procedure which is compatible with the regional seismic hazard in Quebec. The procedure is published in a paper by Karbassi and Nollet (2008).

Table 1.2 Building classification used in NRC-IRC (1992)

Class	Structural Description
WLF	Light wood frame
WPB	Wood post and beam
SMF	Steel Moment resisting frame
SBF	Steel braced frame
SLF	Steel light frame
SCW	Steel frame with concrete shear wall
SIW	Steel frame with infill masonry wall
CMF	Concrete moment resisting frame
CSW	Concrete shear wall
CIW	Concrete frame with unreinforced masonry infill
PCW	Prefabricated concrete wall
PCF	Prefabricated concrete frame
RML	Reinforced masonry bearing walls with wood or metal diaphragms
RMC	Reinforced masonry bearing walls with concrete diaphragms
URM	Unreinforced masonry bearing walls

Score assignment procedure in the United States

The RVS of buildings for potential seismic hazards was initiated in 1988 with the publication of FEMA 154, *Rapid Visual Screening of Buildings for Potential Seismic Hazards: a Handbook*, (ATC 2002a) and its companion, FEMA 155, *Supporting Documentation* (ATC 2002b), both of which were updated in 2002. A major improvement in this update was to link the FEMA 154 screening results to *FEMA 310*, *Handbook for the Seismic Evaluation of Buildings - A Pre-standard* (ASCE 1998) and *FEMA 356*. To this end, the seismic hazard level was changed from 10% probability of being exceeded to 2%, in 50 years. Table 1.3 shows the acronym and description of the building classes considered in the latest version of this manual.

FEMA 154 procedure starts with a visual observation to identify the primary structural lateral-load resisting system based on the construction materials used (Table 1.3). Based on the identified structural system, the next step is to assign a Basic Structural Hazard score (BSH) to each building. The BSH is related to the probability of collapse in a building as a result of earthquakes in the future. As shown in Equation 1.6, the probability of collapse for a building is the product of the probability of the building being in the complete damage state multiplied by the fraction of buildings (of that class) which collapse when in the complete damage state.

$$BSH = -Log_{10}[P(\text{Complete Damage State}) \times P(\text{Collapse} \mid \text{Complete Damage State})] \quad (1.6)$$

In the first edition of FEMA 154, the BSH scores were calculated from the damage probability matrices of ATC 13. In the later edition, however, these probabilities are calculated from the fragility curves presented in the *Earthquake Loss Estimation Methodology Technical Manual* (NIBS 1999).

Finally, the overall score S (Equation 1.7) is calculated by modifying the BSH scores using a set of score modifiers which take into account some structural and site characteristics that are not considered in the calculation of the BSH scores and can be listed as follows.

1. Building's height (midrise and highrise): BSH scores are calculated for lowrise buildings.
2. Vertical and horizontal irregularities.
3. Design and construction year for pre-code and post-benchmark buildings.
4. Buildings constructed on sites with soil classes C, D, or E: BSH scores are calculated for buildings on soil class B.

$$S = BSH\ Score \pm Score\ Modifier \quad (1.7)$$

Table 1.3 Building classification used in ATC (2002b)

Structure Type	Description
W1	Light wood-frame residential and commercial buildings smaller than or equal to 5000 square feet
W2	Light wood-frame buildings larger than 5000 square feet
S1	Steel moment-resisting frame buildings
S2	Braced steel frame buildings
S3	Light metal buildings
S4	Steel frame with cast-in-place concrete shear walls
S5	Steel frame buildings with unreinforced masonry infill walls
C1	Concrete moment-resisting frame buildings
C2	Concrete shear-wall buildings
C3	Concrete frame buildings with unreinforced masonry infill walls
PC1	Tilt-up buildings
PC2	Precast concrete frame buildings
RM1	Reinforced masonry buildings with flexible floor and roof diaphragms
RM2	Reinforced masonry buildings with rigid floor and roof diaphragms
URM	Unreinforced masonry bearing –wall buildings

The final score S varies from zero to 9.8. A final score higher than 2.0, which approximately corresponds to a probability of collapse of 1%, indicated that a detailed analysis for the building is required. It should be noted that FEMA-154 methodology is primarily based on United States seismic hazard representations and California building typology defined mostly for data in California.

UBC 100 project (British Columbia)

The UBC 100 is a project that is conducted at the University of British Columbia to develop performance-based seismic risk assessment guidelines for buildings in that province. The

major development of UBC 100 in comparison to traditional seismic assessment methods is the use of performance-based criteria that allows for a more rational and systematic approach to the seismic evaluation and a relative ranking of a large inventory of structures (White et al. 2005). The project is developed for low-rise buildings (1-3 storeys) in British Columbia. The level of ground shaking assumed is consistent with that of the 2005 National Building Code of Canada, which assumes a 2% in 50-year probability of occurrence. UBC 100 covers six distinct seismic zones within British Columbia on soil classes C, D and E.

As the primary goal in every risk mitigation program is to minimize casualties, the performance level with this definition of risk is called "Life-Safety". Two critical drift levels related to casualties are defined: (1) Life Safety Drift Limit (LSDL) which is the amount of the inter-storey drift a structure can sustain with no significant chance of casualties due to structural failure, and (2) the Instability Drift Limit (ISDL) that is the drift at which a structure may completely collapse, resulting in a very high rate of casualties. The displacement coefficient method outlined in FEMA 440 and some other nonlinear dynamic analysis programs were used to determine the maximum inter-storey drift for each case.

The outcome of UBC 100 is the prioritized ranking of one structure in respect to other structures within the same building stock. The prioritization is performed based on the cost-efficiency of structural retrofitting. This priority retrofit index (PRI) reflects the increase in life safety per dollar spent by retrofitting a structure, shown in Equation 1.8.

$$PRI = \frac{casualty\ rate \times occupancy \times 100000}{retrofit\ cost} \tag{1.8}$$

In Equation 1.8, occupancy is in person-year, retrofit cost is the cost required to achieve a low risk level (life-safe building), and casualty rates reflect the casualties per 100,000 persons. These priority indices do not have any damage probability interpretation for an individual building. Moreover, the results of such a methodology is not applicable for

existing buildings in Quebec as the building classification and the seismic demand values used to develop the priority retrofit indices are different from those in Quebec.

The GNDT methodology in Italy

The GNDT methodology that utilizes a composed damage index derived from discrete damage states assigned to different building components, weighted by their relative extension, is used in Italy to assess the vulnerability of masonry buildings (GNDT 1993). The assessment of a building group is done by completing two forms: the first level form gathers the basic informative elements for each building. Consequently, on the second level form, the answers to 11 descriptive and evaluative (typological/qualitative and quantitative, respectively) items are combined to calculate the vulnerability index for each building. According to answers to those items, one of the four classes (A, B, C, or D) is selected. The class D represents the most vulnerable level. Examples of the application of this methodology can be found in (D'Ayala and Speranza 2002) and (Faccioli, Pessina et al. 1999). The most evident problem associated with this approach is the ignorance of the soil behavior on the seismic vulnerability (Augusti and Ciampoli 2000).

1.5 Performance-based seismic vulnerability evaluation of existing buildings

Conventional analytical methods, which examine only the ability of a building to stand significant earthquake excitations, have several major drawbacks. In any of those methods, only a single structural performance (e.g., Collapse Prevention) is considered. As a result, performance-based concepts that include a wider variety of structural performance states of an existing building excited by different levels of earthquake intensities are needed. The performance-based seismic evaluation (PBSE) of an existing building is a process that leads to the assessment of the building's seismic vulnerability with a view to an understanding of the risk of structural and non-structural damages, and human and economic losses that may occur as a result of probable earthquakes (ATC 2009). The structural and/or the non-structural performance state of the building are determined in terms of the damage evaluation for ground motions with different intensity levels. This information is used to estimate the

occupancy and economic losses at each level which can be used consequently to develop loss exceedance probability curves for different seismic hazards.

The PBSE procedure can be divided into the following four stages (Krawinkler and Miranda 2004; ATC 2009).

1. The seismic hazard analysis stage: the seismic hazard data at the structure's site is assessed to produce hazard curves that represent probability of exceedance in terms of an engineering demand parameter, such as the peak ground acceleration or the spectral acceleration values.
2. The structural analysis stage: non-linear time-history analyses are carried out to determine the building's response to a set of ground motions in terms of the engineering demand parameter.
3. The damage analysis stage: the results of the previous stage are used to define the limit states (e.g., performance levels) in terms of structural responses such as maximum storey drifts or roof displacement. The information is then used to produce the building's fragility curves for each limit state.
4. The loss analysis stage: the fragility curves are combined with the hazard curves, produced in the first stage, to calculate the probability of exceeding any of the limit states during a specific period of time. This information is valuable to determine, for example, the operability of the building versus its repair costs and repair duration.

1.6 Loss estimation analysis: mean annual frequency of exceeding damage states

One piece of information sought in a performance-based seismic vulnerability evaluation of existing buildings is to know how often the damage states may be exceeded annually. This information is useful for risk analysis studies, those in charge of managing cost-allocation studies for reinforcing existing buildings, or insurance corporations. The mean annual frequency (MAF) of exceeding a damage state is expressed as the mean annual frequency of the "intensity measure" (e.g. the spectral acceleration) being larger than the capacity-intensity

measure (IM_c) that pushes the building to reach the damage level, multiplied by the probability of such an intensity measure to happen. Once the fragility curves of the corresponding limit states along with the hazard curve for the site of interest is available, the MAF of exceeding those damage states can be calculated as follows (Ibarra and Krawinkler 2005).

$$MAF_{ds} = \int_0^{\infty} FC_{ds}(z) \times \left| dHC(z) \right| \tag{1.9}$$

In Equation 1.9, *FCds(z)* and *dHC(z)* are the values of the fragility curve for the corresponding damage state and the slope of the hazard curve at z = Sa(T), respectively. The hazard curves depend on the geographical location of the building. We will get back to this issue in the loss estimation stage in Chapter 4 where we calculate the MAF for the studied buildings in this research.

1.7 State of the seismic vulnerability evaluation methods in Quebec

Because enough observed earthquake damage data does not exist in the province, based on the literature review in this chapter, the predicted vulnerability method is seen to be a suitable method for the seismic vulnerability evaluation of a group of buildings here. Nevertheless, the application of the available methods in Canada or in other parts of the world for ancient buildings in Quebec faces three major problems.

1. Adequacy of available building classifications.
2. Applicability of existing methods to the seismic hazard representations in Quebec.
3. Complexity level of analytical procedures (modeling, nonlinear analysis, etc.) for masonry buildings.

1.7.1 Building classification in Quebec

A good building classification should be able to comprehend if not all but the majority of the building types in the area, and to consider both the structural characteristics and the

construction materials. By matching an inventory of 89 buildings, located in old Montreal, to the current Canadian building classification (NRC-IRC 1992) presented in Table 1.2, (Lefebvre 2004) showed that the existing buildings in the historical sector of Montreal are not well represented by the available classification in Canada. As seen in Table 1.4, that research work concluded that the major problem with applying the current Canadian building typology to old sectors in Quebec is that it does not present any subclasses for masonry buildings. Four sub-classes that were found to exist in old Montreal are masonry building built with (I) rubble stone, (II) simple stone, (III) massive stone, and (IV) confined bricks. Another study done on a larger community of buildings in the same area for 516 structures (Rodrigue 2006) showed that two more classes (concrete and steel moment resisting frames) can be added to the "present in old Montreal" column in Table 1.4.

To verify the building classes in other regions of the province, the old district of Quebec City was visited in person. The area was investigated street by street, and several pictures were taken for the research database. Based on such visit and the studies mentioned above, the building classification shown in Table 1.5 is proposed for the existing buildings in the historical sectors of the province.

Table 1.4 Comparison of the current Canadian building classification with classes seen in old Montreal according to Lefebvre (2004) and Rodrigue (2006)

Structure type	**NRC-IRC building classes**	**Present in old Montreal**
Wood	WLF	Light wood frame
	WPB	Wood post and beam
Steel	SMF	
	SBF	Steel frame with bracing
	SLF	Steel frame with concrete shear walls
	SCW	Steel frames with masonry in-fills
	SIW	
Concrete	CMF	
	CSW	
	CIW	Concrete frame with unreinforced masonry infills
	PCW	
	PCF	
	RML	
	RMC	
Masonry	URM	Masonry building with rubble stone
		Masonry building with simple stone
		Masonry building with massive stone
		Masonry with confined bricks

It should be noted that in some cases, assigning a class to a building from those proposed in Table 1.5 is not straightforward. This is mostly when a combination of two or more structural typologies are used in a building. In such cases, specific decisions should be made to consider the best representation for those buildings.

Table 1.5 Proposed building classification for existing structures in historical areas of Quebec

Structure Type	Description
Wood Structures	light wood frame wood beams and columns
Steel Frame	with bracing with concrete shear walls with unreinforced masonry infills moment resisting frames
Concrete	frame with unreinforced masonry infills (CIW) moment resisting frames
Masonry	with rubble stone with simple stone with massive stone confined bricks unreinforced with wood floors (URMW)

1.7.2 Applicability of existing seismic vulnerability methods for Quebec

Among the existing methods for the seismic vulnerability evaluation of buildings, score assignment method, can be used as the first step of a multi-phase procedure for identifying hazardous buildings. Those buildings must then be analysed in more details. As stated previously, the existing rapid visual screening procedure in Canada, explained in section 1.4.5, relates to NBCC 1990, and has not been developed for ancient buildings. Moreover, the index proposed in that manual does not have any damage probability bases and it can be only used to rank a building in comparison with another. FEMA 154 procedure, on the other hand, is primarily based on United States seismic hazard representations and California building typology defined mostly for data in California. The dissimilarities between the seismic hazard representations in Canada (NRCC 2005) and those introduced in the American codes (BSSC 2003) diminish the validity of the results of any rapid visual evaluation performed in Canada that apply only the FEMA 154 scores without modifications.

1.7.3 Complexity level of analytical procedures for masonry buildings

When considering the seismic vulnerability evaluation of masonry buildings such as those identified in Table 1.4, the complexity of the analytical procedures to represent the progressive collapse poses an additional challenge.

1.7.4 Progressive collapse analysis of structures with masonry: Problem with FEM

The following five failure modes can occur in the progressive collapse—in which the failure of a primary structural element results in the failure of adjoining structural elements, which in turn causes further structural failure—of masonry walls: (1) joint de-bonding, (2) units sliding along bed or head joints, (3) units cracking under direct tension, (4) units diagonal tensile cracking under high compression and shear, and (5) bricks splitting (Mayorca and Megura 2003). As the structural boundaries and load conditions prevent the masonry to fail in compression, only the first three failure modes, shown in Figure 1.6, are generally observed in an earthquake, and considered in this study. Any of these failure modes lead to large displacements and separation of elements.

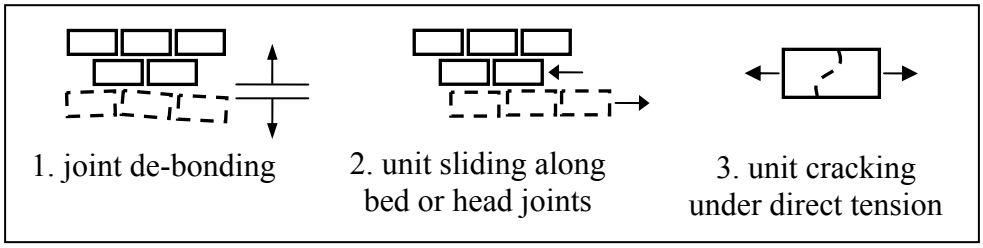

Figure 1.6 Failure modes in masonry walls observed in an earthquake.

The Finite Element-based methods are considered as the main tools for the seismic vulnerability evaluation of existing buildings. However, using a FE-based method—that assumes the material as a continuum (Calderini and Lagomarsino 2008) in a progressive collapse analysis of masonry structures faces two main problems: (1) simulating elements with common nodes but different displacement, and (2) modeling cracks in the elements. In any FE-based analysis, elements are connected at nodes so, it is assumed that all elements

sharing the same node have the same displacement; however, to track the behaviour of each element in an accurate way when element separation occurs in a progressive collapse analysis, elements are considered to displace independently. An alternative is to use multiple node ID's at expected separation points; nevertheless, this technique results in stress singularity and inaccurate stresses at locations of nodal separation that may lead to an uncertain stress distribution within the whole structure (Tagel-Din and Megura 2000).

On the other hand, special techniques must be adapted to model cracks in the elements and to consider the effect of element separation on the building's overall stiffness. Two techniques are generally applied to consider the crack effect in materials such as masonry. The first technique known as "smeared cracks" deals with cracks by considering their effect on stiffness and stress-strain equations (Cervera and Chiumenti 2006). Although showing considerable accuracy in calculating displacements and failure loads, models developed based on this method are relatively complicated. Moreover, special elements should be used in the location of dominant cracks (Meguro and Tagel-Din 2000). This also requires previous knowledge of the location and direction of cracks' propagation. In most cases, the fracture plane is arbitrary and unknown before the analysis. The same problem exists for the other technique known as "discrete cracks" modeling, in which cracks are taken into account as discrete items (Carol et al. 1997). The latter method is more appropriate for cases with few cracks.

Moreover, because of the challenges in material constitutive models and failure modes for masonry structures, predicting the deformation capacity through the application of FE-based methods is a difficult task (Belmouden and Lestuzzi 2007). Consequently, finding the maximum strength and deformations which are essential parameters in developing reliable fragility curves for masonry buildings is difficult.

Some researches have applied elastic (or elastoplastic) FEM analyses [e.g., (Asteris et al. 2005) and (Ismail et al. 2009)] for the seismic vulnerability assessment and rehabilitation of masonry buildings. Although these methods provide simple processes for the repair

methodology of unreinforced buildings under study, the nonlinear behaviour of the materials and consequently, of the whole structure, in a progressive collapse simulation is not fully considered; therefore, such methodologies may not lead to precise fragility curves for masonry buildings.

Applied Element Method

The Applied Element Method is used in this study as an alternative to the FEM. This method, which is based on dividing structural members into virtual elements connected through springs (Figure 1.7), which means that there are no common nodes, can simulate large displacements and elements progressive separation through successive failure of those springs (Meguro and Tagel-Din 2002). Exploration of the approach employed in the Applied Element Method began in 1995 at the University of Tokyo as part of a research study. The term "Applied Element Method," however, was first established in a journal paper in 2000 (Meguro and Tagel-Din 2000).

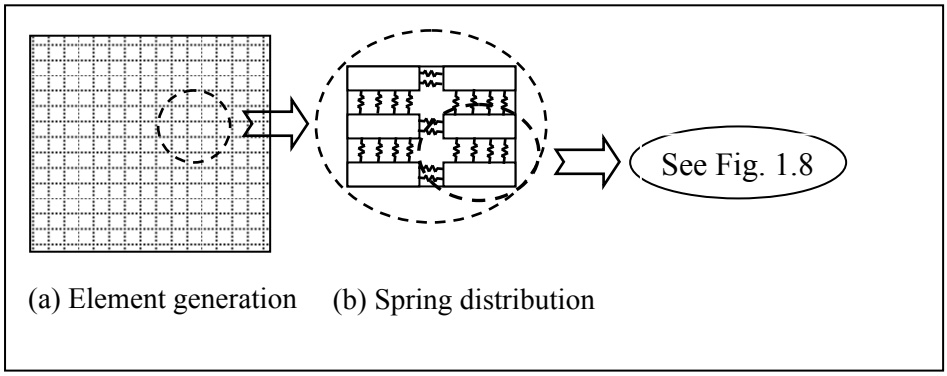

Figure 1.7 Modeling an element in AEM.

As shown in Figure 1.8, pairs of normal and shear springs located at the element contact points, distributed around the edges, represent stresses, strains, and deformations of certain portions of the structure (Meguro and Tagel-Din 2002). Therefore, partial connectivity between elements is allowed during the analysis: while some of the springs fail, others are still effective.

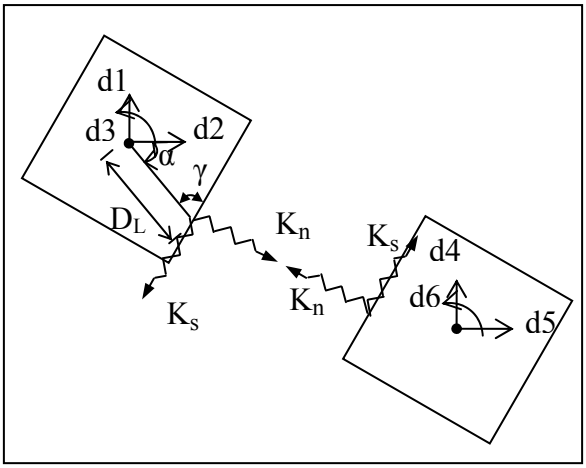

Figure 1.8 Element shape, contact points, and degree of freedom in AEM.
Adapted from (Mayorca and Megura 2003)

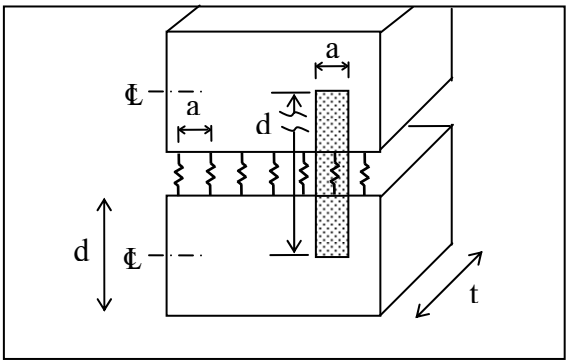

Figure 1.9 Spring distribution and area of influence of each springs pair in AEM.
Adapted from (Mayorca and Megura 2003)

For the normal and shear springs inside the hatched area in Figure 1.9, extended from the centerline of one element to the centerline of the adjacent one, the normal and shear stiffness values are determined as:

$$K_n = \frac{E \cdot a \cdot t}{d} \quad , \; K_s = \frac{G \cdot a \cdot t}{d} \tag{1.10}$$

Where *a* is the distance between the springs, *d* is the length of the represented area by each spring which is actually the element's length, E and G are the Young's and shear modulus of the material, and *t* is the thickness of the element, respectively. Application of this method for masonry buildings and details about its mathematical background are presented in Chapter 3.

1.8 Proposed methodology for the Seismic Vulnerability Evaluation of Buildings with Masonry in Quebec

From the literature review presented in this chapter, it was shown that in situations where there is lack of sufficient observed earthquake damage data, such as in the province of Quebec, the predicted vulnerability technique coupled with a score assignment procedure can be a suitable method for the seismic vulnerability evaluation of a group of buildings. The score assignment procedure can be used to identify the existing buildings which need further study, while the analytical modeling can be applied to develop capacity and fragility curves for those building classes in old sectors of Quebec which are not been well represented in the available building classification in Canada. The proposed methodology for the seismic vulnerability evaluation of existing buildings with masonry in Quebec includes two main components: (1) an adapted rapid visual screening procedure, and (2), a performance-based seismic vulnerability assessment.

a) Rapid visual screening procedure

Considering the shortcoming in the current rapid visual screening method in Canada (NRC-IRC 1992), one of the main objectives of this research work is to develop an updated score assignment method that can be used for cities in Quebec with different seismic hazard levels. A previous study (Nollet et al. 2005) shows that most of the building classes observed in the old sectors of the province—except for the masonry structures, as shown in Table 1.4—can be represented by the current Canadian building typology (NRC-IRC 1992) or the ones available in FEMA 154 (ATC 2002a). Therefore, the available building classification in

(NRC-IRC 1992) and the capacity and fragility curves presented in (NIBS 2003) can be used for most Quebec building classes in the definition of indices for a new rapid visual screening method. The goal of such a screening method is to provide a seismic vulnerability evaluation tool that can be used by urban-decision-makers, to help them identify and prioritize structures requiring seismic risk mitigation plans. The tool can also be used to evaluate the probability of damages in a group of buildings for different levels of seismic hazard. This procedure is developed in Chapter 2.

b) Performance-based seismic vulnerability assessment

Another objective of this research work, on the other hand, is to develop appropriate capacity and fragility curves for the new building classes proposed in Table 1.5. Considering the benefits of the Performance-based Seismic Vulnerability Evaluation for existing buildings, explained in this chapter, only dynamic-based methods are capable of conducting such type of evaluations which take into account the dynamic behaviour of structural models, and static analytical methods such as the Pushover analysis methodology is out of consideration in this case. To this end, the methodology to develop the dynamic capacity and fragility curves for two of the building classes proposed in Table 1.5—unreinforced masonry with wood floors (URMW) and RC frame with unreinforced masonry infills (CIW)—is presented in Chapter 3. The curves are developed at three structural performance levels—Immediate Occupancy, Life Safety, and Collapse Prevention defined in FEMA 356. As will be seen, the methodology uses an Applied Element-based approach to overcome the limitations of a FE-based method in the progressive collapse case for masonry buildings in the Incremental Dynamic Analyses for the buildings studied here.

1.9 Summary

Different seismic vulnerability methods in use in different parts of the world were reviewed in this chapter to assess their applicability for such type of evaluation for the existing buildings in historical sectors of Quebec. The literature review shows that some essential

items for a predicted-based vulnerability method (that was shown to be the suitable method for the case of existing buildings in Quebec) are missing, and should be developed based on the available tools.

1. Although most of the building classes in the current Canadian building typology (NRC-IRC 1992) or the ones available in the American reference (ATC 2002a) can be used to classify the existing buildings in old sectors of the province (Table 1.4), masonry buildings in Quebec are not well represented in those references. For this reason, an adapted building classification was presented in this chapter (Table 1.5).

2. As the first step for a seismic vulnerability evaluation, a rapid visual screening method was shown to be helpful to identify buildings which need further study. Such a screening tool which is in conformity with the seismic demand updates presented in the latest edition of the NBCC 2005 (NRCC 2005) is missing even for the current building classes in (NRC-IRC 1992).

Because of the important effect of material properties and the construction practice (in a region) on the dynamic behaviour of a building, in the context of the seismic vulnerability evaluation, the available capacity and fragility curve data in the literature may not be even close to the reality for some of the building classes (presented in Table 1.4) in Quebec, and have to be checked. To this end, in the second part of Chapter 2, those curves are developed for a typical masonry and a typical concrete frame building with infill masonry.

3. Among the typology identified in Table 1.5, the structural analysis of masonry buildings is complex. However, the Applied Element Method offers an effective alternative to FEM to simulate the progressive collapse of masonry structures.

4. The Performance-based Seismic Vulnerability Evaluation of existing buildings presents the possibility of studying the structural performance of a building (for different seismic

demands) and obtaining the information on the probability of exceeding any of the performance levels.

CHAPTER 2

SCORE ASSIGNMENT METHOD ADAPTED FOR THE SEISMIC HAZARD IN QUEBEC

2.1 Introduction

A rapid visual screening method which is adapted to the seismic demands in Quebec is developed through the application of the latest improvement for nonlinear static analysis procedure proposed in FEMA 440, *Improvement of nonlinear static seismic analysis procedures* (ATC 2005). The seismic demands used in the nonlinear static analysis procedure are those presented in the 2005 edition of the *National building code of Canada* (NBCC) (NRCC 2005) in the form of spectral acceleration response values and spectral amplification factors defined according to the NBCC 2005 site classification. Details of developing the method is published in a journal paper (Karbassi and Nollet 2008).

2.2 Method development principles

Adapting the score assignment method to account for Quebec's different seismic hazard levels relies in part on the methodology applied in the development of scores in FEMA 154. Figure 2.1 illustrates the methodology followed in developing these new indices. The development of such an evaluation tool requires the consideration of three elements: (1) a building classification system defined on the regional basis, (2) the capacity curve for each building class, and (3) an appropriate seismic hazard representation for the area. As stated in the introduction of this chapter, the building classification used in this chapter is the same as that presented in the *Manual for screening of buildings for seismic investigation* (NRC-IRC 1992), shown in Table 1.2. This building classification is in fact similar to the one presented in FEMA 154.

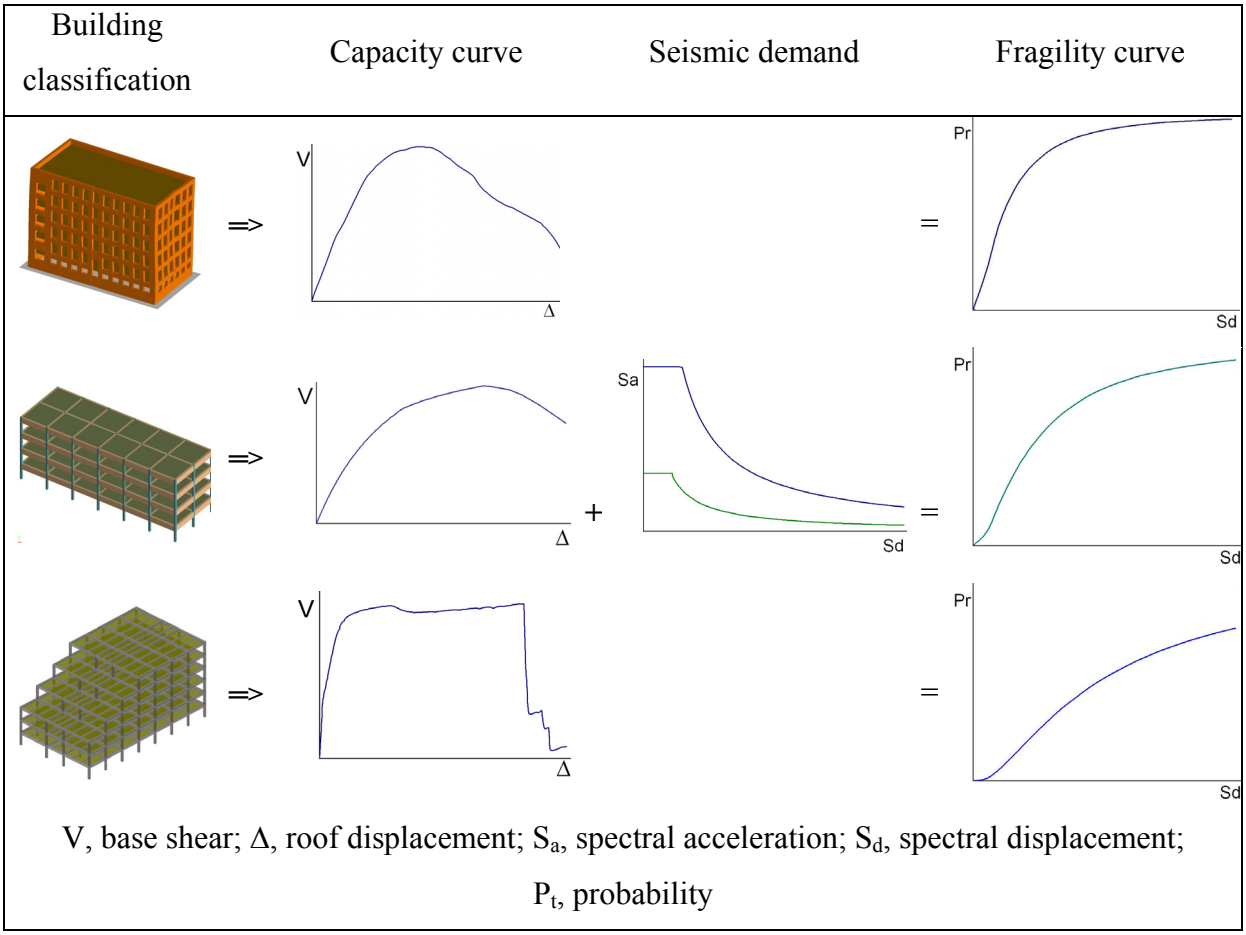

V, base shear; Δ, roof displacement; S_a, spectral acceleration; S_d, spectral displacement; P_t, probability

Figure 2.1 Essential elements for developing the tools for a score assignment method tools.

The NBCC 2005 spectral acceleration response values for the province of Quebec serve as the seismic demand used to calculate a set of structural vulnerability indices and modifiers from the capacity and fragility curves (NIBS 2003) for different building classes. For each seismic hazard level, a structural vulnerability index (SVI) is computed based on the FEMA 440 improved nonlinear static analysis procedure. Index modifiers are also computed for structures that may have different characteristics and deficiencies than those assumed in the calculation of the initial SVI values.

$$\text{SVI final} = \text{SVI} \pm \text{Indices Modifiers} \qquad (2.1)$$

2.3 Seismic hazard regions in Quebec

To differentiate the seismic hazard levels of different cities, acceleration levels as well as spectral shapes must be compared. A city's acceleration level is well represented by its spectral acceleration values at 0.2 s, and the ratio of the spectral acceleration values at 0.2 and 1.0 s is generally used to compare variations in spectral shapes (Heidebrecht 2003). The seismic hazard level of each city in the province is determined using FEMA 310 criteria, which are listed in Table 2.1. Although these criteria have been defined for US cities, reviewing the obtained rational classification (see Appendix I) confirms their application for cities in Quebec. Three seismic hazard levels (low, moderate, and high) are defined according to the spectral acceleration response, S_a, at 0.2 and 1.0 sec. [$S_a(0.2)$ and $S_a(1.0)$], and the peak ground acceleration (PGA) values of the 119 cities and regions presented in NBCC 2005 for the province[1].

Table 2.1 Criteria for specifying the seismic hazard level for cities in Quebec taken from ASCE (1998)

Seismic hazard level	**Spectral acceleration at 0.2 s, $S_a(0.2)$ (g)**	**Spectral acceleration at 1.0 s, $S_a(1.0)$ (g)**
High	> 0.500g	> 0.200g
Moderate	0.167g to 0.500g	0.067g to 0.200g
Low	< 0.167g	< 0.067g

The city with the highest seismic hazard level is La Malbaie, with $S_a(0.2)$ = 2.3g, $S_a(1.0)$ = 0.6g, and PGA = 1.1g. Inukjuak and Kuujjuarapik, on the other hand, have the lowest seismic hazard, with $S_a(0.2)$ = 0.12g, $S_a(1.0)$ = 0.023g, and PGA = 0.059g. The 119 Quebec cities are divided into three groups according to their respective seismic hazard (see Appendix I), and the median of the spectral acceleration values are calculated for each group. The medians are chosen so that the results are consistent with NBCC 2005, which uses median ground motions. It is useful to mention that most of the cities fall in the moderate seismic hazard

[1] Open File 4459, Geology Survey of Canada, available from earthquakescanada.nrcan.gc.ca/hazard/OF4459/index_e.php

group, as expected. Data for adjoining cities with similar spectral values are considered only once in the statistical calculations to avoid data repetition. The spectral acceleration values are used to compute the cumulative probability distribution of $S_a(0.2)$ and $S_a(1.0)$ within each seismic hazard level, as shown in Figure 2.2 and Figure 2.3. The resulting median spectral acceleration values are listed in Table 2.2, and are used to calculate the SVIs for different building classes.

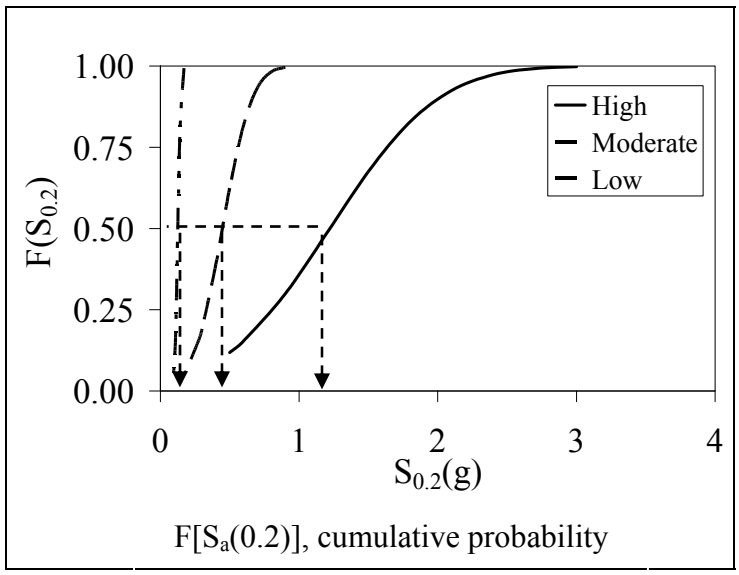

Figure 2.2 Distribution of spectral acceleration values at 0.2 sec, $S_a(0.2)$, in different seismic hazard levels in Quebec.

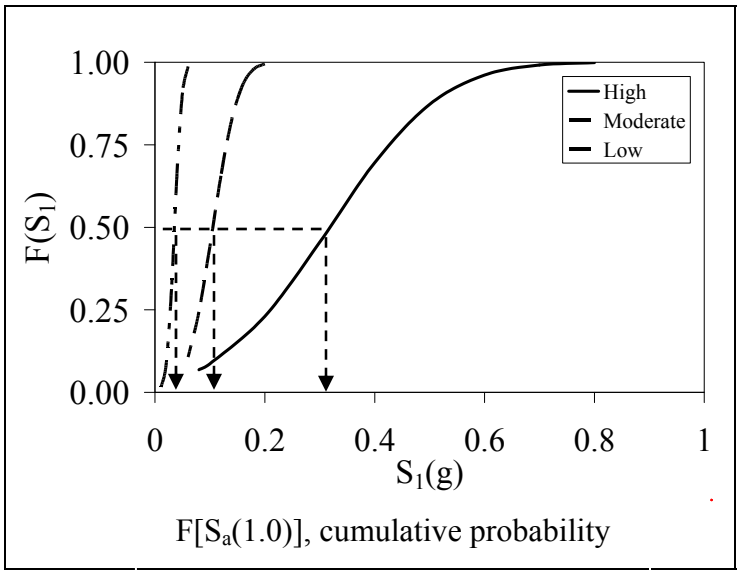

Figure 2.3 Distribution of spectral acceleration values at 1.0 sec, $S_a(1.0)$, in different seismic hazard levels in Quebec.

Table 2.2 Median of spectral acceleration values for different periods at different seismic hazard levels

	Spectral acceleration, g		
	High	**Moderate**	**Low**
$S_a(0.2)$	1.22	0.45	0.13
$S_a(0.5)$	0.66	0.24	0.07
$S_a(1.0)$	0.32	0.11	0.04
$S_a(2.0)$	0.10	0.03	0.01

2.4 Basic assumptions in the calculation of indices

In the improved capacity spectrum method of FEMA 440 considered in this research project, we start off by plotting the capacity curves provided in the *Multi-hazard loss estimation model HAZUS-MH MR 1 technical user's manual* (NIBS 2003) and the seismic demand spectra developed from the spectral acceleration values proposed in Table 2.2 in acceleration-displacement response spectrum (ADRS) format as shown in Figure 2.4. In Figure 2.4, T_0 is the initial period of the building (in the elastic mode), T_{eq} is the period of the building at the

performance point, and β_{eff} is the effective damping. The next step is to find the performance point, which is the maximum displacement of each building group representation. This is a point on the capacity spectrum that lies on the appropriate demand response spectrum, reduced for the nonlinear effects by a reduction factor B defined in FEMA 440 by Equation 2.2.

$$B = \frac{4}{5.6 - \ln(\beta_{eff})} \tag{2.2}$$

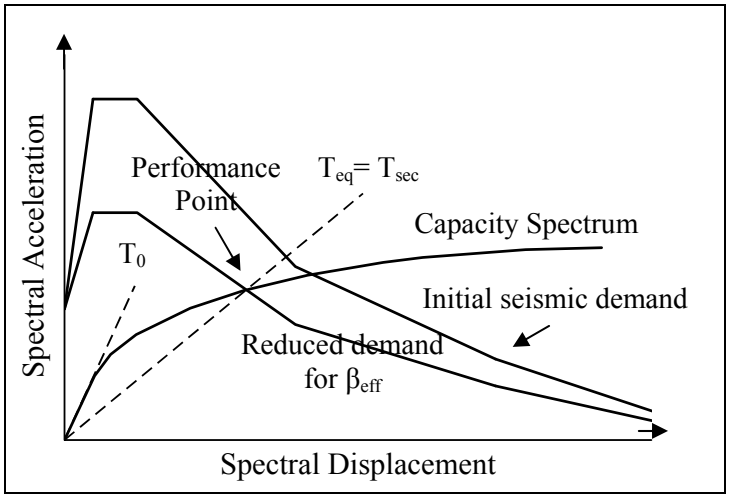

Figure 2.4 Graphical illustration of the Capacity-Spectrum Method.
Adapted from (ATC 2005)

The effective damping in Equation 2.2, β_{eff}, consists of the hysteretic damping and the elastic damping (β_0) for each building class. Equations for calculating hysteretic damping are normally based on the inelastic behaviour and ductility of the structure, whereas the equations used here (proposed by FEMA 440) are those that are independent of the hysteretic model of the structure and have been optimized for use in any capacity curve over a wide range of ductilities. Based on the inelastic behaviour and ductility factor μ_1 of the structure, β_{eff} is calculated from one of the following equations.

$$\text{For } 1.0 < \mu_1 < 4.0: \quad \beta_{eff} = 4.9(\mu_1 - 1)^2 - 1.1(\mu_1 - 1)^3 + \beta_0 \tag{2.3}$$

$$\text{For } 4.0 \leq \mu_1 \leq 6.5: \quad \beta_{eff} = 14.0 + 0.32(\mu_1 - 1) + \beta_0 \tag{2.4}$$

$$\text{For } \mu_1 > 6.5: \quad \beta_{\text{eff}} = 19\left[\frac{0.64(\mu_1 - 1) - 1}{[0.64(\mu_1 - 1)]^2}\right]\left(\frac{T_{eq}}{T_0}\right)^2 + \beta_0 \tag{2.5}$$

The equivalent period in Equation (2.5) is computed from the following equation.

$$T_{eq} = \left[0.89\left[\sqrt{\frac{(\mu_1 - 1)}{1 + 0.05(\mu_1 - 2)}} - 1\right] + 1\right]T_0 \tag{2.6}$$

It should be noted that the above equations are applicable for buildings with initial period between 0.2 to 2.0 sec.

The elastic damping values used in this study are selected according to building type to reflect inherent differences in the damping behaviour of different materials. Recommended damping values are given in (Newmark and Hall 1982) for two levels of stress: working stress and stresses at or just below the yield point (Table 2.3). Upper-bound values are to be used for ordinary structures, whereas lower-bound ones may better reflect the elastic damping in special structures, which should be designed more conservatively (Chopra 2001).

Table 2.3 Recommended Damping Values
taken from (Newmark and Hall 1982)

Stress Level	Building Type	Damping Ratio (%)
Working stress	Welded steel, pre-stressed concrete, well-reinforced concrete (slight cracking)	2-3
	Reinforced concrete with considerable cracking	3-5
	Bolted and/or riveted steel, wood structures with nailed or bolted joints	5-7
At or just below yield point	Welded steel, pre-stressed concrete (without complete loss in pre-stress)	5-7
	Pre-stress concrete with no pre-stress left	7-10
	Reinforced concrete	7-10
	Bolted and/or riveted steel, wood structures with bolted joints	10-15
	Wood structures with nailed joints	15-20

The recommended damping values for unreinforced and reinforced masonry structures are 3% and 7%, respectively; however, most building codes disregard the variation in damping with structural materials and consider a 5% damping ratio for all building types. The elastic damping values considered in the calculations of this chapter, which are similar to those proposed by (NIBS 2003), are presented in Table 2.4.

Table 2.4 Suggested values for the elastic damping used in this chapter

Building Type	Damping (% of critical)
Steel Buildings	5 – 7
Reinforced Concrete and Pre-cast Concrete Buildings	7
Reinforced Masonry Buildings	7- 10
Unreinforced Masonry Bearing Wall and Infill Buildings	10
Wood Buildings	10 – 15

The performance point determination requires a trial-and-error. As shown in Figure 2.4, this point represents the situation for which the seismic capacity of the structure is equal to the seismic demand imposed on it by a specific ground motion (ATC 1996). The performance point is then used to compute the probability of complete damage, which is determined from complete damage state curves produced from past earthquake damage observation data and (or) analytical models (Figure 2.5).

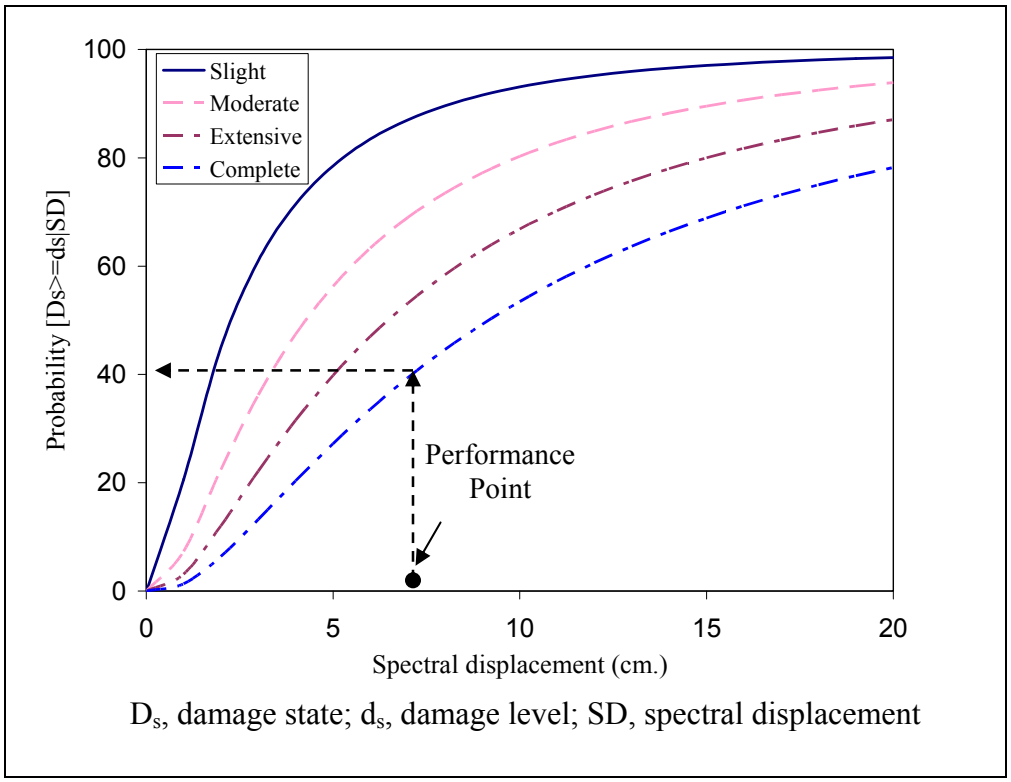

Figure 2.5 Example of fragility curves for unreinforced masonry buildings.

The complete damage state is used in calculating the scores, as the score assignment procedure is generally used to identify those structures within a group that have the highest probability of collapse. Other damage states curves can be considered when developing scores for more important structures, such as hospitals or fire stations that require an operational performance level after an earthquake.

As for the basic structural hazard (BSH) scores in FEMA 154, the proposed SVIs are defined as the negative of the logarithm (base 10) of the probability of collapse given the seismic demand corresponding to the seismic hazard level considered for each region (Equation 2.7).

$$SVI = - \text{Log}_{10}[P(\text{collapse} \mid \text{seismic demand})] \quad (2.7)$$

In developing the fragility and capacity curves, different design criteria are defined for different seismic design zones. The SVIs for the various building types are calculated for buildings constructed after the first national seismic codes were adopted, and before they were substantially improved. These criteria correspond to buildings constructed between 1953 and 1970 in Canada (Table 2.5). In regions with low seismic hazard, the SVIs are calculated for buildings constructed before the initial adoption of the seismic codes.

Soil type C, with an average shear wave velocity of 360-750 m/s in the uppermost 30 m, is the reference soil class in NBCC 2005 (Adams and Atkinson. 2003) and is used in the calculation of the SVIs. Specific modifiers are then considered to adapt these SVIs to reflect the effects from other site classes (types D and E). These modifiers are not proposed for the sites with soil classes A and B, and thus SVIs for buildings do not benefit from the better soil condition.

Table 2.5 Selection of the Canadian seismic design level as a function of the design date and the seismic hazard level

	Design date		
Seismic hazard level	**After 1970**	**1953-1970**	**Before 1953**
High	High-Code	Moderate-Code	Pre-Code
Moderate	Moderate-Code	Low-Code	Pre-Code
Low	Low-Code	Pre-Code	Pre-Code

Figure 2.6 illustrates the detailed procedure to calculate the SVI for one of the building classes, the URM building class, for regions with a high seismic hazard level.

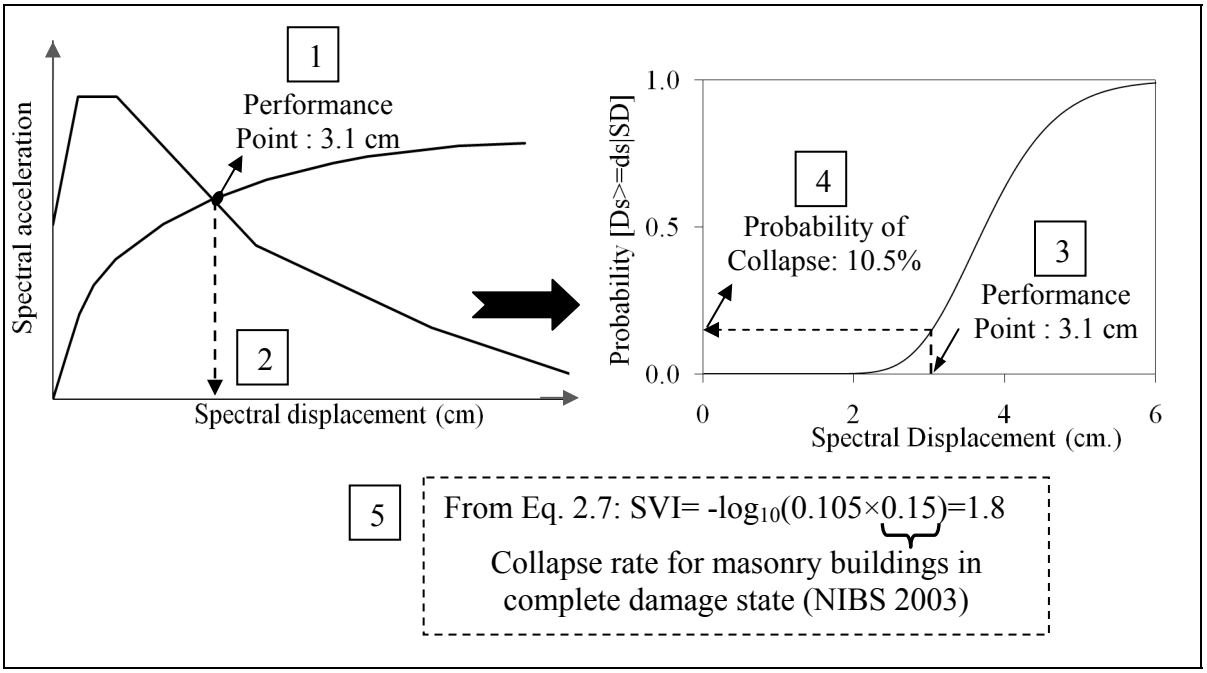

Figure 2.6 Graphical illustration of the process of calculating the BSH for the URM building class.

A major modification is made in the calculation of these scores, versus those in the second edition of FEMA 154/155, through a different consideration of the seismic hazard level in the application of the seismic demand. The maximum earthquake ground motions considered in American provisions (ASCE 2000) are based on a set of rules that depend on the seismic hazard of an individual region. The design ground motions are based on a lower bound estimate of the margin against collapse inherent in structures designed to the provisions. Based on experience, this lower bound is deemed to correspond to a factor of about 1.5 in ground motions. Consequently, the design earthquake ground motion is selected at a ground shaking level that is 1/1.5 (2/3) of the maximum considered earthquake ground motion. The Canadian code for its part, however, considers the median seismic hazard values in the presentation of the spectral acceleration values therefore, the "2/3" reduction factor is ignored in this case (Adams and Atkinson 2003).

The developed structural vulnerability indices for the fifteen building classes of Table 1.2 are presented in Table 2.6.

Table 2.6 Structural vulnerability indices for different building classes in Quebec
Refer to Table 1.2 for building class definitions

Seismic hazard	**Building Class**							
Level	WLF	WPB	SMF	SBF	SLF	SCW	SIW	CMF
High	3.3	4.0	2.9	3.1	2.9	2.8	2.1	2.5
Moderate	5.1	5.4	3.9	4.1	4.0	4.0	3.8	3.6
Low	7.4	7.6	6.0	6.1	6.1	6.1	6.0	5.7
	CSW	CIW	PCW	PCF	RML	RMC	URM	
High	2.9	1.8	2.2	2.6	2.7	2.7	1.8	
Moderate	3.9	3.5	3.8	3.6	4.2	4.2	3.0	
Low	6.4	5.7	5.1	6.1	6.1	6.3	3.9	

2.5 Development of index modifiers

The structural vulnerability indices presented in Table 2.6 have been calculated for the low-rise building class on type C soil for each seismic hazard level. However, the procedure should be able to screen other buildings that may have different characteristics from those assumed in the calculation of the SVIs. For this reason, a variety of index modifiers need to be developed to account for the probable conditions that may exist within the building classes. In this study, modifiers have been developed to take into account the following variances from the SVI basic assumptions:

1. Sites with soil classes D and E as defined in the NBCC 2005.
2. Buildings with horizontal and vertical irregularities.
3. Design and construction years that are pre-code and post-benchmark.
4. Building heights that are mid-rise and high-rise.

The medians of the spectral acceleration values for each seismic hazard level (Table 2.2) are applied as the seismic demands in the calculation of index modifiers.

Index modifiers for soil classes D and E

Soil modification factors, F_a and F_v, for different soil classes are presented in NBCC 2005. These coefficients are used to incorporate the soil amplification effect on earthquake ground shaking in the spectral acceleration values. Index modifiers used to consider the effect of soil types D and E are computed based on the differences that would be obtained for the SVIs were the basic indices to be calculated for these soil classes by applying soil modification factors (F_a and F_y) on the demand spectra. The index modifiers for soil type D for each seismic hazard level are determined by subtracting the SVIs calculated for this soil class from the original SVIs computed for the reference soil class, C. Similar calculations are performed for soil class E, and the results are presented in Table 2.7.

Table 2.7 Index modifiers for soil classes D and E

Seismic hazard level	**Soil Class**	**Building Class**							
		WLF	WPB	SMF	SBF	SLF	SCW	SIW	CMF
High	D	-0.3	-0.3	-0.3	-0.3	-0.2	-0.3	-0.2	-0.3
	E	-0.7	-1.0	-0.7	-0.8	-0.7	-0.8	-0.5	-0.7
Moderate	D	-0.5	-0.7	-0.6	-0.5	-0.5	-0.7	-0.3	-0.6
	E	-0.5	-0.7	-0.6	-0.5	-0.5	-0.7	-0.3	-0.6
Low	D	-0.6	-0.7	-0.7	-0.6	-0.6	-0.6	-0.6	-0.7
	E	-0.6	-0.7	-0.7	-0.6	-0.6	-0.6	-0.6	-0.7
		CSW	CIW	PCW	PCF	RML	RMC	URM	
High	D	-0.4	-0.2	-0.1	-0.3	-0.2	-0.2	-0.2	
	E	-0.4	-0.2	-0.1	-0.3	-0.2	-0.2	-0.2	
Moderate	D	-0.6	-0.5	-0.7	-0.5	-0.8	-0.8	-0.4	
	E	-0.6	-0.5	-0.7	-0.5	-0.8	-0.8	-0.4	
Low	D	-0.7	-0.6	-0.5	-0.7	-0.6	-0.7	-0.4	
	E	-0.7	-0.6	-0.5	-0.7	-0.6	-0.7	-0.4	

Index modifiers for plan and vertical irregularities

Any type of plan irregularity is directly related to the characteristics of each individual building, and so it is somewhat difficult to obtain any index modifier that can precisely account for the effect of this phenomenon (ATC 2002b). Similar to the FEMA 155 approach,

plan irregularity modifiers (Table 2.8) are computed by first calculating an interim index using a 50% increase in the seismic demand of each seismic hazard level (Table 2.2) to take into account the effect of the increased seismic load due to this type of irregularity. The index modifier is then calculated based on the difference of this interim index and the SVIs in Table 2.6. The seismic design code level and soil class assumed are the same ones considered in the calculation of the original SVIs.

Table 2.8 Index modifiers for plan irregularities

Seismic hayard level	**Building Class**							
	WLF	WPB	SMF	SBF	SLF	SCW	SIW	CMF
High	-0.5	-0.8	-0.6	-0.7	-0.5	-0.6	-0.4	-0.6
Moderate	-0.8	-0.8	-0.7	-0.7	-0.6	-0.8	-0.7	-0.7
Low	-0.9	-0.9	-0.9	-0.8	-0.9	-0.9	-0.9	-0.9
	CSW	CIW	PCW	PCF	RML	RMC	URM	
High	-0.8	-0.4	-0.4	-0.7	-0.6	-0.6	-0.4	
Moderate	-0.8	-0.7	-0.9	-0.7	-0.8	-0.8	-0.5	
Low	-0.9	-0.9	-0.8	-0.9	-0.9	-0.9	-0.5	

Because of the large variety of factors that can cause vertical irregularity in a building, it is not easy to numerically quantify the effect of this type of irregularity on SVIs. Similar to the FEMA 154 and FEMA 155 methodology, these index modifiers are calculated based on the assumption that, were they the only modifiers to be considered in the evaluation process, the final index would be below the cutoff index (which will later be shown to be equal to 2'). The values of these irregularity modifiers are provided in Table 2.9.

Because of the minor risk in regions with low seismic hazard, the vertical irregularity modifiers are considered the same as for the moderate seismic hazard level regions, meaning that in regions with low seismic hazard, the vertical irregularity modifier does not solely result in a final index smaller than the cutoff index.

Table 2.9 Index modifiers for vertical irregularities

Seismic hazard level	**Building Class**							
	WLF	WPB	SMF	SBF	SLF	SCW	SIW	CMF
High	-1.4	-2.1	-0.9	-1.1	NA	-0.9	NA	-0.6
Moderate	-3.1	-3.5	-2.0	-2.2	NA	-2.0	-1.9	-1.6
Low	-5.5	-3.5	-2.0	-2.2	NA	-2.0	-1.9	-1.6
	CSW	CIW	PCW	PCF	RML	RMC	URM	
High	-1.0	NA	NA	-0.7	-0.7	-0.7	NA	
Moderate	-2.0	-1.5	NA	-1.7	-2.2	-2.3	-1.0	
Low	-2.0	-1.5	NA	-1.7	-2.2	-2.3	-1.0	

Note: NA, Not Applicable

Index modifier for design and construction date

These modifiers account for SVI variations attributable to different building design and construction dates than those assumed in the calculation of the SVIs. The criteria proposed in Table 2.5, which specify the assumed seismic code design levels for various time domains (post-1970, 1953-1970, and pre-1953), are used in the development of these index modifiers. Post-benchmark modifiers are calculated from the difference between an interim SVI for each seismic hazard level and the original SVI for each building class. The interim indices are calculated for buildings designed after the benchmark year (i.e., when provisions were revised and improved in the seismic code of Canada) using the application capacity and fragility curve data for the appropriate design level. The soil type used in these calculations is class C.

The methodology for the calculation of the pre-code design modifiers is similar to that mentioned above, but with just one exception: the pre-code modifiers do not apply for regions with low seismic hazard, where the design level considered in Table 2.5 is constant and independent of the construction year. The values calculated for these modifiers are provided in Tables 2.10 and 2.11.

Table 2.10 Index modifiers for post-benchmark buildings

Seismic hazard level	**Building Class**							
	WLF	WPB	SMF	SBF	SLF	SCW	SIW	CMF
High	0.7	1.4	1.4	1.1	0.1	1.0	NA	1.0
Moderate	0.0	0.7	0.8	0.8	0.6	1.0	NA	1.1
Low	0.0	0.7	0.4	0.5	0.4	0.5	0.5	0.4
	CSW	CIW	PCW	PCF	RML	RMC	URM	
High	0.6	NA	0.6	0.5	0.4	0.5	NA	
Moderate	1.2	NA	0.0	1.1	0.4	0.4	NA	
Low	0.3	0.6	1.2	0.2	0.8	0.7	0.8	

Note: NA, Not Applicable

Table 2.11 Index modifiers for pre-code buildings

Seismic hazard level	**Building Class**							
	WLF	WPB	SMF	SBF	SLF	SCW	SIW	CMF
High	0.0	-0.9	-0.7	-0.8	-0.6	-0.8	-0.2	-0.7
Moderate	0.0	-0.5	-0.3	-0.3	-0.3	-0.3	-0.2	-0.3
Low	NA	NA	NA	NA	NA	NA	NA	NA
	CSW	CIW	PCW	PCF	RML	RMC	URM	
High	-1.0	-0.2	-0.5	-0.9	-0.8	-0.8	-0.2	
Moderate	-0.3	-0.4	-0.7	-0.2	-0.5	-0.5	-0.4	
Low	NA	NA	NA	NA	NA	NA	NA	

Note: NA, Not Applicable

Index modifiers for mid-rise and high-rise buildings

Two sets of interim indices for each seismic hazard level, one for mid-rise and the other for high-rise buildings, are calculated from the capacity and fragility curves data (NIBS 2003) for midrise and high-rise buildings, respectively. The modifiers for mid-rise buildings are then computed by deducting the original SVIs obtained for low-rise structures from the interim indices calculated for mid-rise buildings. A similar procedure is used for high-rise buildings. The NBCC 2005 (NRCC 2005) reference soil class is considered in the calculations of the above interim indices. The results are shown in Table 2.12 and 2.13.

Table 2.12 Index modifiers for mid-rise buildings

Seismic hazard level	**Building Class**							
	WLF	WPB	SMF	SBF	SLF	SCW	SIW	CMF
High	NA	NA	0.5	0.3	NA	0.5	0.5	0.5
Moderate	NA	NA	0.3	0.1	NA	0.3	0.2	0.3
Low	NA	NA	-0.7	-0.5	NA	-0.3	-0.5	-0.4
	CSW	CIW	PCW	PCF	RML	RMC	URM	
High	0.2	0.4	NA	0.2	0.5	0.5	0.2	
Moderate	0.2	0.0	NA	0.2	0.0	0.0	0.6	
Low	-0.5	-0.4	NA	-0.6	-0.1	-0.3	1.0*	

NA: Not Applicable

*Modifier decreased from 1.9 to 1.0, based on judgment, to cause more buildings to have final indices less than 2.0

Table 2.13 Index modifiers for high-rise buildings

Seismic hazard level	**Building Class**							
	WLF	WPB	SMF	SBF	SLF	SCW	SIW	CMF
High	NA	NA	0.8	1.0	NA	0.9	1.0	0.9
Moderate	NA	NA	1.0	1.0	NA	0.7	0.6	0.9
Low	NA	NA	0.6	0.9	NA	0.0	-0.2	-0.2
	CSW	CIW	PCW	PCF	RML	RMC	URM	
High	0.7	0.7	NA	0.4	NA	0.7	NA	
Moderate	0.6	0.1	NA	0.3	NA	0.1	NA	
Low	-0.6	-0.7	NA	-0.7	NA	-0.4	NA	

NA: Not Applicable

2.6 Cutoff index

According to Equation 2.7, the SVI is proportional to the collapse probability of a building at a specific level of seismic hazard. Normally, a cutoff index determines whether further seismic evaluation is needed for that structure. The cutoff index for any region can be calculated by conducting a cost-benefit analysis that compares the costs of a detailed review with the benefits of increased seismic safety (ATC 2002b). As an example, Table 2.14 presents the building typology distribution of a city with a high seismic hazard, a population of 10 000, and a building inventory of 3000 structures. Based on the SVIs calculated for

different building classes in Table 2.6, the approximate number of buildings expected to collapse is computed assuming that no index modifier is applicable. It can be seen that the total number of the buildings to collapse is 32, which is about 1.06% of the building inventory. This represents an index of 1.97 according to the definition of the SVI in Equation 2.7.

$$- \mathrm{Log}_{10}[1.06\%] = 1.97 \tag{2.8}$$

Table 2.14 Example 1 building inventory used to evaluate the cutoff index

Building Class	**No. of Buildings**	**SVI**	**Probability of Collapse**	**No. of buildings expected to collapse**
URM	1320	1.8	0.0158	21
SCW	300	2.8	0.00158	0
SIW	900	2.1	0.00794	7
CIW	240	1.8	0.0158	4
WLF	240	3.3	0.000501	0
Total :	3000			32

Note: SVI, structural vulnerability index

This example is repeated for another region with high seismic hazard but a different building inventory of 2500 buildings (Table 2.15). It is observed that the total number of the buildings to collapse will be 13, which represents an index of 2.3 in this case.

Ideally, each community should give some thought to the costs and benefits associated with seismic safety, and then decide what cutoff index is appropriate for their particular situation. According to the above explanation, for the province of Quebec, a cutoff index equal to 2 can be considered acceptable for all building classes at this time. An SVI of 2 represents a 1% probability of collapse, given the considered level of seismic hazard for the area.

Table 2.15 Example 2 building inventory used to evaluate the cutoff index

Building Class	No. of Buildings	SVI	Probability of Collapse	No. of buildings expected to collapse
URM	700	1.8	0.0158	11
CMF	175	2.5	0.00316	1
WLF	1625	3.3	0.000501	1
Total :	2500			13

Note: SVI, structural vulnerability index

2.7 Discussion of the SVI scores

The differences between the indices obtained here (Table 2.6) and the scores presented in the latest edition of FEMA 154 demonstrate the effect of the seismic demand modification on SVI scores (Figures 2.7, 2.8, and 2.9). It should be noted that although different assumptions are made in the calculation of these indices in some cases (i.e., the assumption for the reference soil), the calculated indices show a trend similar to that seen with the FEMA 154 scores.

For region with high seismic hazard, the indices developed for Quebec are close to the FEMA 154 scores, except in the case of light wood frame buildings (WLF). This is a result of a difference in the seismic demand spectrum shape as shown in Figure 2.10. The shape of the spectrum for regions with high seismic hazard in Quebec in comparison with the one for the spectrum of FEMA 154 results in a higher performance point for the case in Quebec which leads to a higher vulnerability index. The same explanation applies to the differences found between the indices calculated for the URM building class in regions with moderate and low seismic hazard in Quebec and the equivalent indices calculated in FEMA 154. For the moderate and low seismic hazard regions in Quebec, FEMA 154 scores are generally smaller than indices developed in this research. According to Equation 2.7, this means that the performance points in FEMA models have generally larger values than the performance point values here.

A comparison of Figures 2.7 through 2.9 shows that for most of the building classes, the differences between the indices developed in this chapter and the basic structural hazard scores of FEMA 154 decrease when the seismic hazard level increases. Therefore, for regions with higher seismic hazard levels, the shape of the capacity curve could become an important factor in calculating the performance point in the capacity spectrum method. In other words, capacity (and consequently the fragility) curves which are developed based on the regional structural properties for common building classes in an area should be used in the process of calculating such indices.

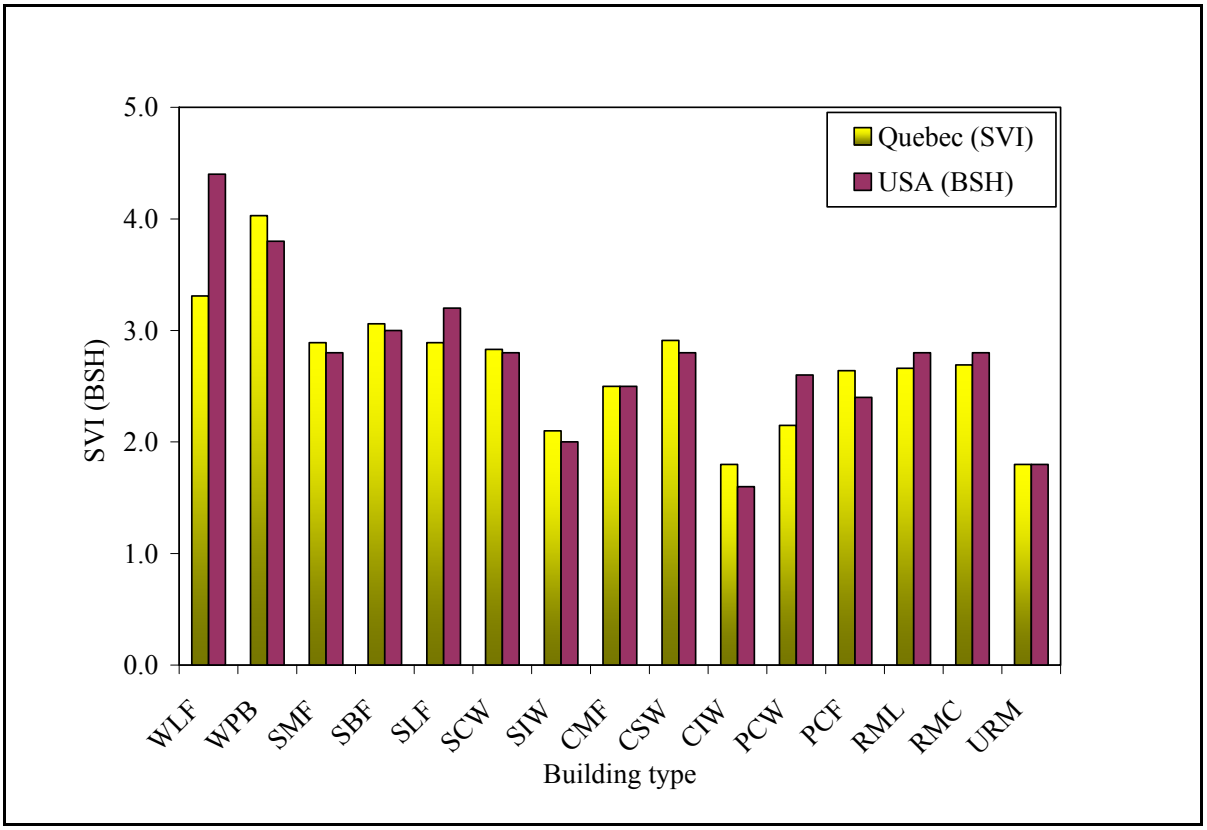

Figure 2.7 Comparison of the seismic vulnerability indices (SVI) in Quebec and the basic structural hazard (BSH) scores in the USA, in regions with high seismic hazard.

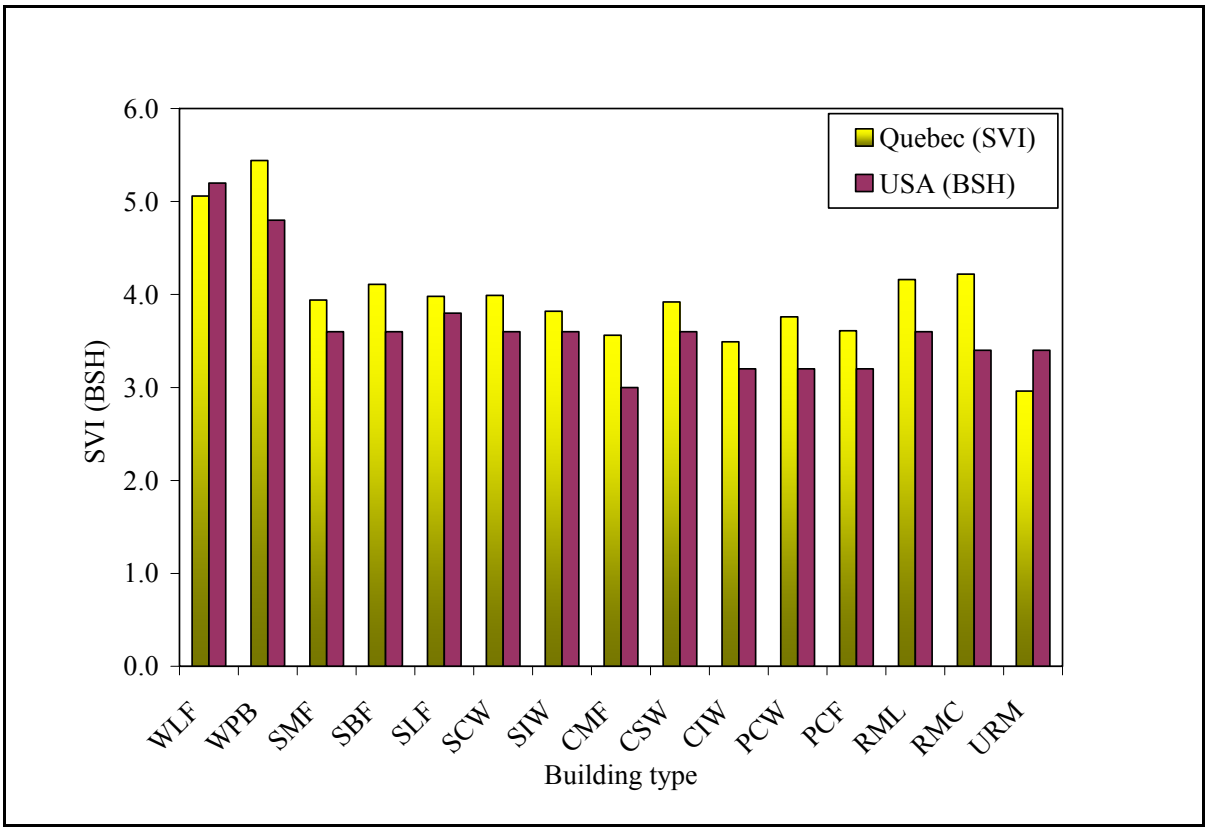

Figure 2.8 Comparison of the seismic vulnerability indices (SVI) in Quebec and the basic structural hazard (BSH) scores in the USA, in regions with moderate seismic hazard.

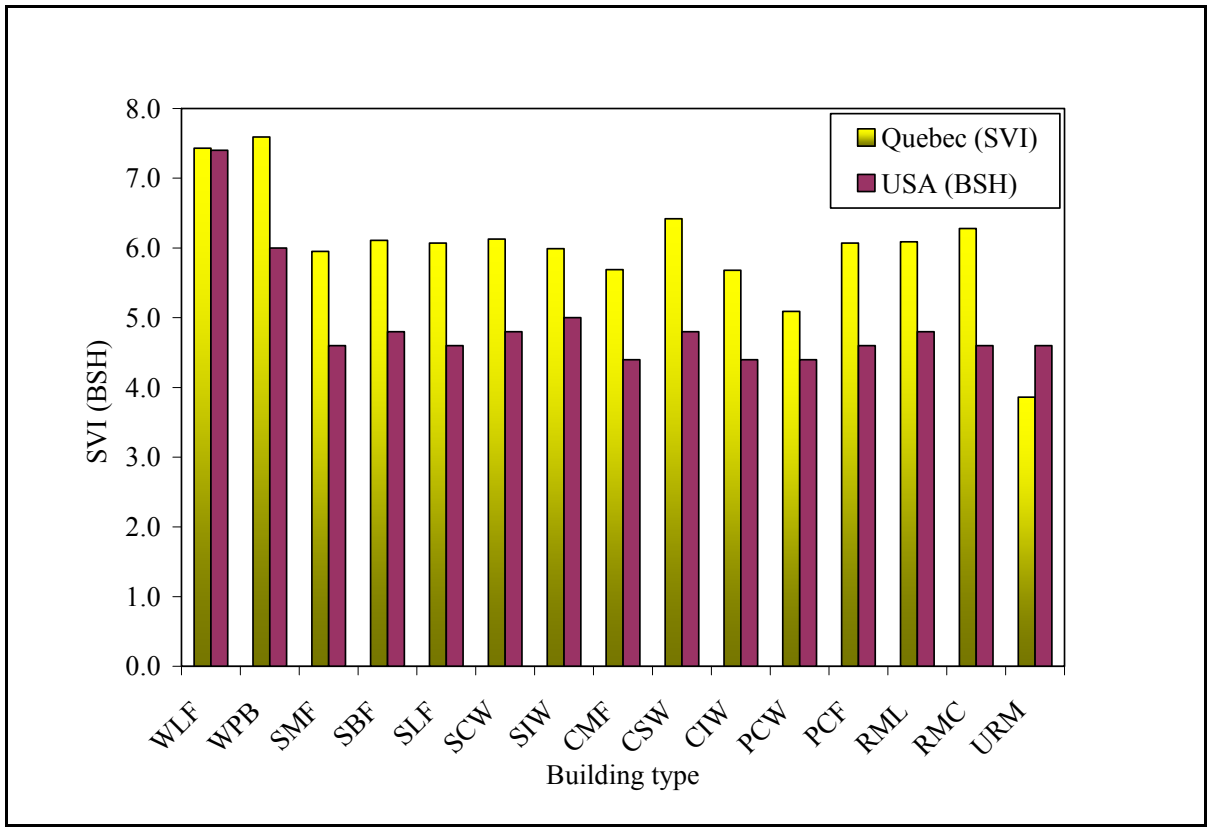

Figure 2.9 Comparison of the seismic vulnerability indices (SVI) in Quebec and the basic structural hazard (BSH) scores in the USA, in regions with low seismic hazard.

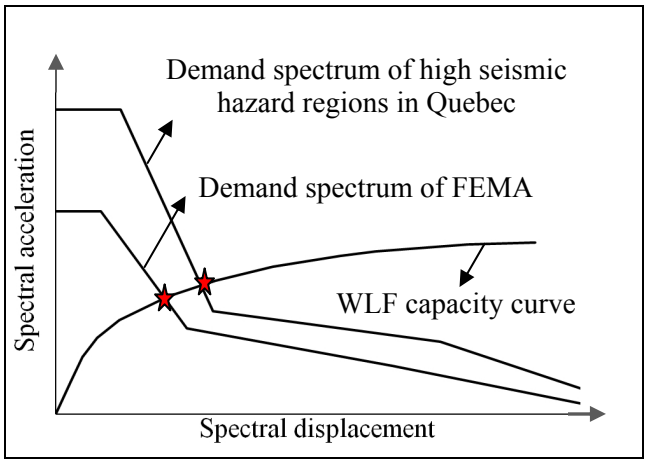

Figure 2.10 Graphical illustration of the spectrum shape effect on the calculation of the performance point for WLF class.

2.8 Application of proposed procedure

The adapted RVS method proposed in this chapter can be used to pursue two objectives: (i) establishment of a priority list for buildings in view of a more detailed evaluation and (ii) estimation of the damage distribution for a large population of buildings. To ascertain the applicability of the proposed method in establishing priorities, the result of a recent comprehensive study of a group of buildings in Quebec City using the proposed RVS method is compared with results obtained using the current Canadian procedure (NRC-IRC 1992) on the same building population. Building information was gathered through the review of available documentation (drawings and reports) and on-site visual inspections of the 106 buildings included in the study. The seismic soil class was obtained from the microzonation maps of the Quebec City area (LeBoeuf and Nollet 2006).

It is observed that for all structures considered "critical" according to the current Canadian procedure, the final index determined using the proposed procedure is below 1.9 (15% of the buildings). There are some constructions with a final index below 2.0 that obtained a "high" or "moderate" priority label using the Canadian procedure (8% and 11%, respectively). Seventy-eight percent of the buildings that had final indices above 2.5 were considered to be low priority in terms of the need for further study, based on the current Canadian procedure.

If an SVI lower than 2.0 is considered equivalent to the "critical" and "high" categories of the current Canadian procedure, the developed procedure turns out to be more sensitive in determining which buildings need further evaluation (49% versus 26%). This can be explained by a number of factors:

5. The seismic priority index (SPI) indicates if the structure is in conformity with the seismic provision of the 1990 NBCC (NRCC 1990), while the final indices of the developed RVS method is an indication of the probability of collapse.

6. In the developed RVS method, the index modifiers for vertical irregularity have been calculated assuming that, if these irregularities were the only modifiers to be considered in the evaluation process, the final index would be below the cutoff.

7. Consideration of site effect (soil class) is observed to have a more significant effect on indices calculated using the developed RVS method than those obtained using the current Canadian procedure.

Both methods offer the possibility of ranking the buildings according to structural seismic vulnerability; however, only the adapted RVS method can lead to a damage probability distribution of building groups in the region. Based on the building type distribution in the Quebec City project (Figure 2.11), and similar to the examples presented in the cutoff index section, the distribution of the collapse probability for the different building classes can be seen in Figure 2.12.

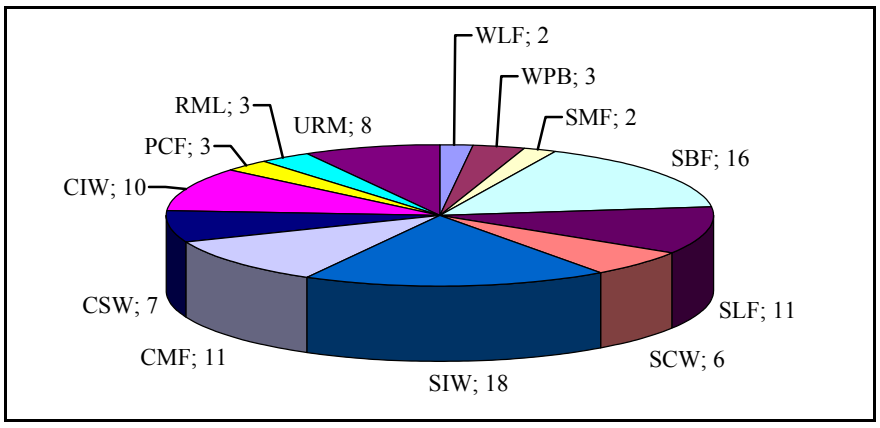

Figure 2.11 Distribution of building types in the Quebec City project.

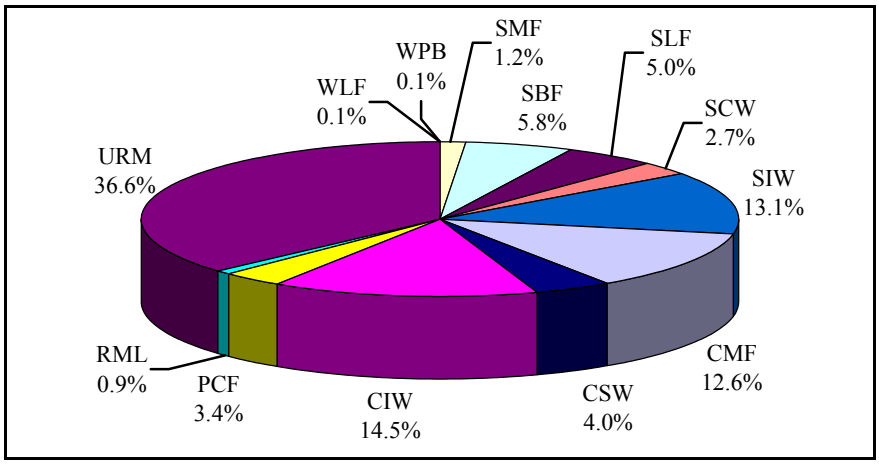

Figure 2.12 Distribution of collapse probability among existing building types in a damage scenario in the Quebec City project.

It should be noted that Fig. 2.12 shows the contribution of the different building types in a damage scenario given the seismic demand considered (spectral acceleration values for regions with moderate seismic hazard in Quebec).

2.9 Summary

A score assignment method for the seismic vulnerability evaluation of a group of buildings in old sectors of Quebec was developed in this chapter. The methodology is adapted to the seismic demand in the province in the form of the spectral acceleration response values of the National building code of Canada (NRCC 2005). Considering that most of the building classes observed in the old sectors of the province—exceptions are masonry structures—can be represented by the current Canadian building typology (NRC-IRC 1992) or the ones available in FEMA 154 (ATC 2002a), the available building classification in (NRC-IRC 1992) and the capacity and fragility curves presented in NIBS (2003) were used in the procedure of calculating the indices for a new rapid visual screening method.

CHAPTER 3

PERFORMANCE-BASED SEISMIC VULNERABILITY EVALUATION OF BUILDINGS WITH MASONRY IN QUEBEC: STRUCTURAL ANALYSE STAGE

3.1 Introduction

The purpose of this chapter is to present a complete approach to the development of dynamic capacity and fragility curves for two of the building classes in Table 1.5: (1) unreinforced brick masonry buildings with wood floors (URMW) which represent the structures in the old industrial sectors at the beginning of the century, and (2) RC frames with unreinforced masonry infill walls (CIW) which used to be a very popular building type between 1930 and 1950.

3.2 Description of the studied buildings

The unreinforced brick masonry construction is used widely in old sectors of the province. Because of the common vulnerability of masonry to resist lateral loads, this building class is selected for further studies in this research work. RC frames with unreinforced masonry infill walls, on the other hand, were used as a very common construction in Quebec before the official regulation for seismic-resistant design of buildings in Canada in historical sectors of Montreal and other cities in the province. Adequate knowledge of the dynamic behaviour is required to assess the seismic vulnerability of those structures and to reduce loss to lives and properties associated with possible structural failures. This building class has been the subject of many researches due to the complexity of the infill walls effects on the overall dynamic behaviour of this building class. For this reason, a typical building from this class is studied later in this chapter.

3.2.1 First studied building: unreinforced brick masonry (URMW)

The studied building in this section is a masonry building which typifies the industrial structures built in the beginning of the century in Eastern Canada (Lefebvre 2004). Figure 3.1 shows a view of such a building with window openings on the two adjacent faces.

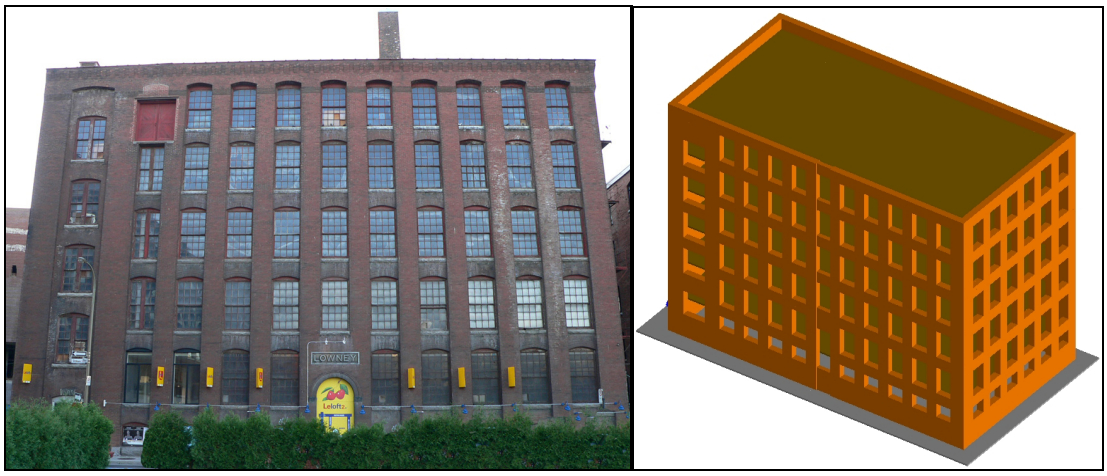

Figure 3.1 Three-dimensional views of the unreinforced masonry structure.

The structural characteristics of the building are shown in Table 3.1, and the material properties used in the dynamic analysis of this chapter are indicated in Table 3.2. These properties are chosen based on a literature review of buildings with masonry construction in Eastern Canada and especially in Quebec (Canadian Standards Association 2004; Beaulieu 2006; Nollet et al. 2009).

Table 3.1 Structural characteristics of the building shown in Figure 3.1

	URMW building
Number of stories	6
Year of construction	1905
Structural system	Columns and beams of steel and wood
Lateral load Resisting system	Exterior masonry walls
Floor material	Wood
1st mode period (longer dir.)	T= 0.38 sec.
1st mode period (shorter dir.)	T= 0.69 sec.

Table 3.2 Material properties used in the Incremental Dynamic Analyses

	Brick	**Mortar**
Modulus of elasticity (GPa)	14	0.5
Compression strength (MPa)	10	1.0
Tensile strength (MPa)	1.0	0.5
Density (KN/m^3)	18	15

3.2.2 Second studied building: RC frame with unreinforced masonry infill walls (CIW)

The structural model for the concrete frame building in this study is constructed based on the typical geometrical properties of this building class in Quebec (Lefebvre and Nollet 2009). A 3-D view of the building is shown in Figure 3.2.

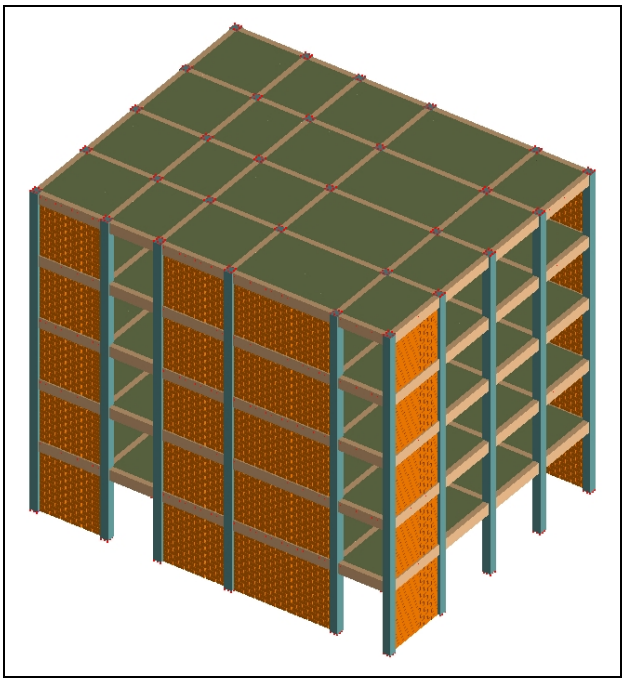

Figure 3.2 Three-dimensional views of the RC frame with unreinforced masonry infill walls.

The structural characteristics of this building are shown in Table 3.3. The material properties for the concrete used in the dynamic analysis of this section, on the other hand, are shown in Table 3.4.

Table 3.3 Structural characteristics of the building shown in Figure 3.2

	CIW building
Number of stories	5
Year of construction	1930-1950
Structural system	Concrete columns and beams
Lateral load Resisting system	Moment resisting joints and infill walls
Floor material	Concrete
1st mode period (longer dir.)	T= 0.29 sec.
1st mode period (shorter dir.)	T= 0.37 sec.

These properties are chosen based on a literature review of buildings with concrete frame with masonry in-fills construction in Eastern Canada and especially in Quebec (Gauthier 1976; Biddah 1997; Arrien and Lemyre 2003). For masonry, the same properties indicated in Table 3.2 are applied.

Table 3.4 Properties used for the concrete in the Incremental Dynamic Analyses

	Concrete
Modulus of elasticity (GPa)	23.2
Compression strength (MPa)	21
Density (KN/m^3)	23.6

3.3 Analytical modeling

3.3.1 Application of the Applied Element Method for Masonry

To apply the AEM method (explained in section 1.7.3) for masonry, two types of springs are needed to represent bricks and the brick-mortar interaction. The values of stiffness for springs which model forces and displacements in bricks are calculated from Equation 1.10 as they connect elements of identical materials. For brick-mortar springs, however, the equivalent values for normal and shear stiffness (Kn_{eq} and Ks_{eq}) are calculated based on a series-system of springs shown in Figure 3.3. The equivalent stiffness is therefore calculated as follows.

$$\frac{1}{Kn_{eq.}} = \frac{d - t_m}{E_b \times a \times t} + \frac{t_m}{E_m \times a \times t}, \tag{3.1}$$

and

$$\frac{1}{Ks_{eq.}} = \frac{d - t_m}{G_b \times a \times t} + \frac{t_m}{G_m \times a \times t} \tag{3.2}$$

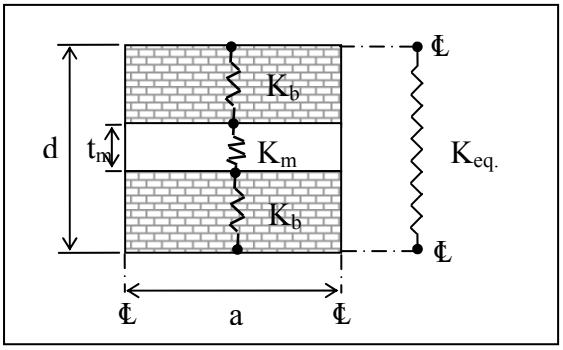

Figure 3.3 Modeling masonry in AEM.

Where E_b, G_b, E_m, and G_m are the brick and mortar Young's and shear modulus, respectively. On the other hand, t and t_m are the element and mortar thicknesses. Referring to Figure 1.6, we observe that failure modes 1 and 2, which are joint de-bonding and unit sliding along bed or head joints, should be reflected in brick-mortar springs and failure mode 3, defined as units cracking under direct tension, has to be modeled with brick springs.

Three degrees of freedom are assumed for each element, one for rotation and two for translation in X and Y directions. Since internal deformations are represented by the springs, the assembly of elements is deformable, in spite of the fact that an element's shape remains unchanged during the analysis. The elements in Figure 1.8 are connected by one pair of normal and shear springs at a general point. The components of the 6×6 stiffness matrix is determined by calculating the forces required at the centroid of each element to restrain all other degrees of freedom, and to satisfy equilibrium conditions against the unit displacement at the corresponding degree of freedom. Equation 3.3 shows the components of the upper left quarter of the stiffness matrix; for masonry, Kn_{eq} and Ks_{eq} are calculated from Equations 3.1 and 3.2. Other parameters in Equation 3.3 are shown in Figure 1.8. As seen in this equation, the matrix components depend on the spring's stiffness and the contact point location. It should be noted that Equation 3.3 presents the stiffness matrix for a case in which only one pair of springs exists between the two elements. However, the global stiffness matrix is determined by combining the stiffness matrices of all the individual spring pairs around the element.

$$K_{3\times3}=\left[\begin{array}{l|l|l} Sin^2(\alpha+\gamma)Kn_{eq} & -Kn_{eq}Sin(\alpha+\gamma)Cos(\alpha+\gamma) & Cos(\alpha+\gamma)Ks_{eq}D_LSin(\gamma) \\ +Cos^2(\alpha+\gamma)Ks_{eq} & +Ks_{eq}Sin(\alpha+\gamma)Cos(\alpha+\gamma) & -Sin(\alpha+\gamma)Kn_{eq}D_LCos(\gamma) \\ \hline -Kn_{eq}Sin(\alpha+\gamma)Cos(\alpha+\gamma) & Sin^2(\alpha+\gamma)Ks_{eq} & Cos(\alpha+\gamma)Kn_{eq}D_LCos(\gamma) \\ +Ks_{eq}Sin(\alpha+\gamma)Cos(\alpha+\gamma) & +Cos^2(\alpha+\gamma)Kn_{eq} & +Sin(\alpha+\gamma)Ks_{eq}D_LCos(\gamma) \\ \hline Cos(\alpha+\gamma)Ks_{eq}D_LSin(\gamma) & Cos(\alpha+\gamma)Kn_{eq}D_LCos(\gamma) & D_L{}^2Cos^2(\gamma)Kn_{eq} \\ -Sin(\alpha+\gamma)Kn_{eq}D_LCos(\gamma) & +Sin(\alpha+\gamma)Ks_{eq}D_LCos(\gamma) & +D_L{}^2Sin^2(\gamma)Ks_{eq} \end{array}\right] \quad (3.3)$$

3.3.2 Application of AEM in the Incremental Dynamic Analysis

In a performance base seismic evaluation (PBSE) process, the calculated responses are sensitive to the characteristics of the individual ground motion used as the seismic input. Therefore, different ground motion records are required to obtain a good estimation of the building's responses. To this end, the Incremental Dynamic Analysis (IDA) is shown to be an effective tool for thoroughly examining the structural performance of buildings under seismic loads (Christovasilis, Filiatrault et al. 2009; Lagaros 2009). An IDA involves subjecting a structural model to various ground motion records, each scaled to multiple levels of intensity up to the point at which a limit state is reached (Vamvatsikos and Cornell 2002). The approach has the potential to demonstrate the variation of structural responses, as measured by a damage measure (DM, e.g., inter-storey drift), versus the ground motion intensity level, measured by an intensity measure (IM, e.g., peak ground acceleration or the first-mode spectral acceleration). In other words, the IDA procedure provides dynamic capacity curves for different ground motion levels.

To apply the Applied Element Method in the IDA procedure, large deformations of an element under dynamic loads are calculated by the following general dynamic equation of motion (Tagel-Din and Meguro 2000).

$$[M][\Delta U'']+[C][\Delta U']+[K][\Delta U]=\Delta f(t)+R_m+R_G \quad (3.4)$$

In Equation 3.4, *[M]* is the mass, *[C]* is the damping, and *[K]* is the stiffness matrix. Moreover, $\Delta f(t)$ is the incremental applied load vector, $[\Delta U]$ is the incremental displacement

vectors, and $[\Delta U']$ and $[\Delta U'']$ are the incremental velocity and acceleration vectors, respectively. The vector R_m in Equation 3.4 stands for the residual forces caused by cracking, or the incompatibility between strains and stresses at the spring location due the nonlinear behaviour of materials. The vector R_G, on the other hand, represents the residual forces caused by geometrical changes of the structure during loading. In this regard, the AEM has an advantage over the FEM noting that the latter considers the redistribution of internal forces resulting from geometrical changes by adopting a geometrical stiffness matrix. The nonlinear material behavior in the AEM is taken into account in calculating [K] and $R_{m.}$ The reader is referred to (Tagel-Din and Meguro 2000) for more information regarding the solution process of Equation 3.4, the Eigen value analysis, and the methodology to calculate the displacement of elements.

3.4 Structural analysis stage for the URMW building

A total number of 5 springs is used on each face of the elements in the Applied Element Model for the URMW building. The size of the meshing is picked in a way to avoid creating elements with large aspect ratios. Therefore, an approximate number of 10'000 elements are used for this building. The floors are modeled as wood elements (semi-rigid). However, as they are of less interest, in comparison to the masonry walls, beams, and columns in this study, a bigger meshing size is chosen for them.

3.4.1 Time-history analysis of the building: selection of Accelograms

Although it is possible to utilize a single record in an IDA procedure, it is essential to consider variations in ground motion content when utilizing IDA in a performance-based assessment. For this reason, the selection of ground motion records that takes into consideration site characteristics and source mechanisms is critical. Previous studies show that 10 to 20 records are sufficient to predict, with acceptable accuracy, the seismic demand of a mid-rise building (Shome et al. 1998). Therefore, the time-history analyses of this chapter have been carried out using a set of 14 synthetic and historic ground motion records. The synthetic ground motions considered in this study belong to three M and R categories

chosen based on seismic hazard de-aggregation of Eastern Canada (Halchuk et al. 2007) which determine the dominant earthquakes contributing to spectral acceleration values of a site. For each category, four sets of ground motions have been developed with identical durations (Atkinson and Beresnev 1998). The historic ground motion records used, on the other hand, include the data from the Saguenay[1] (1988) and Nahanni[2] (1985) earthquakes. Table 3.5 shows the characteristics of each set of these ground motion records. Figure 3.4 to Figure 3.7 illustrate examples of these ground motion records along with their spectral acceleration curves.

Table 3.5 Characteristics of records used in the Incremental Dynamic Analyses

		M	**R (km)**	**Duration (sec.)**	**Time step (sec.)**	**PGA (g)**	***Site***
Categ. 1	Set1	6.0	30	8.8	0.01	0.43	-
	Set2	6.0	30	8.8	0.01	0.52	-
	Set3	6.0	30	8.8	0.01	0.47	-
	Set4	6.0	30	8.8	0.01	0.44	-
Categ. 2	Set1	7.0	70	24.0	0.01	0.30	-
	Set2	7.0	70	24.0	0.01	0.29	-
	Set3	7.0	70	24.0	0.01	0.34	-
	Set4	7.0	70	24.0	0.01	0.29	-
Categ. 3	Set1	7.0	20	15.2	0.01	1.71	-
	Set2	7.0	20	15.2	0.01	1.69	-
	Set3	7.0	20	15.2	0.01	1.93	-
	Set4	7.0	20	15.2	0.01	1.62	-
Historic EarthQ.	Saguenay (1988)	5.9*	-	17.7	0.005	0.12	*S7 (Baie-St-Paul)*
	Nahanni (1985)	*6.8**	-	*9.8*	*0.005*	*0.07*	*S3 (Battlement Creek)*

* Moment magnitude

[1] http://earthquakescanada.nrcan.gc.ca/historic_eq/20th/saguenay88/saguenay88_e.php

[2] http://earthquakescanada.nrcan.gc.ca/historic_eq/20th/nahanni/nahanni85_e.php

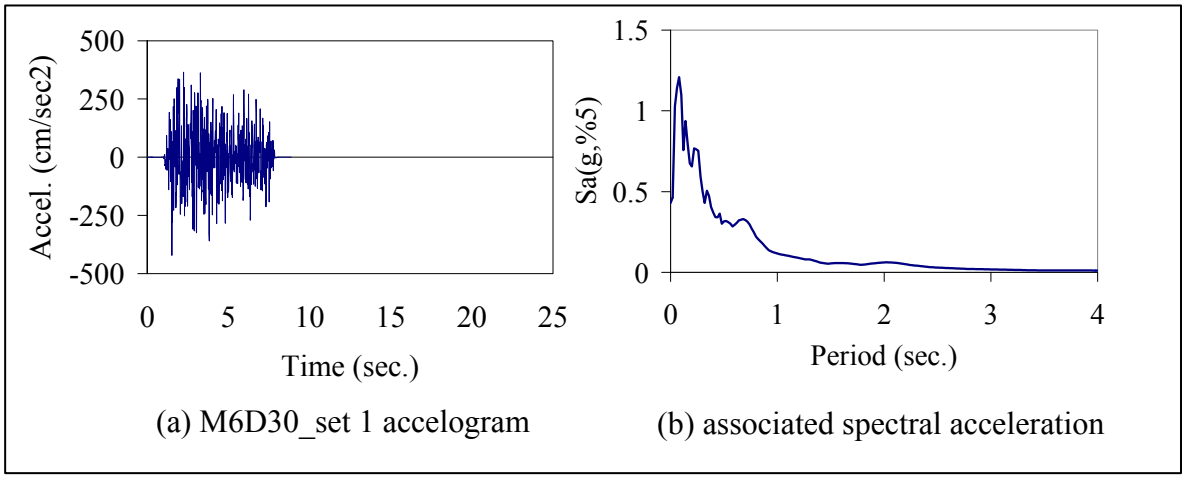

Figure 3.4 M6D30 set 1 time-history record used in the IDA of the URMW.

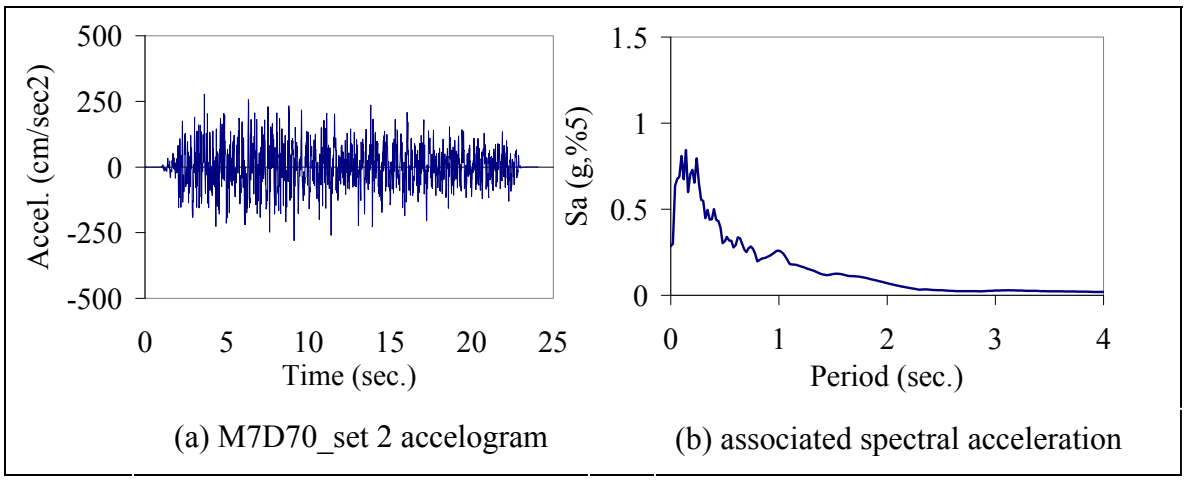

Figure 3.5 M7D70 set 2 time-history record used in the IDA of the URMW.

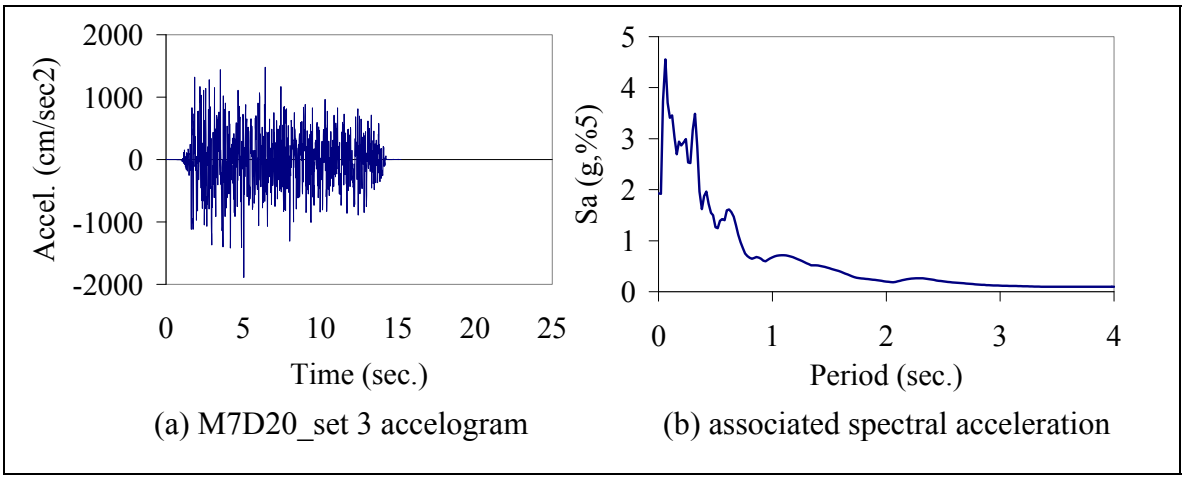

(a) M7D20_set 3 accelogram (b) associated spectral acceleration

Figure 3.6 M7D20 set 3 time-history record used in the IDA of the URMW.

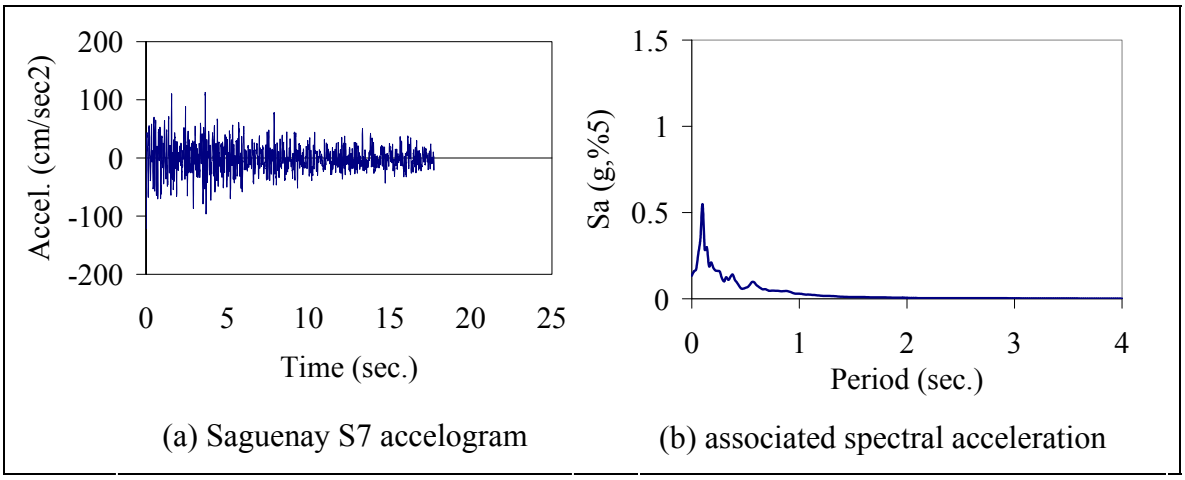

(a) Saguenay S7 accelogram (b) associated spectral acceleration

Figure 3.7 Saguenay S7 time-history record used in the IDA of the URMW.

Studies show that scaling records to a specific value within each category, e.g. the bin-median spectral acceleration, reduces the dispersion of nonlinear responses without affecting the median estimates of most measures of nonlinear behaviour (Shome et al. 1998). The same reference states that this scaling also decreases the response dependency to M and R given a specific S_a intensity. The bias in estimating structural responses and the number of required records are also shown to decrease significantly when records are scaled to match a target spectrum over a range of periods (Hancock et al. 2008).

The selected ground motion records used for the time history analyses have to be compatible with the seismic hazard of the building's site. Considering that one objective of this study is to assess the seismic performance of masonry buildings in Quebec (but not at any specific location), the ground motion records of Table 3.5 are scaled to a target spectrum (Table 3.6), in the frequency domain, that represents the spectral acceleration medians of regions with a high seismic hazard in Quebec, as defined in Table 2.2. By matching those accelograms to such a target spectrum, we also aim to avoid the bias reported in the structural responses (Baker and Cornell 2006) when the accelograms are magnified by big scaling factors in the incremental dynamic analysis, to push the structure to enter its nonlinear range.

The scaling process starts with calculating the spectral acceleration values of each accelogram in Table 3.5. Next, the calculated spectral acceleration values at different periods are matched to the target spectrum within 3 iterations in the frequency domain. In this way, the frequency content of each ground motion record does not change. Finally, an inverse Fourier Transform is applied to calculate the associated ground motion records. Figure 3.8 shows the matched spectral acceleration values of the 14 accelograms. The matching results in 14 sets of accelograms that are then used in the IDA of a masonry building.

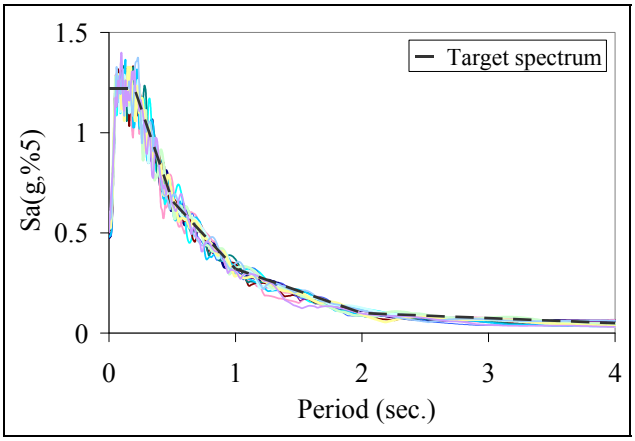

Figure 3.8 5%-damped elastic response from records in Table 3.3 matched to the target spectrum.

Table 3.6 Spectral acceleration values of the target spectrum at different periods

T (sec.)	0.2	0.5	1.0	0.2
S_a (T)	1.22	0.66	0.32	0.10

3.4.2 Application of the Incremental Dynamic Analysis

The application of the IDA method for the masonry building helps us to calculate displacements thoroughly, and to observe collapse progress under seismic loads. For the first-mode-dominated masonry building shown in Figure 3.1, the spectral acceleration value at the first-mode period is selected as the intensity measure (IM) for the IDA because the structure is sensitive to the power of the frequency content near the first-mode. In this way, no extra energy is imposed on the structure as a result of increasing the intensity of the ground motion records in the Incremental Dynamic Analysis. The inter-storey drift (ISD), on the other hand, is picked as the damage measure (DM) because it relates well to joint rotations and the storey local and global collapse (Vamvatsikos and Cornell 2002).

To assess the masonry building's strength in both directions, the IDA curves are developed for both longer and shorter directions, separately. In other words, the structure is assumed as two systems with different first modes of vibration, T_1= 0.69 sec. and 0.38 sec. in the shorter and longer directions, respectively. Overall, 308 time-history analyses have been carried out, on an analytical model which consists of about 10000 elements, using the Extreme Loading® for Structures (Applied Science International 2007) which is a AEM-based software. Verifications of the application of this tool for the nonlinear analysis of masonry and concrete structures are presented in Appendix II.

Each of the 14 ground motions presented previously is scaled to multiple levels of intensity according to its spectral acceleration value at the building's first-mode period in each direction and the nonlinear dynamic analyses are carried out at each level of intensity using the Applied Element Method. The intensity measure is increased up to the point at which a small increase in that value results in a large increase in the damage measure (inter-storey

drift) or until complete collapse occurs in the analytical model. The results are shown in Figure 3.9 where the incremental dynamic analysis curves for the masonry building are illustrated in both the longer and shorter directions for all ground motions.

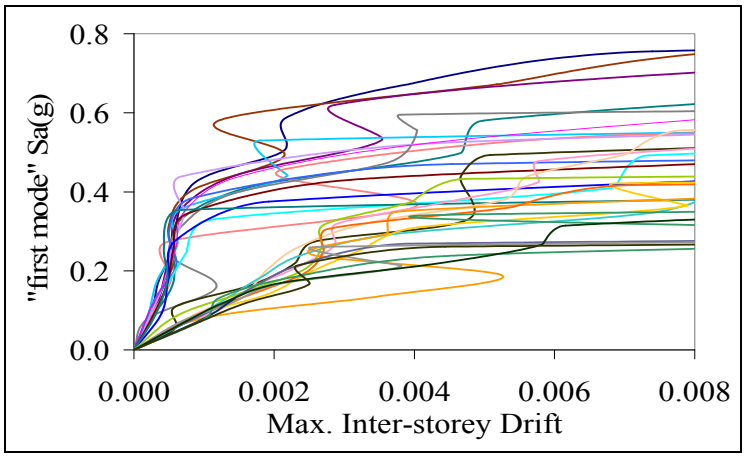

Figure 3.9 IDA curves for both the longer and shorter directions of the URMW building.

3.4.3 Distribution of structural performance levels

The next step toward the PBSE of the masonry building is to determine the limit states on the IDA curves shown in Figure 3.9. To conduct the seismic vulnerability evaluation with a performance-based approach, the three structural performance levels—Immediate Occupancy (IO), Life Safety (LS), and Collapse Prevention (CP)—defined in FEMA 356 (ASCE 2000) are used here. Table 3.7 presents the definition of each performance level for unreinforced masonry walls along with the typical inter-storey drift ratios for the in-plane behaviour (bed-joint sliding). These typical values are not used to determine the limit states here. Instead, in this research, the IO limit-state is set as the ultimate point in the elastic region where the structure's stiffness is almost the same as the elastic value, as shown in Figure 3.10. The CP limit-state, on the other hand, is defined as the point at which the building is on the verge of collapse, but still stable. However, any increase in the lateral force will produce instability in the system. Finally, The Life Safety limit state is determined as the point which represents three-fourth of the deformation capacity which is the Collapse Prevention level in this document (Abrams 2001).

Table 3.7 Definition of Structural Performance levels
taken from ASCE (2000)

Performance levels	**Description of damages**	**ASCE inter-storey drift ratio**	**Interpretation of DM in this study**
Immediate Occupancy (IO)	Minor cracking of veneers. Minor spalling in veneers at few corner openings. No observable out-of-plane offsets	0.1%	Ultimate point in the elastic region
Life Safety (LS)	Extensive cracking. Noticeable in-plane offsets of masonry and minor out-of-plane offsets	0.3%	Three-fourth of the deformation capacity
Collapse Prevention (CP)	Extensive cracking; face course and veneer may peel off. Noticeable in-plane and out-of-plane offsets	0.4%	The verge of collapse, but still stable

This means that the LS limit-state is chosen as the point where extensive cracking exists in the masonry walls but there is an acceptable safety margin to prevent collapse in the structure. Figure 3.11 to Figure 3.13 show the damage states at those performance levels in the masonry building subjected to Nahanni's ground motion record. In Figure 3.11 showing the Immediate Occupancy level, minor cracks are seen in the masonry walls around the structure. These cracks, however, have not yet affected the lateral strength of the building. At the Life Safety level, noticeable cracks are seen in one corner of the building in Figure 3.12. The wood slab is also detached from the masonry wall in few places. In the Collapse Prevention level, significant cracks are formed all around the masonry wall in Figure 3.13. The slabs are almost detached from the wall. As a result, the building is on the verge of collapse, but still stable. Based on the interpretation of the damage measures in Table 3.7, the DM and IM values at each performance level are calculated for each ground motion record, and presented in Chapter 3.

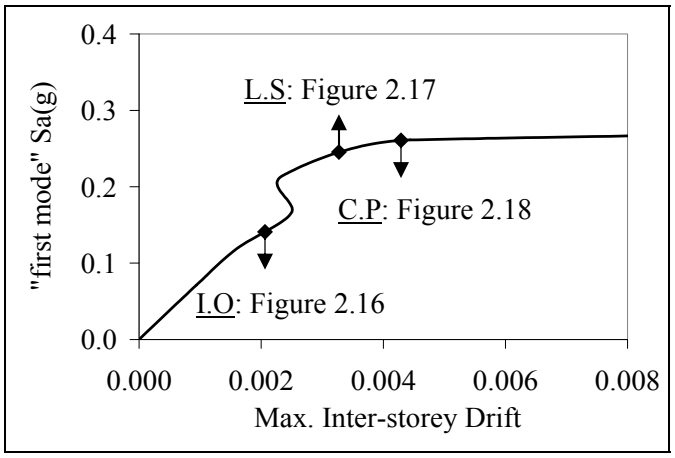

Figure 3.10 IDA curve of the URMW building in the shorter direction for Nahanni ground motion.

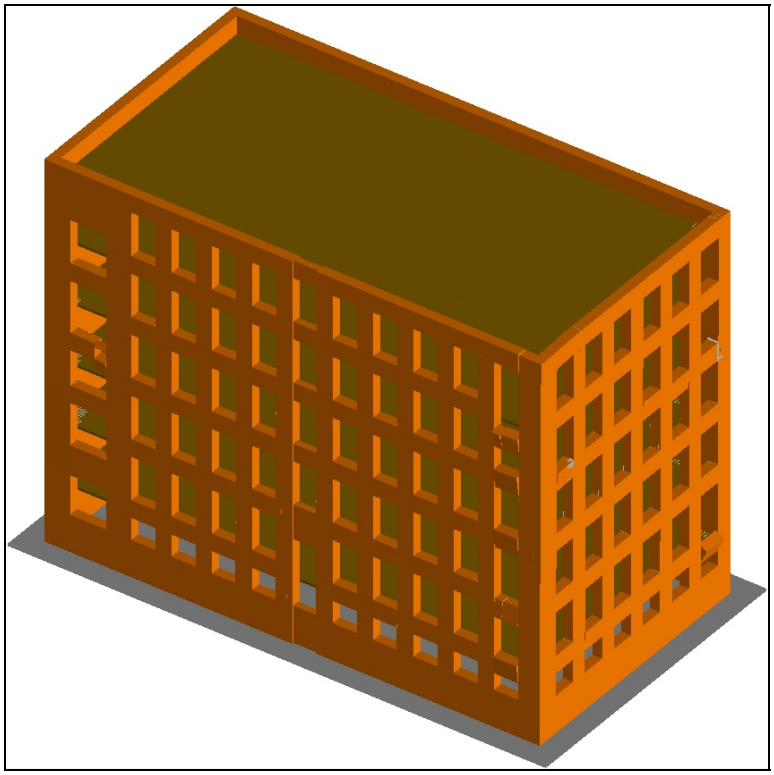

Figure 3.11 URMW building at Immediate Occupancy level for Nahanni S3-EN1 ground motion record.

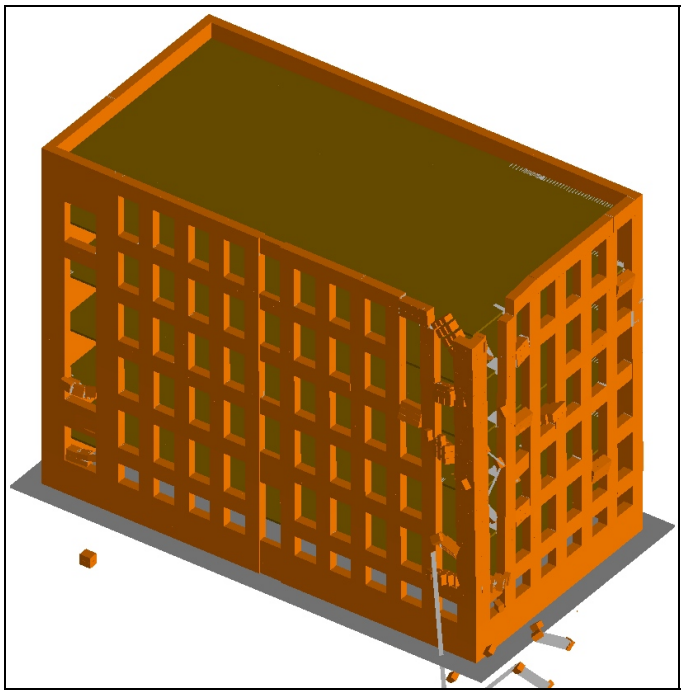

Figure 3.12 URMW building at Life Safety level for Nahanni S3-EN1 ground motion record.

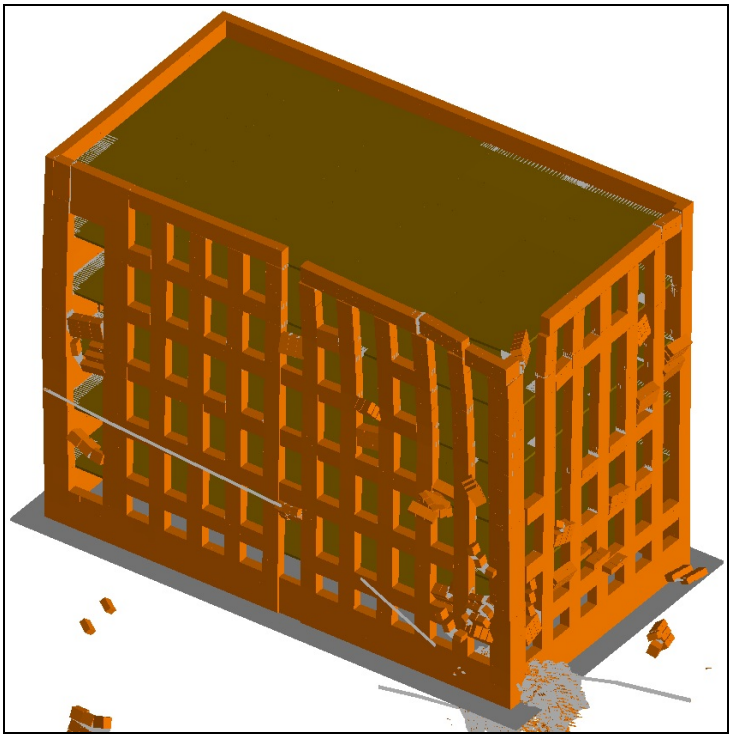

Figure 3.13 URMW building at Collapse Prevention level for Nahanni S3-EN1 ground motion record.

3.5 Structural analysis stage for the CIW building

The same number of springs per element face (five) is used in the Applied Element Model for the CIW building. The size of the meshing is again picked in a way to avoid creating elements with large aspect ratios in the beams, columns, and masonry infill walls. Therefore, an approximate number of 12'000 elements are used for this building. The RC floors were modeled as rigid slabs with bigger meshing size in comparison to the other structural elements in the building. The perfect way to model the masonry infill walls would be to connect the masonry and the concrete frame with a gap through which only friction forces keep the masonry inside the frame. As such precise detailing is not possible, the masonry bricks are attached to the concrete elements through springs which have combined properties from both materials (Mayorca and Megura 2003).

3.5.1 Time-history analysis of the building: selection of Accelograms

At the time of this part of the research, synthetic ground motions compatible with the 2005 *National building code of Canada* (NRCC 2005) uniform hazard spectrum became available (Atkinson 2009). Unlike the synthetic ground motions used for the dynamic analysis of the masonry building in the previous section which could only be used to conduct one-directional structural analysis, these recent ground motions can be used to simulate bi-directional seismic loads (as a real earthquake) on the structural model. Therefore, in this section, full 3D Incremental dynamic Analyses are performed to develop the dynamic capacity and fragility curves for the concrete frame building with unreinforced masonry infill walls.

To select the ground motion records for the Incremental Dynamic Analyses from (Atkinson 2009), the spectral acceleration data of the ground motion records for three of the earthquake scenarios (M6 at 20-30 km, M7 at 15-25 km, and M7 at 50-100 km) were compared with the target spectrum presented in Table 3.6 (Figure 3.14 to Figure 3.16). According to the instruction provided in that reference, for each ground motion, the mean of the fraction

($S_{a\ target}/S_{a\ record}$)—over a range of period from 0.1 to 0.5 sec. for M6 scenarios and from 0.5 to 2 sec. for M7 ones—were calculated. Out of the 45 ground motion records in each scenario, those sets which have a mean of the fraction ($S_{a\ target}/S_{a\ record}$) in the approximate range from 0.5 to 2.5 and the lowest standard deviation values, were selected (Table 3.8). Later, each selected set was scaled to its own ($S_{a\ target}/S_{a\ record}$) ratio, according to the instructions in Atkinson (2009). Each two sets then formed a group which are used as the two perpendicular components of the earthquake scenario in the dynamic analysis of the CIW building.

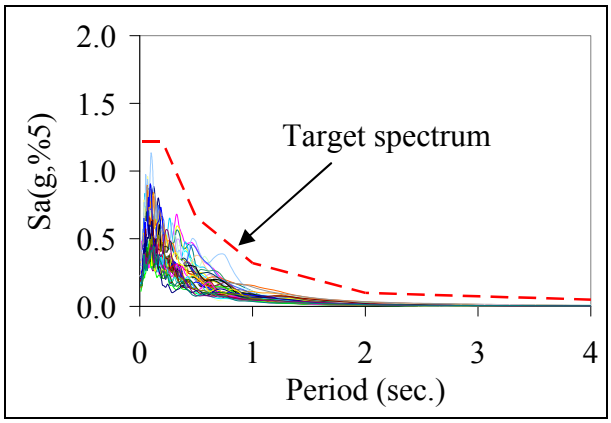

Figure 3.14 Comparison of the spectral acceleration data for M6 at D20-30 ground motion records (Table 3.5) with the target spectrum in Table 3.6

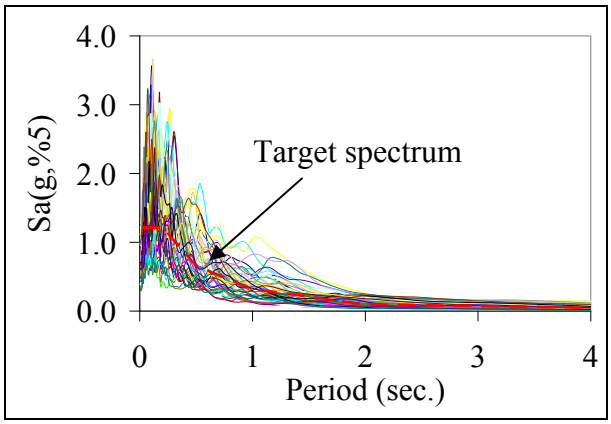

Figure 3.15 Comparison of the spectral acceleration data for M7 at D15-25 ground motion records (Table 3.5) with the target spectrum in Table 3.6

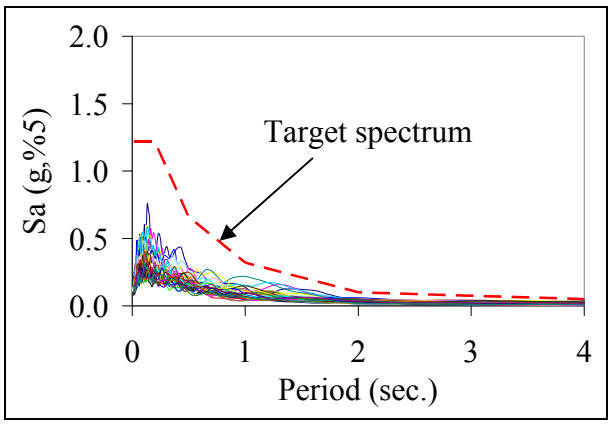

Figure 3.16 Comparison of the spectral acceleration data for M7 at D50-100 ground motion records (Table 3.5) with the target spectrum in Table 3.6

Table 3.8 Characteristics of synthetic ground motion records used in the Incremental Dynamic Analyses

		M	R (km)	Duration (sec.)	Time step (sec.)	PGA (g)
Group 1	Set 1	6.0	20-30	7.2	0.002	0.59
	Set 8	6.0	20-30	7.2	0.002	0.63
Group 2	Set 7	6.0	20-30	9.0	0.002	0.65
	Set 9	6.0	20-30	9.0	0.002	0.71
Group 3	Set 11	6.0	20-30	4.5	0.002	0.65
	Set 4	6.0	20-30	4.5	0.002	0.86
Group 4	Set 5	6.0	20-30	4.5	0.002	0.75
	Set 13	6.0	20-30	4.5	0.002	0.68
Group 5	Set 1	7.0	15-25	12.7	0.002	0.73
	Set 6	7.0	15-25	12.7	0.002	0.87
Group 6	Set 11	7.0	15-25	13.9	0.002	1.03
	Set 25	7.0	15-25	13.9	0.002	0.59
Group 7	Set 18	7.0	15-25	12.0	0.002	0.57
	Set 45	7.0	15-25	12.0	0.002	0.86
Group 8	Set 1	7.0	50-100	16.7	0.002	0.47
	Set 8	7.0	50-100	16.7	0.002	0.51
Group 9	Set 3	7.0	50-100	12.75	0.002	0.57
	Set 9	7.0	50-100	12.75	0.002	0.50
Group 10	Set 7	7.0	50-100	14.0	0.002	0.51
	Set 14	7.0	50-100	14.0	0.002	0.45

3.5.2 Application of the Incremental Dynamic Analysis

Similar to IDA analysis for the URMW building, for the CIW building, the spectral acceleration value at the first-mode period is selected as the intensity measure (IM), and the inter-storey drift (ISD), on the other hand, is chosen as the damage measure (DM). The two

components in each group are scaled to Sa(T_x,5%)—spectral acceleration value at the period of the first mode of vibration in the longer direction. This is achieved by scaling the set in each group which has higher Sa(T_x,5%), while the second set would follow the scaling rule, thus preserving their relative ratio (Lagaros 2009). About 100 three-dimensional time-history analyses have been carried out, on an analytical model which consists of about 12000 elements, using the AEM method. The resulted IDA curves are seen in Figure 3.17.

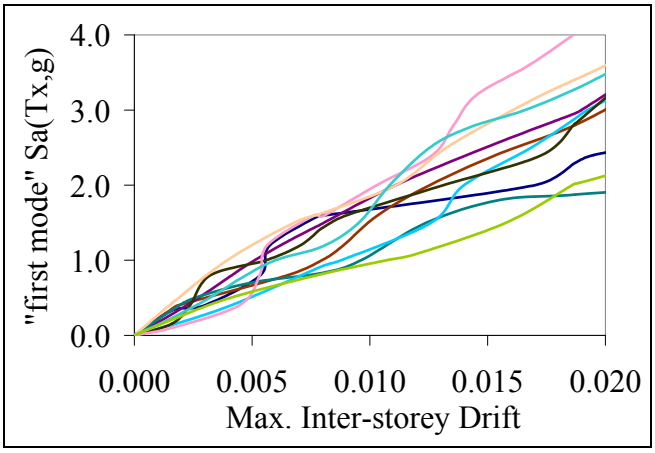

Figure 3.17 Two-dimensional IDA curves for the CIW building.

3.5.3 Distribution of structural performance levels

For each ground motion record group, the intensity measure was increased with the goal to reach to a point at which a small increase in that value would result in a large increase in the damage measure (inter-storey drift) or until complete collapse would happen in the analytical model. However, as seen in Figure 3.17, the IDA curves do not show any sign of complete collapse or instability (curves turning downwards) even when the Intensity Measure reached a value of 4g. At such an extreme intensity, the infill masonry walls were extensively cracked. However, because there was no perfect way to model the out-of-plan behaviour for those walls through the connection of the walls with the concrete frame, the walls stayed within the concrete frame. This means that the masonry walls would still partially contribute to the stiffness of the frames. Nevertheless, in reality this is not the case. For this reason, to determine the inter-storey drift values at the three structural performance levels—Immediate

Occupancy (IO), Life Safety (LS), and Collapse Prevention (CP)—in the case of the CIW building, the values of this drift ratio at the damage states introduced in NIBS (1999) for this building class are used instead (Table 3.9). These values are very close to the ISD threshold values presented in Rossetto and Elnashai (2005) for this building class.

Table 3.9 Definition of buildings damage states
taken from NIBS (1999)

Damage level	**Description**	**Inter-storey drift ratio**
Slight (≈ IO)	Diagonal hairline cracks on most infill walls; cracks at frame-infill interfaces	0.0016
Extensive (≈ LS)	Most infill walls exhibit large cracks; some bricks may dislodge and fall; some infill walls may bulge out-of-plane; few walls may fall partially or full; few concrete columns or beams may fail in shear resulting partial collapse.	0.008
Complete (≈ CP)	Structure is in imminent danger of collapse due to a combination of total failure of the infill walls and non ductile failure of the concrete beams and columns.	0.0187

Based on the above assumptions, the DM and IM values at each performance level (damage states) are calculated and presented in the next chapter.

3.6 Summary

In this chapter, for two buildings—an unreinforced masonry building with wood floors and an RC frame building with unreinforced masonry infill walls—which represent two of the building classes introduced in Table 1.5, the dynamic capacity curves were developed by applying the Applied Element Method in an Incremental Dynamic Analyses of the structural models. The intensity and damage measures for each building are calculated in the next chapter. These values are then used to develop the fragility curves for each building class which will be presented in Chapter 4.

CHAPTER 4

STRUCTURAL ANALYSIS RESULTS: DAMAGE ANALYSIS AND LOSS ANALYSIS STAGES

4.1 Introduction

In this chapter, the structural analysis results for the dynamic analyses conducted for the two buildings explained in Chapter 3 are presented. In the first place, for each building, the values of the intensity (IM) and damage measures (DM) on the IDA curves are determined based on the criteria explained in sections 3.4.3 and 3.5.3. Later on, the fragility curves for each building class studied in this research work are presented along with a loss estimation study for each building.

4.2 Damage analysis for the URMW building

4.2.1 Distribution of the structural performance levels

Using the assumptions explained in section 3.4.3, the DM and IM values for the URMW (shown in Figure 3.1) at each performance level are calculated in each direction, and shown in Table 4.1 and Table 4.2. From those performance levels, the Immediate Occupancy and the Collapse Prevention are pointed out on the IDA curves, shown in Figure 4.1 (The Life Safety performance level is not shown just to avoid unclear figures with several points).

Table 4.1 The IM and DM values at the three performance levels of the URMW building in the longer direction

	$S_a(T_1)/g$				ISD (Inter-storey Drift)		
Ground motion	**IO**	**LS**	**CP**		**IO**	**LS**	**CP**
M6D30_Set1	0.42	0.59	0.76		8.43E-04	2.17E-03	7.39E-03
M6D30_Set2	0.40	0.49	0.72		8.24E-04	2.15E-03	7.16E-03
M6D30_Set3	0.35	0.49	0.62		6.60E-04	2.51E-03	2.86E-03
M6D30_Set4	0.33	0.46	0.62		6.77E-04	3.18E-03	9.20E-03
M7D70_Set1	0.21	0.39	0.47		6.01E-04	8.44E-04	4.54E-03
M7D70_Set2	0.26	0.39	0.52		6.01E-04	1.09E-03	4.23E-03
M7D70_Set3	0.16	0.25	0.33		4.78E-04	7.46E-04	1.06E-03
M7D70_Set4	0.26	0.43	0.60		5.67E-04	3.09E-03	1.29E-02
M7D20_Set1	0.27	0.44	0.54		6.16E-04	2.19E-03	4.00E-03
M7D20_Set2	0.27	0.36	0.50		4.71E-04	4.03E-03	4.76E-03
M7D20_Set3	0.16	0.40	0.60		1.18E-03	1.44E-03	3.80E-03
M7D20_Set4	0.26	0.35	0.48		5.52E-04	7.19E-04	2.69E-03
Saguenay (S7)	0.24	0.33	0.42		5.59E-04	1.27E-03	9.26E-03
Nahanni (S3)	0.18	0.27	0.36		4.76E-04	4.31E-04	6.70E-04

Table 4.2 The IM and DM values at the three performance levels of the URMW building in the shorter direction

	$S_a(T_1)/g$				ISD (Inter-storey Drift)		
Ground motion	**IO**	**LS**	**CP**		**IO**	**LS**	**CP**
M6D30_Set1	0.22	0.30	0.49		2.30E-03	3.81E-03	5.08E-03
M6D30_Set2	0.21	0.37	0.48		2.36E-03	4.32E-03	5.77E-03
M6D30_Set3	0.26	0.45	0.56		2.38E-03	5.88E-03	7.84E-03
M6D30_Set4	0.24	0.37	0.45		2.38E-03	7.77E-03	1.04E-02
M7D70_Set1	0.16	0.24	0.27		1.73E-03	2.96E-03	3.95E-03
M7D70_Set2	0.12	0.19	0.26		1.38E-03	1.97E-03	2.62E-03
M7D70_Set3	0.08	0.09	0.13		9.83E-04	1.08E-03	1.44E-03
M7D70_Set4	0.11	0.21	0.24		1.12E-03	3.32E-03	4.43E-03
M7D20_Set1	0.20	0.36	0.43		2.41E-03	3.54E-03	4.73E-03
M7D20_Set2	0.14	0.33	0.42		1.90E-03	5.18E-03	6.90E-03
M7D20_Set3	0.13	0.35	0.38		3.45E-03	3.95E-03	5.26E-03
M7D20_Set4	0.17	0.36	0.42		2.04E-03	5.31E-03	7.075E-03
Saguenay (S7)	0.15	0.23	0.31		1.70E-03	4.62E-03	6.16E-03
Nahanni (S3)	0.14	0.24	0.26		2.05E-03	3.33E-03	4.44E-03

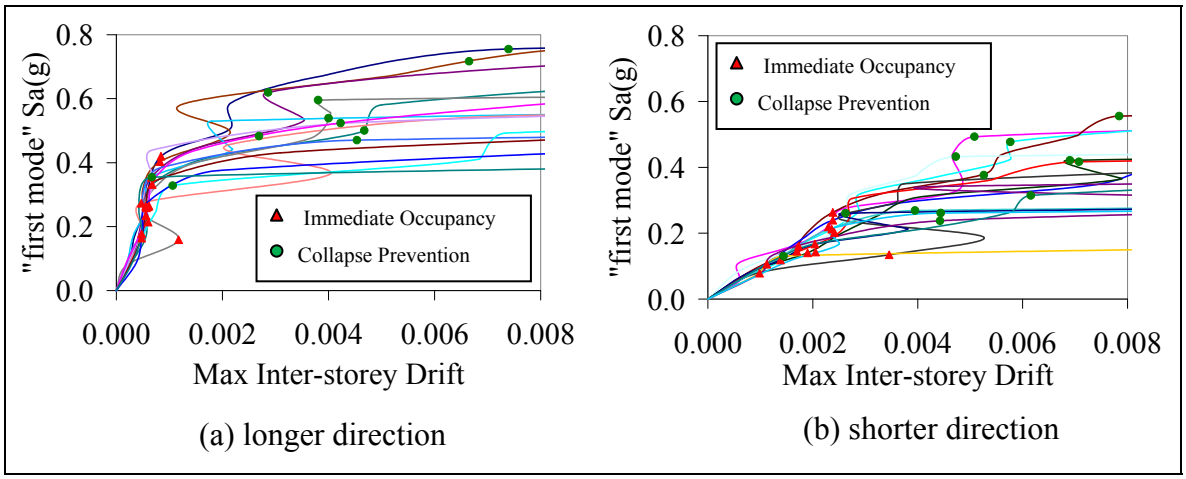

Figure 4.1 Distribution of the IO and CP performance levels on the URMW's IDA curves.

4.2.2 Development of the fragility curves for the URMW building

General methodology

According to the definition of the fragility curves presented in Chapter 1, the fragility curves can be developed using Equation 1.2 by calculating the median and the standard deviation of the logarithmic values of the IM measures at each performance level. The intensity measure values that will be calculated in the next chapter for the masonry building and the concrete frame building are used to develop the fragility curves at the three desired performance levels.

As seen in Equation 1.2, the intensity measure values at each performance levels are supposed to have a normal distribution. This assumption is checked through a normality test for the IM's calculated for each building.

Normality check

Example of this check is presented in Figure 4.2 in which the intensity measure values (S_a) in Table 4.1 and Table 4.2 at the Collapse Prevention level are plotted along with the values

which those measures would have had, were their distribution perfectly normal. As seen, a 1:1 straight line can be fitted to those data (with R^2 = 0.92 and 0.89) which shows that the normal distribution assumption for the IM values is completely valid.

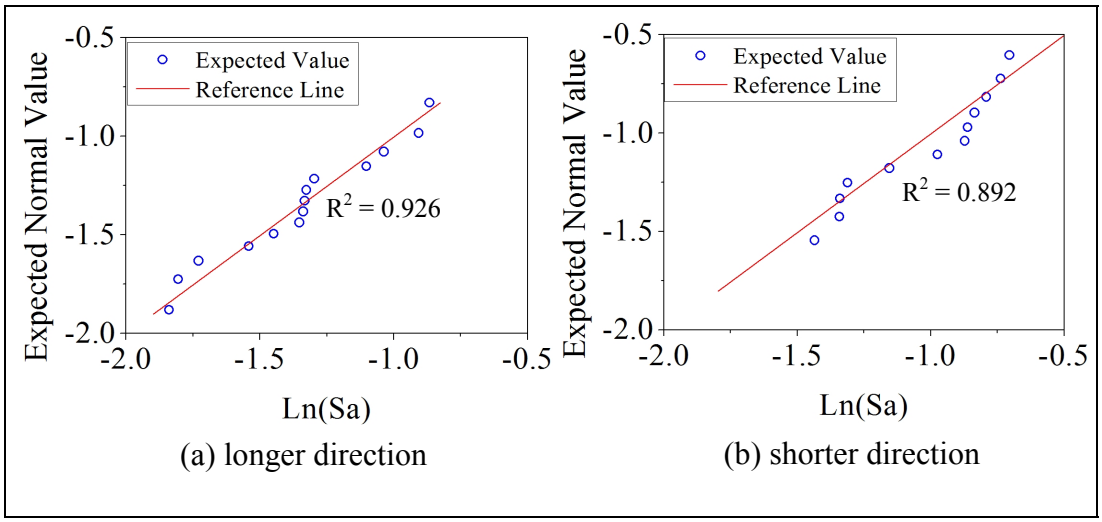

Figure 4.2 Q-Q plots for the IM values at the Collapse Prevention level.

Fragility curves for the URMW building

By calculating the median and the standard deviation of the logarithmic values of the IM measures shown in Table 4.1 and Table 4.2 at each performance level, the fragility curves can be developed using Equation 1.2. To this end, the first step is to calculate the logarithmic values of the IM's, as shown in Table 4.3 and Table 4.4.

Table 4.3 Logarithmic values of the URMW's intensity measures in Table 4.1 for the three performance levels, in the longer direction

		$\ln[S_a(T_1)/g]$				$\ln[S_d(T_1)]$		
Ground Motion		**IO**	**LS**	**CP**		**IO**	**LS**	**CP**
M6D30_Set1		-0.868	-0.335	-0.281		0.42	0.96	1.01
M6D30_Set2		-0.908	-0.391	-0.333		0.38	0.90	0.96
M6D30_Set3		-1.038	-0.638	-0.478		0.25	0.65	0.81
M6D30_Set4		-1.104	-0.662	-0.476		0.19	0.63	0.82
M7D70_Set1		-1.328	-0.810	-0.618		-0.04	0.48	0.67
M7D70_Set2		-1.298	-1.044	-0.692		0.00	0.25	0.60
M7D70_Set3		-1.840	-0.803	-0.518		-0.54	0.49	0.78
M7D70_Set4		-1.334	-0.759	-0.728		-0.04	0.53	0.57
M7D20_Set1		-1.543	-0.813	-0.754		-0.25	0.48	0.54
M7D20_Set2		-1.340	-0.712	-0.647		-0.05	0.58	0.65
M7D20_Set3		-1.807	-1.348	-1.114		-0.51	-0.05	0.18
M7D20_Set4		-1.354	-0.606	-0.506		-0.06	0.69	0.79
Saguenay (S7)		-1.450	-0.899	-0.863		-0.16	0.39	0.43
Nahanni (S3)		-1.730	-1.118	-1.037		-0.44	0.18	0.26

Table 4.4 Logarithmic values of the URMW's intensity measures in Table 4.2 for the three performance levels, in the shorter direction

		$\ln[S_a(T_1)/g]$				$\ln[S_d(T_1)]$		
Ground Motion		**IO**	**LS**	**CP**		**IO**	**LS**	**CP**
M6D30_Set1		-1.518	-1.212	-0.707		0.94	1.25	1.75
M6D30_Set2		-1.551	-1.001	-0.740		0.91	1.46	1.72
M6D30_Set3		-1.335	-0.799	-0.587		1.12	1.66	1.87
M6D30_Set4		-1.430	-1.005	-0.794		1.03	1.46	1.67
M7D70_Set1		-1.600	-1.034	-0.838		0.86	1.43	1.62
M7D70_Set2		-1.963	-1.121	-0.864		0.49	1.34	1.59
M7D70_Set3		-2.006	-1.046	-0.977		0.45	1.41	1.48
M7D70_Set4		-1.791	-1.022	-0.875		0.67	1.44	1.59
M7D20_Set1		-1.824	-1.448	-1.313		0.63	1.01	1.14
M7D20_Set2		-2.133	-1.680	-1.344		0.33	0.78	1.11
M7D20_Set3		-2.547	-2.415	-2.036		-0.09	0.04	0.42
M7D20_Set4		-2.248	-1.560	-1.437		0.21	0.90	1.02
Saguenay (S7)		-1.930	-1.478	-1.156		0.53	0.98	1.30
Nahanni (S3)		-1.948	-1.432	-1.342		0.51	1.03	1.12

The median and the standard deviation of those logarithmical values are then computed (Table 4.5 and Table 4.6), and used in Equation 1.2 to develop the fragility curves for each performance level. The acceleration and displacement based curves are shown in Figure 4.3 and Figure 4.4, for the longer and shorter directions, respectively. The relation between spectral displacement (S_d) and spectral acceleration (S_a) is given in Equation 4.1 in which T is the period of the first mode of vibration.

$$S_a = \left(\frac{2.\pi}{T}\right)^2 \times S_d \tag{4.1}$$

Table 4.5 Median and standard deviation values of ln[S_a(g)] shown in Table 4.3 and Table 4.4

		Longer dir.			**Shorter dir.**	
		μ	σ		μ	σ
IO		-1.337	0.308		-1.877	0.338
LS		-0.781	0.269		-1.166	0.412
CP		-0.632	0.242		-0.926	0.390

Table 4.6 Median and standard deviation values of ln[S_d(cm)] shown in Table 4.3 and Table 4.4

		Longer dir.			**Shorter dir.**	
		μ	σ		μ	σ
IO		-0.044	0.307		0.582	0.338
LS		0.513	0.269		1.292	0.412
CP		0.660	0.242		1.533	0.390

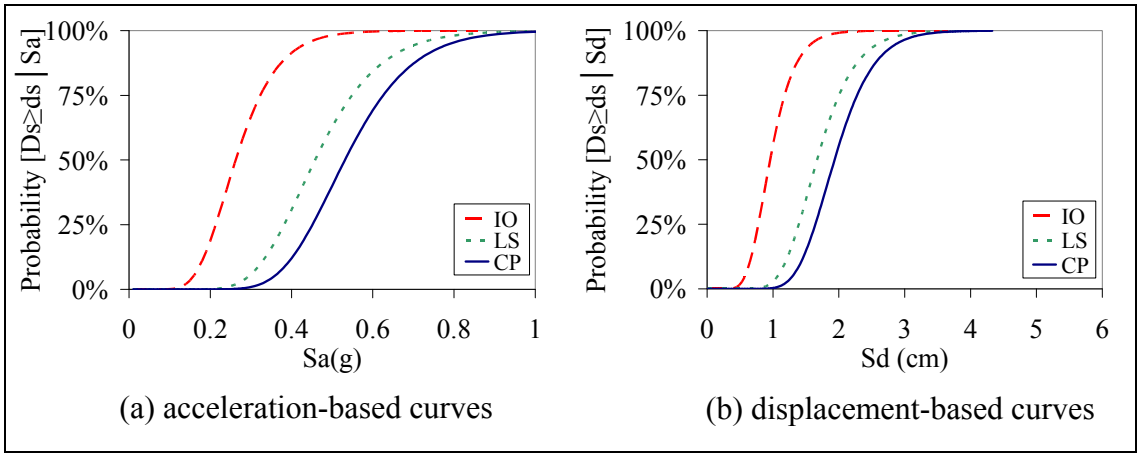

Figure 4.3 Fragility curves for the three performance levels, URMW longer direction.

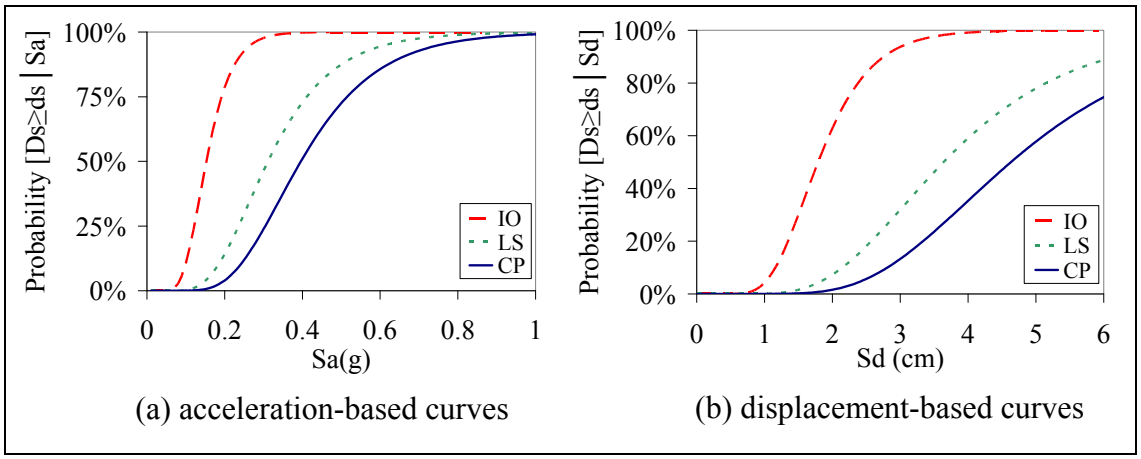

Figure 4.4 Fragility curves for the three performance levels, URMW shorter direction.

4.2.3 Combined fragility curves for the URMW building

Because the synthetic ground motion records used for the URMW building are not developed for bidirectional structural analysis, the analytical studies for that building have been conducted for the longer and shorter directions of the structure, separately. However, in a real situation, the direction in which an earthquake hits a building is arbitrary; therefore, unified fragility curves considering the dynamic behaviour of the building in both directions should be developed.

To this end, the weakest link theory is applied in this study to obtain the combined fragility curves for the masonry building: it is assumed that the overall structural performance of the building exceeds any of the limit states—Immediate Occupancy, Life Safety, or Collapse Prevention—if the performance level in either direction exceeds those limit states. In other words, the building is considered as a series-type system in which the failure of one component results in the failure of the system. According to the theory of reliability (Haldar and Mahadevan 2000), the first-order upper and lower bounds on the failure probability of such a system is defined as follows.

$$\max[FC_x(z), FC_y(z)] \le FC_T(z) \le \min\left[\sum_i^{x,y} FC_i(z), 1\right] \tag{4.2}$$

Where $FC_x(z)$ and $FC_x(z)$ are the probability of exceeding a damage state in the longer and shorter directions, respectively, and $FC_T(z)$ is the building's overall fragility. The lower bound in Equation 4.2 shows the case in which the events are perfectly dependent, and the upper bound represents the situation in which the events are mutually exclusive. If exceeding the damage levels in the longer and shorter directions are assumed marginally independent, Equation 4.2 can be written as follows.

$$\max[FC_x(z), FC_y(z)] \le FC_T(z) \le 1 - \prod_i^{x,y} [1 - FC_i(z)] \tag{4.3}$$

Equation 4.3 shows that at each IM level, the lower bound of the building's fragility is the fragility of the longer or shorter direction, whichever is weaker, while its upper bound is a combination of the fragility of the two main directions.

Using Equation 4.3, the upper and lower bounds of the combined acceleration and displacement-based fragility curves for the URMW building are developed and shown in Figure 4.5. Results show that the combined acceleration-based fragility curves are closer to the fragility curve of the direction that is weaker in strength, which is the shorter direction. On the other hand, the combined displacement-based fragility curves are closer to the fragility curve of the direction that is stiffer, the longer direction. This means that because of the lower level of ductility in the longer direction, applying the same amount of displacement in both directions produces more damages in the longer direction than in the shorter one.

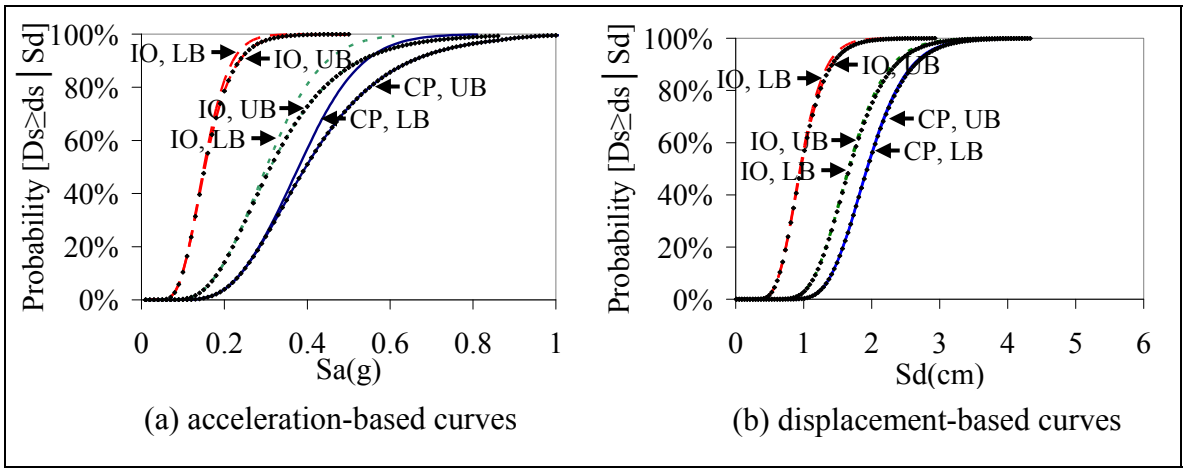

Figure 4.5 Upper (UB) and lower bounds (LB) of the fragility curves.

4.3 Damage analysis for the CIW building

4.3.1 Distribution of the structural performance levels

Using the assumptions explained in Table 3.9, the DM (Inter-storey Drift) and IM (Spectral Acceleration) values for the concrete building with masonry infill walls (shown in Figure 3.2) at each performance level are calculated, and shown in Table 4.7. As seen in that table, due to the criteria used to determine the damage measures (DM) in this case, the values of Inter-storey Drifts at each performance level is identical. From those performance levels, the Immediate Occupancy and the Collapse Prevention are pointed out on the IDA curves, shown in Figure 4.6.

Table 4.7 The IM and DM values at the three performance levels of the CIW building

	$S_a(T_1)/g$				ISD (Inter-storey Drift)		
Ground motion	**IO**	**LS**	**CP**		**IO**	**LS**	**CP**
M7D20_Group 1	0.33	1.62	2.29		1.60E-03	8.00E-03	1.87E-02
M7D20_Group 2	0.16	1.43	2.82		1.60E-03	8.00E-03	1.87E-02
M6D30_Group 3	0.35	1.01	2.80		1.60E-03	8.00E-03	1.87E-02
M6D30_Group 4	0.10	1.59	4.01		1.60E-03	8.00E-03	1.87E-02
M7D20_Group 5	0.28	1.49	2.96		1.60E-03	8.00E-03	1.87E-02
M7D75_Group 6	0.43	1.63	3.40		1.60E-03	8.00E-03	1.87E-02
M7D75_Group 7	0.34	0.83	1.87		1.60E-03	8.00E-03	1.87E-02
M6D30_Group 8	0.23	1.19	3.28		1.60E-03	8.00E-03	1.87E-02
M6D30_Group 9	0.14	0.92	2.88		1.60E-03	8.00E-03	1.87E-02
M7D75_Group 10	0.21	0.82	2.02		1.60E-03	8.00E-03	1.87E-02

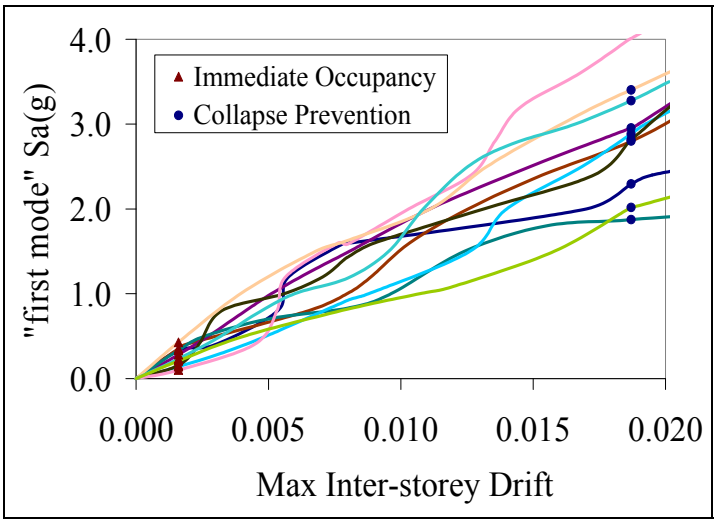

Figure 4.6 Distribution of the IO and CP performance levels on the CIW's IDA curves.

4.3.2 Development of the fragility curves for the CIW building

Normality check

Example of this check for the CIW building is presented in Figure 4.7 in which the intensity measure values (S_a) in Table 4.7 at the Collapse Prevention level are plotted along with the values which those measures would have had, were their distribution perfectly normal. As seen, a 1:1 straight line can be fitted to those data (with $R^2 = 0.86$) which shows that the normal distribution assumption for the IM values is valid.

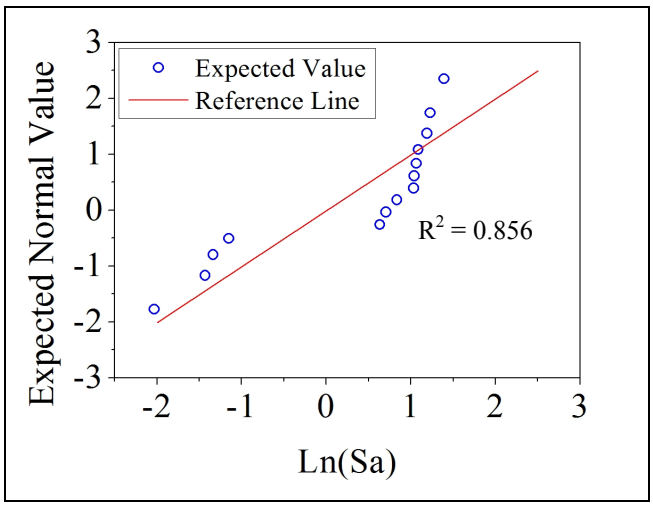

Figure 4.7 Q-Q plots for the IM values at the Collapse Prevention level.

Fragility curves for the CIW building

By calculating the median and the standard deviation of the logarithmic values of the IM measures shown in Table 4.7 at each performance level, the fragility curves can be developed using Equation 1.2. To this end, the first step is to calculate the logarithmic values of the IM's, as shown in Table 4.8.

Table 4.8 Logarithmic values of the CIW's intensity measures in Table 4.9 for the three limit states

		$\ln[S_a(T_x)/g]$				$\ln[S_d(T_x)]$		
Ground Motion		**IO**	**LS**	**CP**		**IO**	**LS**	**CP**
M7D20_Group 1		-1.103	0.483	0.831		-0.366	1.219	1.567
M7D20_Group 2		-1.850	0.360	1.035		-1.113	1.097	1.772
M6D30_Group 3		-1.039	0.007	1.030		-0.302	0.744	1.766
M6D30_Group 4		-2.291	0.461	1.389		-1.555	1.198	2.125
M7D20_Group 5		-1.264	0.399	1.084		-0.527	1.136	1.820
M7D75_Group 6		-0.848	0.489	1.225		-0.112	1.225	1.961
M7D75_Group 7		-1.092	-0.183	0.628		-0.355	0.553	1.365
M6D30_Group 8		-1.464	0.171	1.187		-0.727	0.907	1.924
M6D30_Group 9		-1.962	-0.079	1.059		-1.226	0.657	1.796
M7D75_Group 10		-1.565	-0.198	0.702		-0.828	0.538	1.439

The median and the standard deviation of those logarithmical values are then computed (Table 4.12), and used in Equation 1.2 to develop the fragility curves for each performance level. The results are shown in Figure 4.8 and Figure 4.9.

Table 4.9 Median and standard deviation values for $\ln[S_a(g)]$ and $\ln[S_d(cm)]$, shown in Table 4.8

		$\ln[S_a(g)]$			$\ln[S_d(cm)]$	
		μ	σ		μ	σ
IO		-1.448	0.466		-0.711	0.466
LS		0.191	0.282		0.928	0.282
CP		1.017	0.236		1.754	0.236

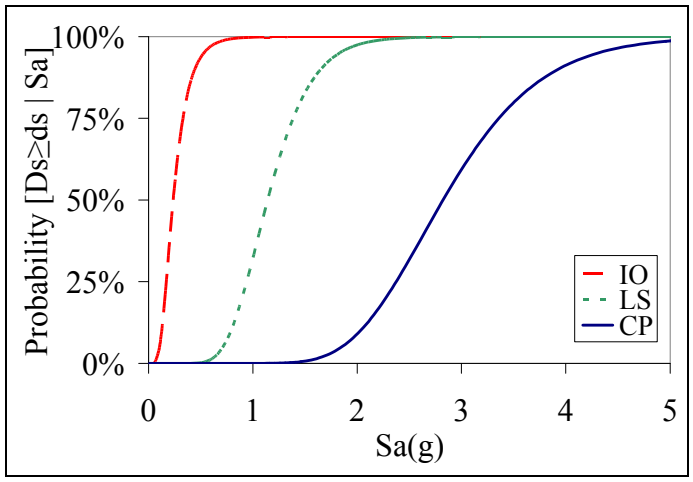

Figure 4.8 Acceleration-based fragility curves for the CIW building at the three performance levels.

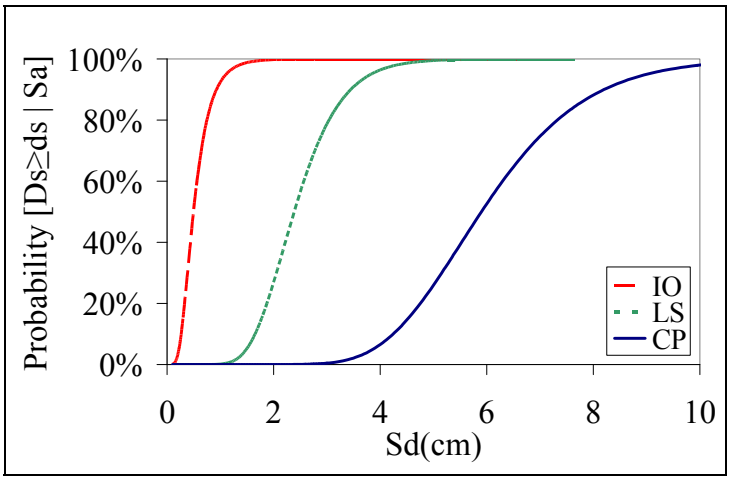

Figure 4.9 Displacement-based fragility curves for the CIW building at the three performance levels.

4.4 Loss analysis stage: mean annual frequency of exceeding the damage states

To calculate the MAF (explained in Chapter 1) of exceeding the limit states—Immediate Occupancy, Life Safety, and Collapse Prevention, here—for the buildings studied in this document, the hazard curves are obtained from the geological studies of Geological Survey of Canada conducted for different sites in the country. Considering that the ground motion records were scaled to the acceleration spectrum of the regions with high seismic hazard in

Quebec, the results are independent from the de-aggregation of any specific city in the province (Shome et al. 1998). Therefore, we can assume that, for example, both buildings are located in La Malbaie, Quebec, the spectral acceleration values[1] at different periods for different probabilities of exceedance, for this city is shown in Table 4.10 and illustrated in Figure 4.10.

Table 4.10 Spectral acceleration values (g) with different probability of exceedance in La Malbaie, Quebec

T(sec.)		**2% in 50 yrs.**	**5% in 50 yrs.**	**10% in 50 yrs.**	**40% in 50 yrs.**
0 (PGA)		1.11	0.79	0.58	0.27
0.2		2.28	1.53	1.01	0.37
0.29†		1.95	1.30	0.85	0.30
0.37†		1.65	1.09	0.71	0.24
0.38‡		1.61	1.06	0.69	0.23
0.5		1.18	0.77	0.48	0.14
0.69‡		0.85	0.52	0.30	0.08
1.0		0.59	0.34	0.20	0.05
2.0		0.19	0.10	0.06	0.015
4.0		0.093	0.052	0.030	0.0075

† Concrete frame building's first mode of vibration in the two directions
‡ Masonry building's first mode of vibration in the two directions

[1] http://earthquakescanada.nrcan.gc.ca/hazard-alea/interpolat/

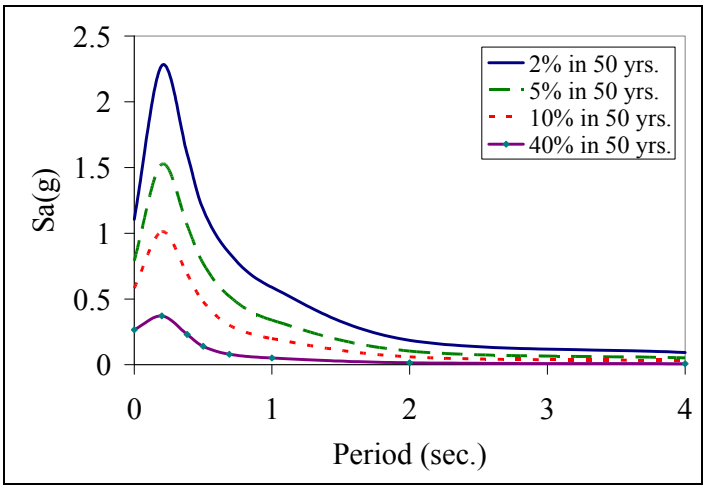

Figure 4.10 Spectral acceleration curves with different probability of exceedance in 50 years for La Malbaie, Quebec.

4.4.1 URMW building

For the masonry building, the lower bound of the combined fragility curves shown in Figure 4.5, which represent a more realistic case of the interaction between the two main directions, are applied is Equation 1.9. The hazard curves for the annual probability of exceedance at T_x=0.38 sec. and T_y=0.69 sec are illustrated in Figure 4.11. The equations for the curves that best fit the hazard data are also shown on that figure.

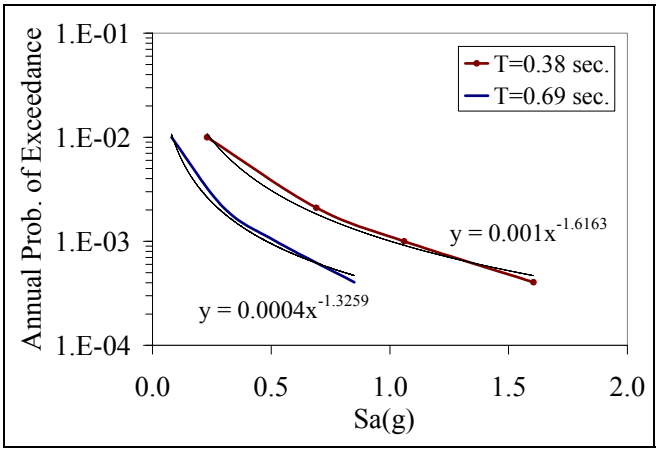

Figure 4.11 Hazard curves calculated at the URMW building's fundamental periods in the longer and shorter directions.

To calculate the MAF from Equation 1.9, the hazard curves shown in Figure 4.11 are illustrated along with the lower bound of the combined fragility curves, in Figure 4.12.

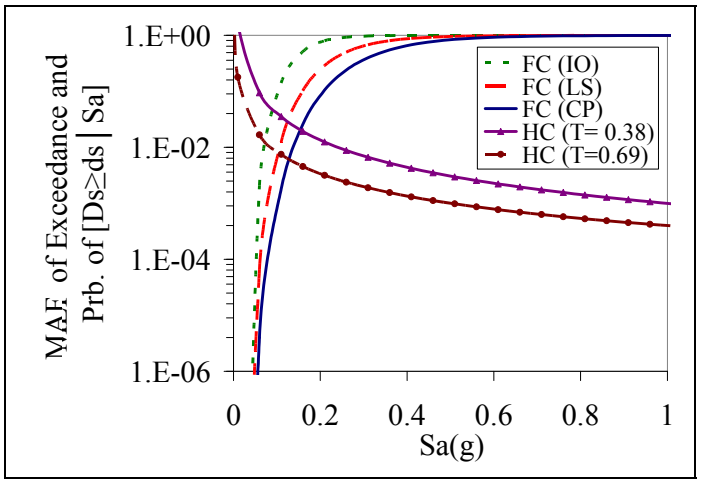

Figure 4.12 Lower bound of the combined fragility curves along with the hazard curves at the URMW building's dominant modes of vibration.

The MAF at any $S_a(T)$—the inner part of the integration in Equation 1.9—which is equal to the value of the corresponding fragility curve multiplied by the slope of the hazard curve at that point is calculated and shown in Figure 4.13 to Figure 4.15, for the three performance levels.

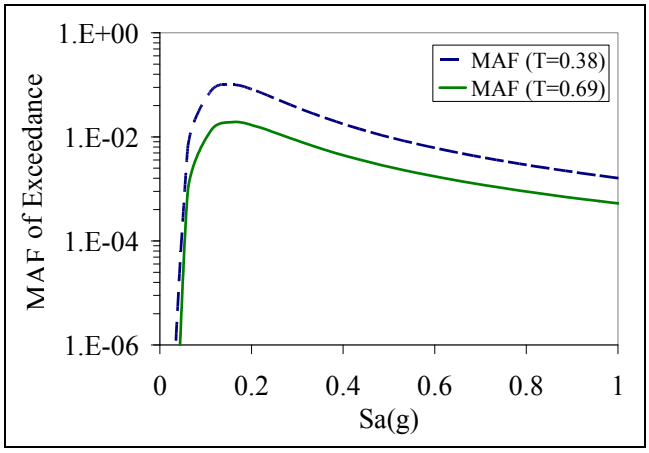

Figure 4.13 URMW building's mean annual frequency of exceeding the Immediate Occupancy performance level, due to $S_a = z$.

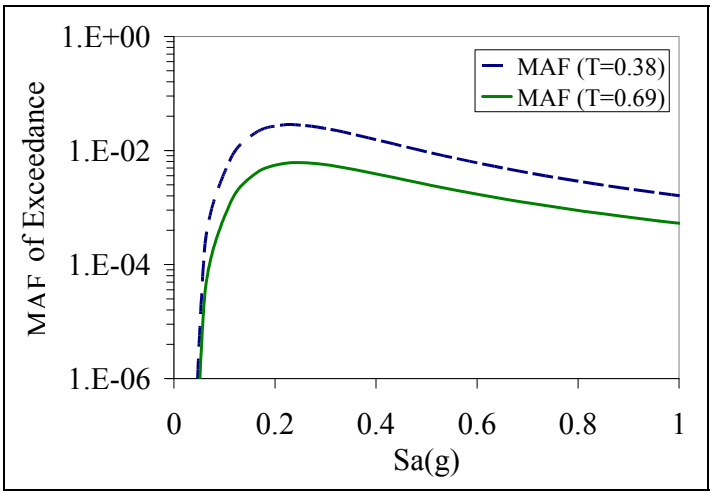

Figure 4.14 The URMW building's mean annual frequency of exceeding the Life Safety performance level, due to S_a = z.

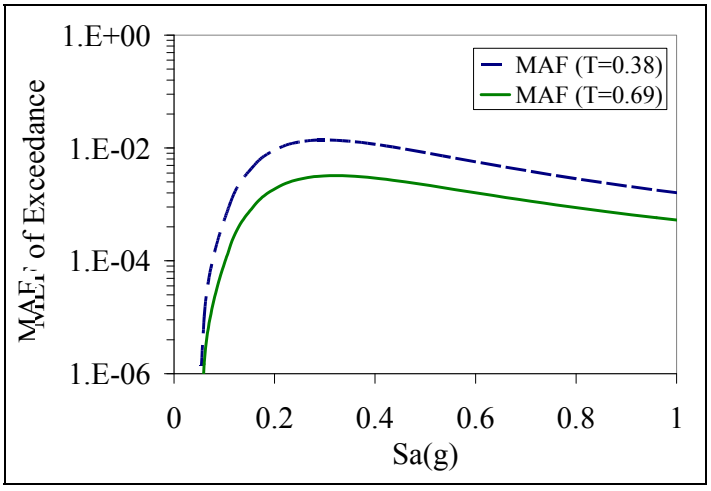

Figure 4.15 The URMW building's mean annual frequency of exceeding the Collapse Prevention performance level, due to S_a = z.

The curves shown in any of these figures have a descending trend as the slope of the hazard curves tends toward zero for large values of S_a. The total MAF of exceeding any of the performance levels, on the other hand, is equal to the area under the curves shown in Figure 4.13 to Figure 4.15, from zero to the infinity. The MAF of exceedance for each of the two dominant modes of vibration are presented in Table 4.11 and Table 4.15. The mean "return

period" of the damage-state exceedance, on the other hand, can be computed by inverting the values expressed for the MAF of exceedance.

Table 4.11 MAF's of exceedance and return periods of violating the performance levels, displacement in the longer direction (T=0.38 sec.)

		IO	**LS**	**CP**
MAF of exceedance		0.0228	0.0106	0.0069
Return period (yrs.)		43	94	144

Table 4.12 MAF's of exceedance and return periods of violating the performance levels, displacement in the shorter direction (T=0.69 sec.)

		IO	**LS**	**CP**
MAF of exceedance		0.0051	0.0027	0.0018
Return period (yrs.)		196	370	555

To pick the right MAF for each damage state, the weakest link theory is applied again. As seen in Table 4.11 and Table 4.15, the mode of vibration in the longer direction governs in this case as it results in higher MAF of exceedance (lower return period, consequently). Therefore, the values in Table 4.11 are chosen as the main annual frequency of exceedance for the three damage states. It should be noted that the epistemic uncertainties related to the structural properties as well as our geological knowledge can influence these results.

4.4.2 CIW building

For the RC frame building with unreinforced masonry infill walls, the fragility curves shown in Figure 4.8 are applied is Equation 1.9. The hazard curves for the annual probability of exceedance at T_x=0.29 sec. and T_y=0.37 sec. are illustrated in Figure 4.16. The equations for the curves that best fit the hazard data are also shown on that figure.

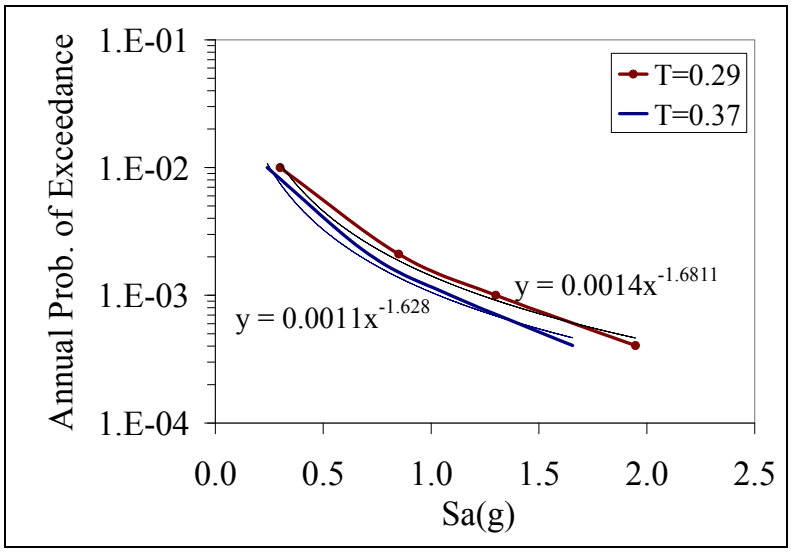

Figure 4.16 Hazard curves at the CIW building's fundamental periods in the longer and shorter directions.

To calculate the MAF from Equation 1.9, the hazard curves shown in Figure 4.16 are illustrated in Figure 4.17 along with the calculated fragility curves.

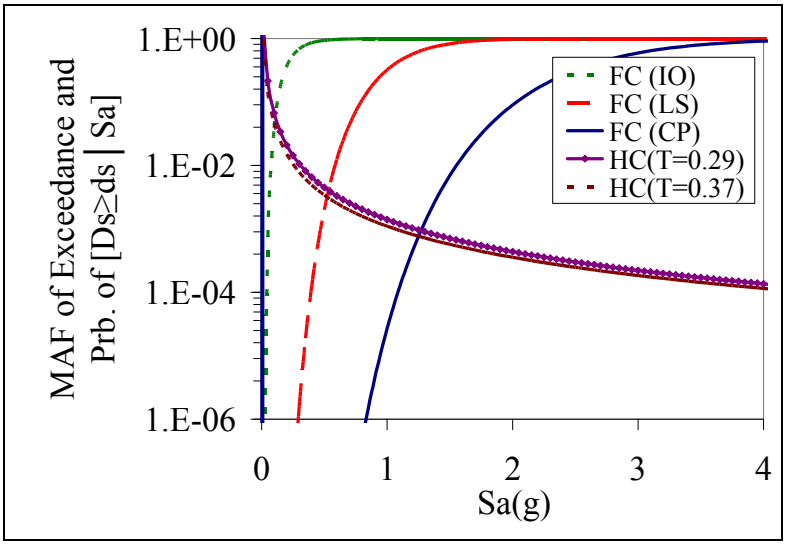

Figure 4.17 CIW building's fragility curves with the hazard curves at building's dominant modes of vibration.

It is seen in Figure 4.17 that the hazard curves for the two dominant period of vibration are very close. Therefore, only one of those curves which is the hazard curve for T=0.29 sec. is

considered for the rest of our calculations. The MAF at any $S_a(T)$—the inner part of the integration in Equation 1.9—which is equal to the value of the corresponding fragility curve multiplied by the slope of the hazard curve at that point is calculated and shown in Figure 4.18, for the three performance levels.

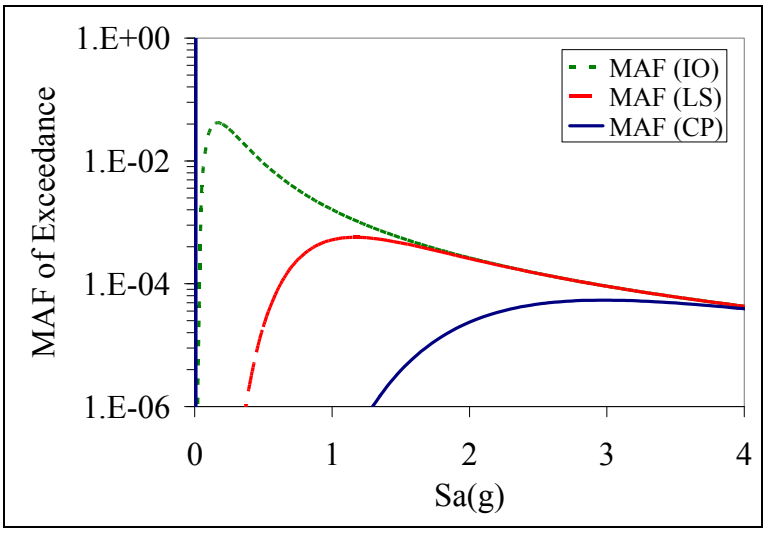

Figure 4.18 The CIW building's mean annual frequency of exceeding the three performance levels, due to $S_a = z$.

The total MAF of exceeding any of the performance levels, on the other hand, is equal to the area under the curves shown in Figure 4.18, from zero to the infinity. The MAF of exceedance for each of the performance levels are presented in Table 4.13. The mean "return period" of the damage-state exceedance, on the other hand, can be computed by inverting the values expressed for the MAF of exceedance.

Table 4.13 MAF's of exceedance and return periods of violating the performance levels

		IO	LS	CP
MAF of exceedance		0.014	0.00086	0.00016
Return period (yrs.)		71	1162	6250

As seen in Table 4.13, such a building in La Malbaie exceeds the Collapse Prevention performance level for an earthquake with a return period which surpasses the actual NBCC 2005 design earthquake. This result is surprising considering that concrete frame with masonry infill wall structures in Quebec are generally considered to be among the most vulnerable structures towards seismic loads (Lefebvre and Nollet 2009). However, as seen in Table 4.13, such a result only applies to the Collapse Prevention level (risk of complete damage), and the Life Safety and Immediate Occupancy performance levels for the building are expected to exceed within the return period considered in the seismic design of buildings according to the building code. This means that vulnerability can be high in buildings which are expected to stay functional after the earthquake (IO level) or buildings in which high number of people live or work (LS level). Moreover, it should be kept in mind that the current knowledge on the behaviour of RC frames with unreinforced masonry infill walls subjected to seismic loads is mostly a result of observed damages. Those observations confirm that the seismic vulnerability of such structures is highly related to either the out-of-plane failure of the masonry infill or the shear failure of the concrete columns. Although the second phenomenon is well represented by the AEM methodology, it is difficult to simulate the out-of-plane failure. As long as masonry elements stay inside the frame, there is a certain lateral rigidity and resistance that is, in fact, lost in case of out-of-plane failures. This may partially explain the results of Table 4.13. One should also consider that the results were obtained from an IDA which considers the dynamic properties of the structure; therefore, the methodology leads to different results from those generally found from static non-linear analysis. In any case, the results in Table 4.13 should be interpreted with caution as it has been developed for only one building. Analytical modeling of more buildings from this class will allow us to obtain even a better idea about the general behaviour of this building class. The epistemic uncertainties related to the structural properties as well as better geological knowledge can influence these results.

4.5 Summary

The result of the Incremental Dynamic Analyses in which an Applied Element-based Method was used, was presented in this chapter. The performance-based seismic evaluation (PBSE) for a typical industrial unreinforced masonry building and an RC frame building with unreinforced masonry infill walls led to the development of acceleration and displacement-based fragility curves for those buildings. To summarize the large amount of information regarding the different behaviours of the studied buildings towards each ground motion record, the IDA curves were summarized into their median, 16%, and 84% fractile values using the cross-section fractile method. The lognormal distribution of intensity measures, on the other hand, was used to develop the acceleration and displacement-based fragility curves. The loss estimation studies for existing buildings mainly depend on the geographical location of the structure. In this chapter, the mean annual frequencies of exceeding the three performance levels were calculated assuming that the studied buildings were located in La Malbaie which has the highest seismic hazard level in Quebec. The calculations show that the masonry and the concrete frame buildings will exceed the Collapse Prevention level within about 150 and 6250 years, respectively. Considering the age of some unreinforced masonry buildings in the province, such a return period is not much and can raise the red flag for many masonry buildings. It should be noted that the MAF of exceeding the performance levels decreases with the decrease of the seismic hazard level.

CHAPTER 5

DISCUSSION OF THE RESULTS

5.1 Introduction

In this chapter we will discuss the results of the structural analyses which were presented in the previous chapters. First of all, the statistical analysis of the information obtained from the IDA curves is presented and those curves are used to study the local dynamic behaviour of each building. This section is followed by a comparison of our fragility curves with those presented in the Technical and User's Manual of HAZUS (NIBS 2003) for the similar building classes. Later, the application of the newly developed fragility curves, for the buildings studied in this research work, to develop vulnerability scores is presented. Finally, a discussion on the application of the AEM in progressive collapse study is presented and the chapter is concluded with an explanation of the standard error in the estimation of the intensity and damage measure values.

5.2 Statistical analysis of the information obtained from the IDA curves

5.2.1 Unreinforced masonry building

The IDA curves in Figure 4.1 demonstrate a large amount of information regarding the masonry building's different behaviour towards each ground motion record. This information can be analyzed in two different ways.

I. Distribution of DM given the IM

The first way is to classify the obtained information from the IDA curves according to the distribution of the DM (inter-storey drifts here) given the IM (spectral acceleration value at building's first-mode period) and the probability of exceeding any performance level given a specific IM level. The distribution of limit states can be summarized into their medians and

measures showing their dispersion; Table 5.1 and Table 5.2 show the 16%, 50% (median values), and 84% fractiles of DM and IM values at the IO, LS, and CP levels. From the values in these tables, it can be noted that for example, 16% of ground motions cause the building to exceed the Collapse Prevention performance level at a spectral acceleration value of 0.42g—at building's first mode in the longer direction of the building (Table 5.1)—which is equal to an ISD of 0.0027. For the same fractile (16%), the spectral acceleration and the ISD values for exceeding that performance level in the shorter direction are S_a= 0.26g and ISD = 0.0039. This shows that the building is weaker in terms of earthquake intensity resistance and more flexible, in the shorter direction. Considering that the ISD values in Table 3.7 are average values of this damage measure at each performance level, the ISD values in that table can be compared with the median values in Tables 5.1 and 5.2. As seen in these tables, the median values for the ISD in both longer and shorter directions of the URMW building are very close to the values presented in Table 3.7 for CP and LS performance levels (e.g., 3.29E-03 for the LS level in comparison with 0.003 in Table 3.7). In the case of the IO performance level, the 0.1% value in Table 3.7 represents an upper limit for the ISD values in the longer direction and a lower limit for the values in the shorter direction of the URMW building, in Tables 5.1 and 5.2.

Table 5.1 Summary of the limit states in the URMW's longer direction

Fractile	**$S_a(T_1)$/g**				**Max Inter-Storey Drift (ISD)**		
	IO	LS	CP		IO	LS	CP
16%	0.18	0.36	0.42		4.84E-04	2.03E-03	2.70E-03
50%	0.26	0.46	0.53		6.01E-04	3.29E-03	4.38E-03
84%	0.35	0.54	0.62		8.12E-04	6.80E-03	9.06E-03

Table 5.2 Summary of the limit states in the URMW's shorter direction

Fractile	$S_a(T_1)$/g				Max Inter-Storey Drift (ISD)		
	IO	LS	CP		IO	LS	CP
16%	0.12	0.21	0.26		1.41E-03	2.99E-03	3.99E-03
50%	0.15	0.31	0.40		2.05E-03	3.88E-03	5.17E-03
84%	0.22	0.37	0.48		2.38E-03	5.30E-03	7.06E-03

II. Curves in their fractile format

The second way to classify the information obtained from the IDA curves in Figure 3.9 is to present the curves (and not just the DM and IM values) in their fractile format. To this end, the cross-section fractile method (Vamvatsikos and Cornell 2002) is used to present those curves in their median, 16%, and 84% fractile values. Using the sp-line interpolation, for each curve, the DM values are calculated at arbitrary levels of IM's. Therefore, at each seismicity level, this procedure results in fourteen finite or infinite DM values (for the 14 accelograms) at each IM level. These values are used to draw the fractiles of the IDA curves for both the longer and shorter directions, shown in Figure 5.1.

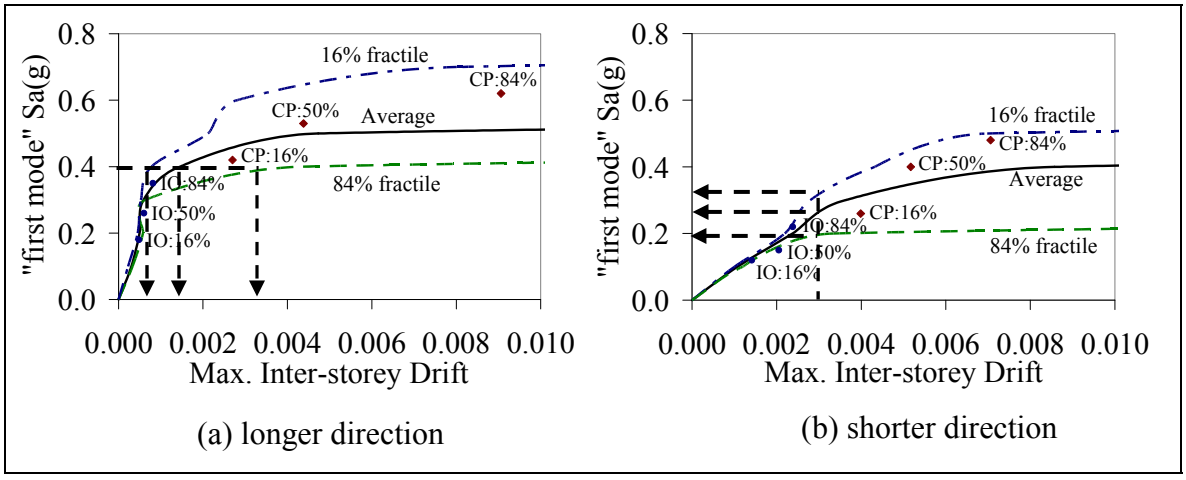

Figure 5.1 Summary of URMW's IDA curves into the median, 16%, and 84% fractiles.

As seen from Figure 5.1.a, in the longer direction of the masonry building, for example, given $S_a(T_1)$ = 0.4g, 84% of the records cause an inter-storey drift smaller than 0.0032, 50% smaller than 0.0015, and 16% smaller than 0.0008. On the other hand, as seen in Figure 5.1.b, for example, to develop an inter-storey drift equal to 0.003 in the shorter direction, the spectral acceleration values of 84% of the records at T= 0.69 sec. (building's period of vibration in that direction) should be scaled to 0.19g or greater, 50% to 0.26g or greater, and 16% to 0.32g or greater.

The median, 16%, and 84% fractiles of the IO and CP performance levels as computed at the beginning of this section are also pointed out on Figure 5.1. The definition described in this section for these limit states results in a different distribution of the performance levels in comparison with those of the IDA curves. As a result, as seen in Figure 5.1, the IO and CP fractiles do not necessarily reside on their corresponding IDA curve fractiles, but do lie quite close to them.

5.2.2 RC frame building with unreinforced masonry infill walls

I. Distribution of DM given the IM

The information included in the IDA curves in Figure 4.6 can be analyzed in the same two different ways stated in section 3.2.2. The first way is to classify the obtained information from the IDA curves according to the distribution of the DM (inter-storey drifts in this paper) given the IM (spectral acceleration value at building's first-mode period) and the probability of exceeding any performance level given a specific IM level. The distribution of limit states are summarized into their medians and measures showing their dispersion; Table 5.3 shows the 16%, 50% (median values), and 84% fractiles of DM and IM values at the IO, LS, and CP levels. From the values in this Table, it can be noted that for example, 16% of ground motions cause the building to exceed the Collapse Prevention performance level at a spectral acceleration value of 2.18g—at building's first mode in the longer direction (Table 5.1)—which is equal to an ISD of 0.0187.

Table 5.3 Summary of the limit states for the CIW building

Fractile	$S_a(T_1)$/g				Max Inter-Storey Drift (ISD)		
	IO	LS	CP		IO	LS	CP
16%	0.15	0.89	2.18		1.60E-03	8.00E-03	1.87E-02
50%	0.22	0.94	2.51		1.60E-03	8.00E-03	1.87E-02
84%	0.34	1.6	3.33		1.60E-03	8.00E-03	1.87E-02

II. Curves in their fractile format

As the second way to classify the information obtained from the IDA, the IDA curves are presented in their median, 16%, and 84% fractile values as shown in Figure 5.2.

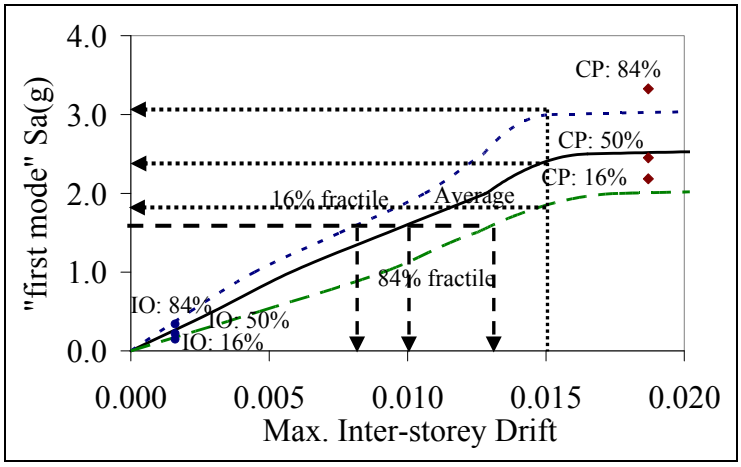

Figure 5.2 Summary of the CIW's IDA curves into the median, 16%, and 84% fractiles.

As seen from Figure 5.2, given $S_a(T_1)$ = 1.5g, 84% of the records cause an inter-storey drift smaller than 0.012, 50% smaller than 0.009, and 16% smaller than 0.007. On the other hand, to develop an inter-storey drift equal to 0.014 or greater, the spectral acceleration values of 84% of the records at T= 0.29 sec. (building's period of vibration in the longer direction) should be scaled to 1.8g or greater, 50% to 2.2g or greater, and 16% to 2.9g or greater. The median, 16%, and 84% fractiles of the IO and CP performance levels are also pointed out on

Figure 5.2. Similar to the case for the URMW building, the IO and CP fractiles for the concrete frame building do not necessarily reside on their corresponding IDA curve fractiles, but do lie quite close to them.

5.3 Studying the structural dynamic behaviour from IDA

5.3.1 Unreinforced masonry building

The information obtained from the IDA can be applied to evaluate the local behaviour of each storey during an earthquake. Figure 5.3 demonstrates the maximum ISD outline of all storeys in both the longer and shorter directions at various IM levels for set 1 ground motion record of category 3 with M=7 and D=20 km (Table 3.5). As seen in this figure, while higher storeys accumulate the deformation at lower intensities (first mode's effect) the second storey accumulates a major part of the deformation at higher intensities, an indication of higher mode effects on the building's overall behaviour.

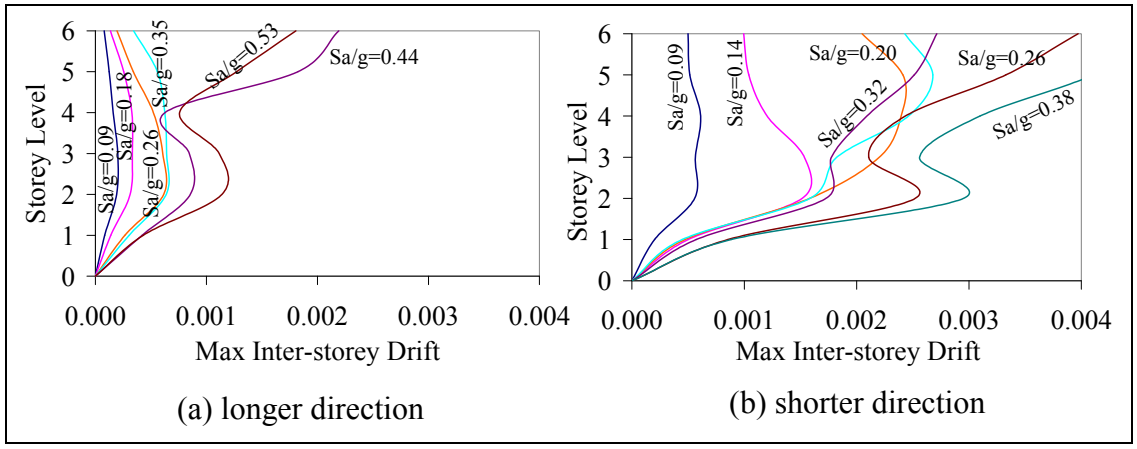

Figure 5.3 URMW's maximum ISD of all storeys at different values of S_a(T1) for set 1 ground motion record of category 3 in Table 3.5.

Another useful piece of information is the incremental behaviour of each storey through the dynamic analysis. Figure 5.4 shows the IDA curves for all the storeys in both directions for the same record used to draw Figure 5.3. In the longer direction (Figure 5.4.a), as soon as the

IM passes the 0.35g value, the fifth and the roof (6^{th}) floors suddenly start to accumulate more and more deformation. In the shorter direction (Figure 5.4.b), however, almost all of the storeys except the first floor accumulate deformation in fairly the same manner. From Figure 5.4, it can be noted that the higher mode effect pointed out in Figure 5.3 seems to be more significant in the longer direction as the IDA curve of the second floor end up to pass other upper floors except the roof and the fifth floor.

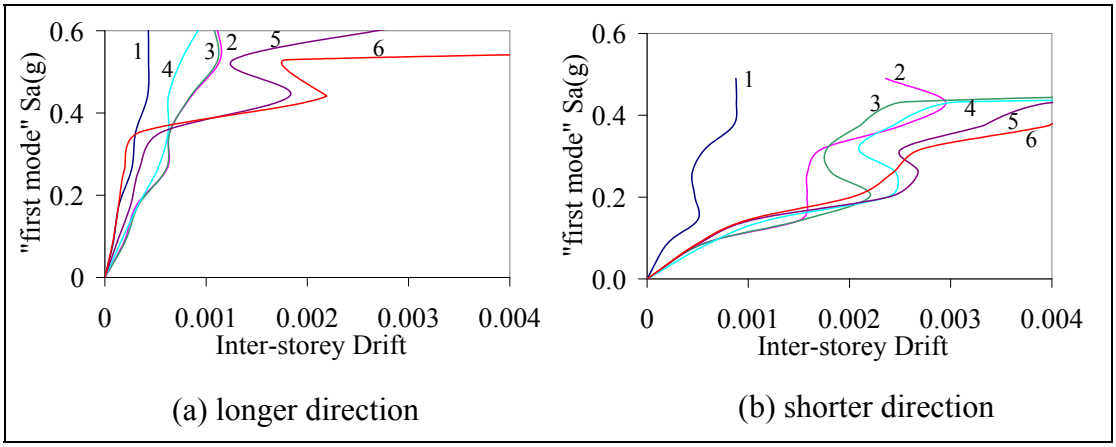

Figure 5.4 IDA curves for each storey of the URMW building, for set 1 ground motion record of category 3.

The IDA results can also be used to evaluate ductility change in the building (Krawinkler et al. 2003), which could be useful to obtain information of structure softening during an earthquake. However, this issue is out of score of this research work.

5.3.2 RC frame building with unreinforced masonry infill walls

Figure 5.5 demonstrates the maximum ISD outline of all storeys at various IM levels for group 5 of the ground motion records in Table 3.8, with M=7 and R=15 to 25 km. As seen in this figure, the building shows a strong higher mode effect even at lower intensities. The first and second storeys accumulate the major part of the deformation at all intensities, which is typical of a structure in which the lateral resisting system is partly constituted from a frame.

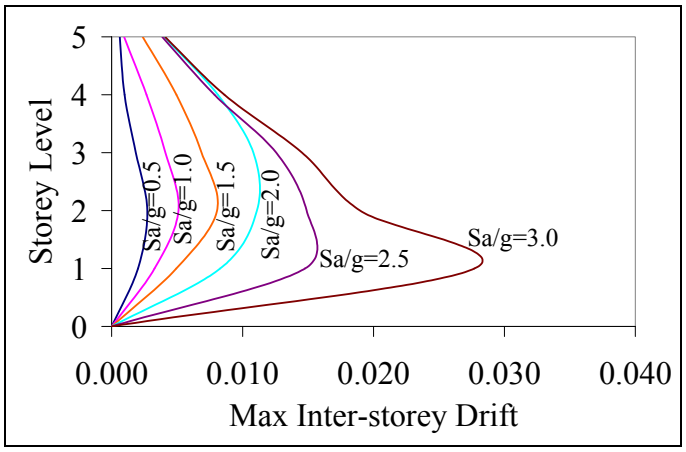

Figure 5.5 CIW's maximum ISD of all storeys at different values of S_a(Tx) for group 5 of the ground motion in Table 3.8.

Figure 5.6, on the other hand, shows the incremental behaviour of each storey through the dynamic analysis. The IDA curves are shown for all the storeys for the same record used to draw Figure 5.5. Up to the IM=2.3 g, the second floor accumulates the most deformation. After this point, it is the first floor which passes the second floor and accumulates the major part of deformation in the building. This observation confirms the behaviour seen in Figure 5.5.

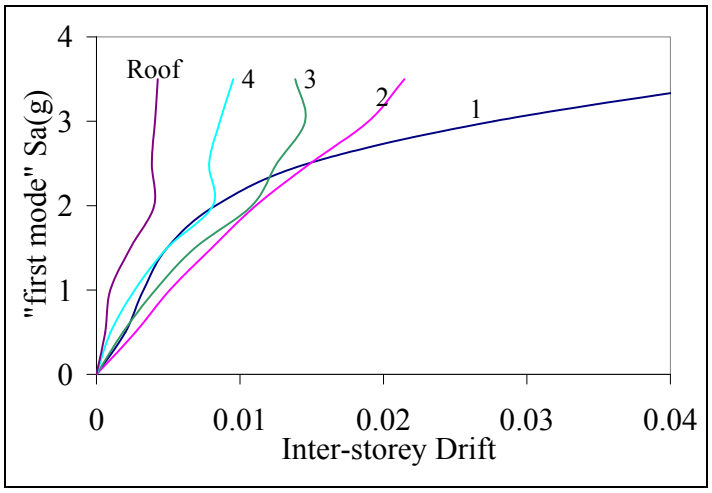

Figure 5.6 IDA curves for each storey of the CIW building, for group 5 of the ground motion records.

Because bi-directional accelograms have been used in the Incremental Dynamic Analysis of the CIW building, the effects of seismic loading in one direction on the deformation of the other direction can be also studied for this building, if the ISD in Figures 5.5 and 5.6 are calculated for each direction, individually.

5.4 Comparing with HAZUS fragility curves

5.4.1 Unreinforced masonry building

The displacement-based fragility curves in Figure 4.3 and Figure 4.4 are compared with those for the medium-rise pre-code masonry building presented in the Technical and User's Manual of HAZUS, which is the closest typology to the building classification of FEMA. It should be noted that HAZUS curves are developed for damage-based states—such as Slight, Moderate, Extensive, and Complete—while the fragility curves in this research work are calculated for performance-based states. Assuming that the Slight Damage state is similar to the Immediate Occupancy level, the Extensive Damage to the Life Safety, and the Complete Damage to Collapse Prevention, the curves are compared in Figure 5.7 and Figure 5.8. As seen in both figures, while the median values (50% probability of occurrence) of the extreme damage states in HAZUS (extensive and complete) are greater than those of the masonry model in this research work, the median values of the slight damage state are close to the IO level in both directions. This means that the model considered here is less ductile than the one in HAZUS. In other words, from a PBSE perspective, the masonry building here is more vulnerable as for the same value of S_d, the probability of exceeding extreme damage states are higher for the masonry building in this research work.

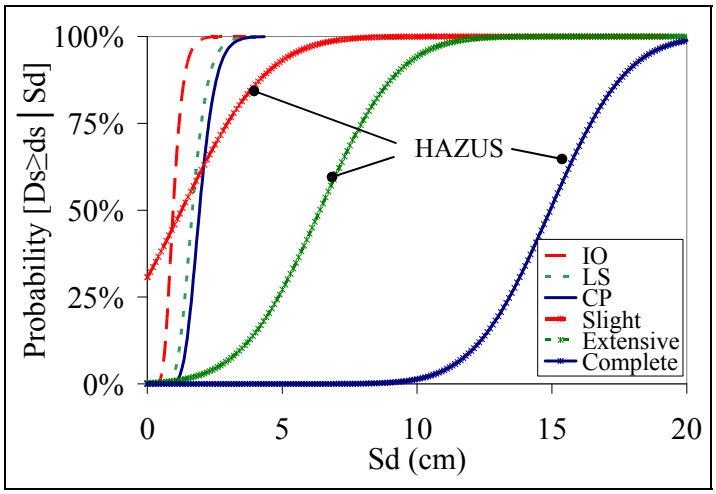

Figure 5.7 Fragility curves of the masonry building in the longer direction compared with HAZUS fragility curves for a pre-code midrise URM.

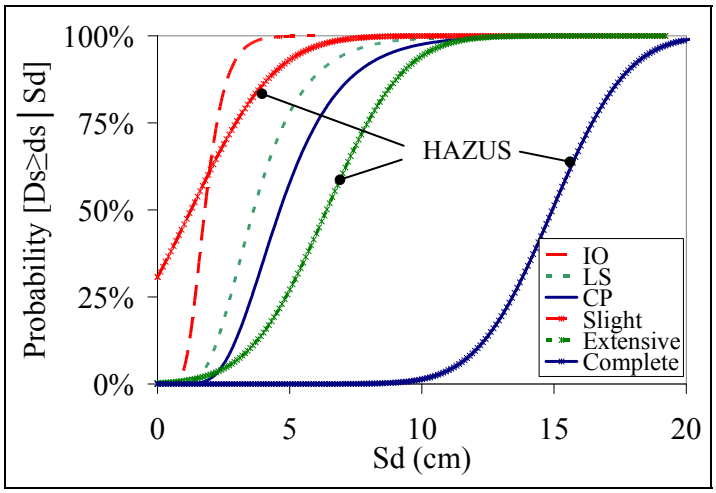

Figure 5.8 Fragility curves of the masonry building in the shorter direction compared with HAZUS fragility curves for a pre-code midrise URM.

One reason for having such different median values in the extreme damage cases is the differences in the buildings' height since NIBS (2003) doesn't present any fragility curves for masonry buildings above 3 storeys. Moreover, the number of openings in the masonry building studied here affects the failure mode which is normally expected in a masonry building. It is expected that having greater height and more openings make the masonry building analyzed here more ductile. However, since the URMW is taller and heavier, the

seismic demand on the building is greater, and more damages is expected to be observed in the 6-storey building than in a 3-storey building, for the same seismic acceleration. Except the first two first floors in the URMW building, other floors stay rigid (Figure 5.5), which means that the total drift of the 6-storeys URMW will be less than HAZUS 3-storeys. This confirms the higher rigidity for the URMW observed in Figures 5.7 and 5.8. The different way of treating masonry properties (dynamic analysis here in comparison to static analysis in HAZUS) could also be the cause of those different results.

Differences in the curves' standard deviations (variances in damage data) also results in curves with different slopes. As seen in Figure 5.7 and Figure 5.8, the fragility curves developed in this document are mostly steeper (smaller standard deviation) than those of (NIBS 2003). There are exceptions though, for the curves in the extreme damage cases in Figure 5.8 where the extensive and complete damage curves are almost parallel to the LS and CP curves. To have a better idea of the differences in the standard deviations, the coefficient of variation (COF), defined in Equation 3.10, is calculated, for fragility curves in Figure 5.7 and Figure 5.8, and presented in Table 5.4.

$$Coefficient\ of\ \text{var}iation = \frac{\sigma}{\mu} \tag{5.1}$$

In Equation 5.1, μ and σ are the mean and standard deviation values of the fragility curves, respectively.

Table 5.4 Coefficient of variation for masonry buildings' fragility curves in HAZUS (NIBS 2003) and those developed in Chapter 4

	HAZUS	**Masonry longer dir.**	**Masonry shorter dir.**
IO (≈ Slight)	1.98	0.30	0.32
LS (≈ Extreme)	0.36	0.26	0.33
CP(≈ Complete)	0.15	0.23	0.33

The coefficient of variation in Table 5.4 for the fragility curves developed here are generally smaller than of those in HAZUS. This can be a result of comparing HAZUS curves that have been developed based on an average behavior of the URM class with this document's curves which have been developed for just one building with average properties.

5.4.2 RC frame building with unreinforced masonry infill walls

The displacement-based fragility curves in Figure 4.9 are compared with those for the medium-rise pre-code concrete frame buildings with infill walls presented in the Technical and User's Manual of HAZUS. Again it is assumed that the Slight Damage state is similar to the Immediate Occupancy level, the Extensive Damage to the Life Safety, and the Complete Damage to Collapse Prevention, the curves are compared in Figure 5.9. The median values (50% probability of occurrence) of all limit states in HAZUS are again greater than those of the concrete frame building in this research work; the median value of the slight damage state is the closest to its corresponding limit state in this document, the IO level.

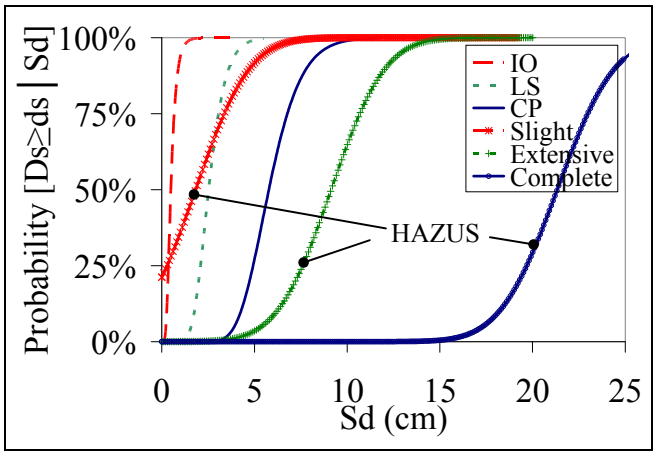

Figure 5.9 Fragility curves of the concrete frame building compared with HAZUS fragility curves for a pre-code midrise C3M.

This means that the RC frame with masonry infill wall model considered here is less ductile than the one in HAZUS. Knowing that the number of storeys and year of construction are somewhat similar, such a difference can be a result of the way that HAZUS takes into

account the effect of the infill walls in its structural models which has resulted in a generally softer structural behavior (larger displacement) than the CIW studied here. Moreover, HAZUS curves are developed based on information from expert opinions and static analyses of structural models, which does not take into account the dynamic characteristics of the structure such as period modification. The advantages of the bi-directional analysis—through which the interaction between the lateral resisting systems in both directions is considered—and the Incremental Dynamic Analysis, applied in this research work should not be ignored in such comparison.

However, same as what explained for the case of the unreinforced masonry building, more RC frame buildings with masonry infill walls analyzed with the methodology proposed here will allow us to obtain even a better idea regarding the differences between the curves in the two documents. Parallel curves in most cases in Figure 5.9, on the other hand, indicates a similar standard deviation calculated in Table 4.12 with those for HAZUS curves.

5.5 Application of the loss estimation studies in developing SVI

Based on the definition of SVI in Equation 2.7, the information calculated in Table 4.11 and Table 4.13 regarding the MAF's of exceeding the Collapse Prevention performance level in the unreinforced masonry and RC frame buildings with masonry infills can be used to develop new basic vulnerability indices for those buildings. The advantage of such new indices is that, unlike the indices presented here, the dynamic behaviour of each building class is considered in the process of index calculation.

As Table 4.11 and Table 4.13 present the probability of exceeding the Collapse Prevention performance level on a yearly based, the first step is to calculate the frequency of the event occurrence in 50 years.

Table 5.5 Probability of exceedance of the Collapse Prevention level in 50 years, calculated from Table 4.11 and Table 4.13

		URMW	**CIW**
Probability (%)		34.5	0.8

Using Equation 2.7, new SVI can then be calculated from the values presented in Table 5.5. These SVI's are presented in Table 5.6.

Table 5.6 Seismic Vulnerability Indices for the two studied buildings in this research work

		URMW	**CIW**
SVI		0.46	2.09

Unlike the results developed for these building classes in Chapter 2, the indices here are developed through a performance-based seismic evaluation of the structural models. Because of such a difference, the results in Table 5.6 are not directly comparable with those presented in Table 2.6 in Chapter 2 for regions with high seismic risk (1.8 for both building classes). However, relative comparison of the results in Table 5.6 indicates that the unreinforced masonry building has a significant lower score which means a higher vulnerability for this building class in comparison to the concrete frame building with infill walls. Considering the differences between the structural behaviour of these two building classes, such a result is more rational than the equal vulnerability indices in Table II.1 (for the regions with high seismic risk).

To have a better idea of the meaning of these indices, on the other hand, a cutoff index should be chosen. If the same seismic risk level considered in developing the seismic demands in the Building Code of Canada (NRCC 2005) is chosen—%2 in 50 years—, using Equation 2.7, the cuttoff index is equal to 1.69. This means that any building with an SVI lower than 1.69 needs to be evaluated in further details. The indices shown in Table 5.6 are

basic ones and they should be modified according to the existence of index modifiers explained in section 2.2.4. In other words, although the RC frame building with masonry infill walls (in regions with high seismic risk) doesn't have a basic index smaller than the cutoff index, structural irregularities or site conditions could cause buildings from this class to require further assessment. According to the basic index in Table 5.6, the unreinforced masonry building in regions with high seismic risk in Quebec will always require further investigation. As the basic index calculated here directly depends on the level of the seismic risk, such a "pre-defined further evaluation" can change in regions with moderate and low seismic risk, such as in Montreal or Quebec City.

It should be noted that the indices shown in Table 5.6 are developed using the performance-based evaluation of one building in each class. As these indices should aim to evaluate the average behaviour of each building class rather than individual buildings, better indices can be developed when the loss estimation is repeated for a number of buildings in each class with different structural characteristics. This is, of course, out of the scope of this research work.

5.6 Application of the AEM in the progressive collapse of the studied structures

As stated in section 1.7.3, the Applied Element Method was used in this research work to overcome the FEM shortcomings in the progressive collapse case of buildings with masonry construction. Thanks to the partial connectivity that can exist between elements during the analysis in this method—some springs fail, while others are still effective—the "joint de-bonding" and "unit sliding along bed or head joint" modes shown in Figure 1.6 were the dominant failure modes (shear failure) which could be captured in the various structural analyses for both models. The "unit cracking under direct tension" mode could only be seen in higher intensity measures. On the other hand, although the RC frame buildings with masonry infill walls are known to be vulnerable to the out-of-plane failure mode, even AEM methodology is deficient about modeling such a failure mode for the CIW building studied here. This may explain the difference between the fragility curves obtained based on expert

opinion methods and analytical models. Due to the high gravity loads, in case of the URMW building, the out-of–plan failure mode was not a controlling factor in the analyses.

The easiness of calculating the performance points on the IDA curves, obtained from the AEM methodology, directly depends on the clarity of the available definition for each performance level. In case of the unreinforced masonry building here, the three performance levels were calculated according to both the criteria explained in section 3.4.3 and the visual damage on the structural model. For the RC frame with unreinforced masonry infill walls, although some local failure were observed in the columns of the first floor, no clear overall damage was observed in the structural model. Therefore, the performance points were determined using the criteria explained in Table 3.9 which are maximum interstorey drift ratios recommended by NIBS (2003). The effect of variations in determining those performance points (which directly affects the IM and DM values) are discussed in the next section.

5.7 Standard error in the estimation of the measured values

The standard errors of estimation (SEE) are used here to determine the preciseness of the calculated damage and intensity measure values for the immediate occupancy, life safety, and collapse prevention levels (presented in Table 4.1, Table 4.2, and Table 4.7), based on the number of the accelograms used in the nonlinear dynamic analysis.

The SEE, which is the standard deviation of the measured values divided by $\sqrt{n}$ (n: the number of accelograms), of the damage and intensity measures are presented in Tables 5.7 and 5.8. As seen in Table 5.7, the standard errors of estimation of the spectral acceleration values at the edge of the URMW building's collapse, life safety, and immediate occupancy are all less than 10% of the estimated median values, which appear to be reliable. The largest error is shown to be in the estimation of the maximum inter-storey drift at the CP and LS performance levels in the longer direction. Later, we will show how to determine the number

of additional records needed for the non-linear analyses to keep those errors under a certain value.

Table 5.7 Medians and standard errors of estimation of DM's and IM's of the URMW building at different performance states

			Median			SEE (% of the median)	
			longer dir.	shorter dir.		longer dir.	Shorter dir.
IO	$S_a(g)$		0.26	0.15		8.3	9.4
	Inter-storey drift		6.01E-04	2.05E-03		8.4	8.2
LS	$S_a(g)$		0.46	0.31		7.2	8.1
	Inter-storey drift		3.29E-03	3.88E-03		20.9	11.5
CP	$S_a(g)$		0.53	0.39		6.2	8.1
	Inter-storey drift		4.38E-03	5.17E-03		21	11.5

In the case of the CIW building, almost all of the errors are around 10% or below. Because the same criteria has been used to determine the damage measures (ISD) for different ground motion records for this building (Table 3.9), the SEE is zero, as shown in Table 5.8.

Table 5.8 Medians and standard errors of estimation of DM's and IM's of the CIW building at different performance states

			Median		SEE (% of the median)
IO	$S_a(g)$		0.22		11.6
	Inter-storey drift		1.60E-03		0.0
LS	$S_a(g)$		0.88		6.1
	Inter-storey drift		8.00E-03		0.0
CP	$S_a(g)$		2.45		8.7
	Inter-storey drift		1.87E-02		0.0

It should be noted that these errors are related to the seismic demand source. In general, there are two other sources of errors: (1) the uncertainty in the performance level thresholds, (2)

variability in the capacity properties of the analytical models. Theses two sources of errors are not considered in this section.

5.8 Discussion on Fragility Curves: Estimation of confidence intervals

As a result of the above errors in the estimation of DM's and IM's for each of the three limit states, there is a statistical variation in the estimation of the fragility curves. Therefore, a confidence interval (CI) which is an interval likely to include those curves, instead of estimating them by a single median and standard deviation value can be presented. To avoid repetition in this section, the procedure to calculate this value is only explained here for the unreinforced masonry building.

For a population with known standard deviation, the confidence intervals for the population's median can be computed as follows (Haldar and Mahadevan 2000).

$$C.I. = \mu \pm z.\frac{\sigma}{\sqrt{n}} \tag{5.2}$$

In Equation 5.2, z is the upper critical value for the standard normal distribution, and μ and σ are the median and standard deviation of the sample population, respectively. From Equation 5.2, the 90% confidence interval—from the Normal Distribution Table, z is equal to 1.64 for this C.I. level—of the medians of the DM and IM values for the most important limit state, the collapse prevention in Table 5.7, are calculated and displayed in Table 5.. A 90% confidence level in Table 5. means that there is only 5% probability that for the CP performance level, the estimated median falls below the lower or above the upper limits indicated in that table.

As an issue raised previously, using Equation 5.2, we can now show with a simple calculation that the number of records (n) required to decrease the SEE and consequently the width of the confidence interval of, for example, the inter-storey drift in the longer direction

(Table 5.7) to, let say, 15% of its median value, results in n = 74. Therefore, to reduce the value of SEE to 15% of the ISD's median value in that specific direction, an additional of 60 ground motion records should be added to the motion records shown in Table 5..

Table 5.9 90% confidence interval of the DM and IM median values for the CP damage state

		90% CI	
		Longer dir.	shorter dir.
S_a(g)		[0.48; 0.58]	[0.34; 0.44]
Inter-storey drift		[2.87E-03; 5.88E-03]	[4.19E-03; 6.14E-03]

As seen in Table 5.9, the typical values for the ISD ratio in Table 3.7 falls within the interval obtained for the longer direction of the URMW building. On the other hand, the 0.4% ISD ratio in Table 3.7 acts as a lower bound for the interval presented in Table 5.9. It can be concluded that the masonry building in this research behaves more similar to the typical URM building in ASCE (2000), in the longer direction.

The IM median's upper and lower limits shown in Table 5. can be used to develop the fragility curves with 5% and 95% confidence, for the longer and shorter direction of the building (Figure 5.10). The standard deviation values used to develop these curves are the same as those used to draw the average curves shown in Figure 4.3 and Figure 4.4.

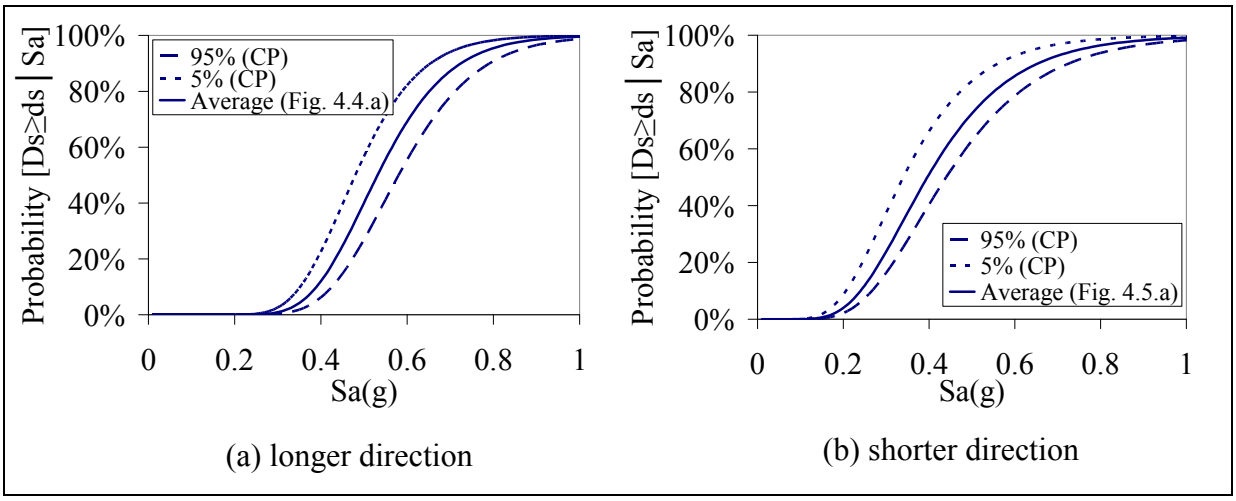

Figure 5.10 The URMW 5% and 95% confidence-level fragility curves, for the CP limit state.

The same procedure used to calculate the combined fragility curves previously is applicable here to derive the combined fragility curves with 5% and 95% confidence levels for the masonry building, as shown in Figure 5.11.

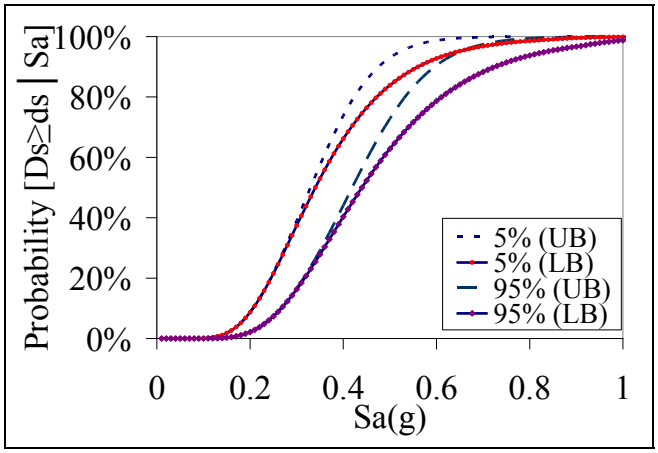

Figure 5.11 Upper and lower bounds of the 5% and 95% confidence-level URMW fragility curves, for the CP limit state.

5.9 Summary

The information obtained from the IDA curves are used to study the dynamic behaviour of each building, in different ways. On one hand, the statistical analysis of those curves

provided us with useful information about the behaviour of the building towards the ground motion records used in the dynamic analysis. On the other hand, the IDA curves presented very useful information regarding the local dynamic behaviour of the building (higher mode effects, etc.).

A comparison of the fragility curves developed in this research work with the curves for the relevant building classes in HAZUS indicated a more vulnerable structural behaviour for both buildings studied here. However, more masonry and concrete frame building with infill walls should be considered and analysed with the methodology presented here to be able to explain the differences in the standard deviations observed between HAZUS curves and those developed here.

The results of the loss estimation in Chapter 4, for each of the buildings studied in this research work, were used here to develop new kind of vulnerability indices which not only include a probabilistic interpretation regarding the building's exceeding a desired limit state, but also are based on considering the dynamic behaviour of each building class. Finally, a thorough explanation of the method to calculate the confidence intervals for the damage and intensity measure values was presented, as well. Those confidence intervals were then used to develop fragility curves with desired confidence-levels (5% and 95% here).

CONCLUSION

Summary

The predicted vulnerability technique coupled with a score assignment procedure is shown to be a suitable method for the seismic vulnerability assessment of a group of buildings for regions in which there is not much observed earthquake damage data available, such as in the province of Quebec. Considering the vulnerability of masonry as a construction material and its massive use in buildings which have been built in the old sectors of the province before the first detailed seismic provisions were incorporated in the National Building Code of Canada in 1953, the main objective of this research work is to develop a predicted-based seismic vulnerability evaluation method for those buildings with masonry construction in old sectors of Quebec. This main objective is achieved at two levels. First of all, using the current building classification in Canada, a rapid visual screening tool which is compatible to the regional seismic hazard of the province, is developed. Later on, for two of the building classes—unreinforced brick masonry buildings and concrete frames with unreinforced masonry infill walls—used largely in old sectors of Quebec and not well represented in the literature, the dynamic capacity and fragility curves are calculated considering the nonlinear dynamic behaviour of the masonry. The Applied Element Method in the form of Incremental Dynamic Analyses is used here to overcome the limitations of a FE-based method in the progressive collapse case of masonry buildings.

The two building classes studied here are chosen from the building classification proposed in chapter one for buildings in old sectors of the province, based on the review of the literature and personal visits in the area. The methodology to achieve the main objectives in this research work is presented in two parts. In the first place in Chapter 2, the procedure to develop a score assignment method which is adapted to the seismic demand in the province, for the seismic vulnerability evaluation of a group of buildings in old sectors of Quebec is explained. Later on, in Chapter 3, the methodology to conduct a performance-based seismic vulnerability evaluation to develop the dynamic capacity curves for the target buildings in

this study is explained. Those curves are calculated through the application of the Applied Element Method in the Incremental Dynamic Analyses of the structural models. The results of those Incremental Dynamic Analyses are presented in Chapter 4 where the lognormal distribution of intensity measures on the IDA curves are used to develop the acceleration and displacement-based fragility curves for each building. The loss estimation study of those buildings, on the other hand, is conducted in the same chapter to evaluate the Mean Annual Frequency of exceeding the performance levels—Immediate Occupancy, Life Safety, and Collapse Prevention—considered in this study. It was shown that if for example, the URMW building is located in La Malbaie, the IO, LS, and CP performance levels will be exceed in 43, 94, and 144 years, respectively. These return periods are calculated to be 71, 1162, and 6250 years for the same performance levels for the CIW building.

In Chapter 5, the information obtained from the IDA curves are used to study the dynamic behaviour of each building. A comparison of the fragility curves developed in this research work with the curves for the relevant building classes in HAZUS is also presented. It is shown that the models considered here are less ductile than the ones in HAZUS. From a PBSE perspective, this means that the unreinforced masonry and concrete frame with infill wall buildings here are more vulnerable as for the same value of S_d, the probability of exceeding extreme damage states are higher. Later, the results of the loss estimation presented in the previous chapter are used to develop new kind of vulnerability indices for the two buildings studied. Finally, the application of the AEM in the progressive collapse of the studied structures is discussed, and a set of standard errors in estimating the intensity and damage measure values at the threshold of each performance level is presented. It is shown that those errors are less than 10% of the estimated median values for most of the cases, which are indications of reliable results in the structural analysis section.

The weakest link theory was used here in this research work to obtain the combined fragility curves for the URMW building. This means that the fragility curves for each direction was calculated and the final results were combined. Another way to face this problem would have been to combine the damage measures (max. inter-storey drift in this research) from the

structural analysis of each direction, and then to obtain bi-directional curves from those results. The problem with this methodology, though, is that the maximum of the inter-storey drifts (ISD) does not necessarily happen at the same time in both directions. Therefore, combining the maximum of ISD's would create conservative curves, in this case.

Original contribution of the research work

The main outcome of this research work is developing dynamic capacity and fragility curves for an unreinforced masonry building and an RC frame with unreinforced masonry infill walls. Other outcomes can be stated as follows (the order of the items does not reflect their level of importance).

1. Proposing a building classification for the existing buildings in old sectors of Quebec considering the masonry as the main construction material

2. Developing a rapid visual screening tool adapted to the seismic demand in Quebec: The indices are calculated through the application of the improved nonlinear static analysis procedure proposed in FEMA 440. It also includes the use of the seismic hazard definition in the 2005 edition of NBCC.

3. Proposing a performance based seismic evaluation methodology for masonry buildings that can be used in regions with few observed earthquake damage data. This methodology includes:

    a. Application of the Applied Element Method to model progressive collapse of URM building and RC building with infill walls
    b. Structural analysis in the form of Incremental Dynamic Analysis to determine the building's response considering dynamic properties: The IDA conducted in this research work consisted of 14 accelograms in 2D analyses for the unreinforced

masonry building and 10 bi-directional accelograms in 3D analyses for the RC frame with unreinforced masonry infill walls.

c. Damage analysis in which three (3) performance levels—Immediate Occupancy, Life Safety, and Collapse Prevention defined in FEMA 356—are located on the IDA curves using the criteria explained in Chapter 3 and used to develop dynamic capacity and fragility curves for the unreinforced masonry building and the RC frame with unreinforced masonry infill walls.
d. Loss estimation analysis in which the return period for exceeding any of the performance levels are evaluated for the studied buildings. Such estimations depend on the geographical location of the building under study. The results of this section are used to develop new type of screen vulnerability indices for the masonry and concrete frame with infill wall buildings.

Difficulties encountered in the application of the Applied Element Method

Although the application of the Applied Element method in this research work provided us with a tool to evaluate the nonlinear dynamic behaviour of the masonry, the process to conduct each step of the Incremental Dynamic Analysis is time-consuming and varies from 4 to 8 hours/step. Knowing that a minimum number of 10 to 15 increments are required for each ground motion record, every effort should be made to minimize the processing time. Items that influence the speed of structural analyses are (i) the size of meshing for the structural elements such as masonry walls, beams and columns, and slabs; and (ii) the length of the ground motion records used in the dynamic analysis.

The meshing size and the number of springs per element face are shown to have great effects on the time required for completing the analysis and the preciseness of the results (Meguro and Tagel-Din 2000). Therefore, the goal should be decreasing those numbers without sacrificing the output results. In this research work, it was seen that increasing the number of springs (per face) above 5 would not necessarily change the results of the IDA. Therefore, such a number was chosen in all cases. On the other hand, the size of element meshing was

picked in a way to avoid creating elements with large aspect ratios. Such a decision resulted in a total number of approximately 10’000 and 12’000 elements for the unreinforced masonry and the RC frame with masonry infill walls, respectively.

The length of the ground motion records, on the other hand, significantly affects the time required to conduct the dynamic analysis. This factor is out of our control as there is limited number of ground motion records available for Eastern Canada. Therefore, the IDA can not be necessary done only for shorter records.

One the other hand, experimental tests are known to be the best way to validate the results obtained from analytical models and the results of this research work are not an exception. The cost of such experiment test, however, can be very high considering the equipments (size of the shaking table, etc.) required for performing a reliable test. Therefore, there may not be a clear solution for such a validation, at the present time.

RECOMMENDATIONS

5.9.1 Rapid Visual Screening procedure

It was shown in section 5.5 that the results of the Performance-based Seismic Vulnerability Evaluation can be used to develop vulnerability indices for the building classes under study. The advantage of such indices is that, unlike the indices presented in Chapter 2, the dynamic behaviour of each building class is considered in the process of index calculation. Therefore, the methodology in this research work can be applied to develop new indices for all the building classes in Table 1.5.

As explained previously in Chapter 2, the vertical irregularity modifiers for the index assignment method proposed here are calculated based on the assumption that if these irregularities were the only modifiers to be considered in the evaluation process, then the final index would be below the cutoff index. The experience of an assessment project conducted in Quebec City indicates that this may not be the best way to consider the existence of such irregularities in the seismic evaluation of a group of buildings, as it may unnecessarily penalize structures with SVIs well above the cutoff, causing them to fall below the cutoff. This has the potential of unreasonably increasing the cost of the detailed evaluation phase, which is usually performed after the RVS stage. The following steps can be done to better consider the effect of such irregularity in a rapid visual screening methodology.

1. For each building class (concrete, masonry, etc.), a set of structural models with different vertical irregularities should be developed.
2. The capacity curve for each analytical model should be calculated, and the interim vulnerability index for each one should be developed.
3. Within each building class, the different interim SVI should be compared with the rest to obtain a pattern for the average analytical behaviour for each building class when vertical irregularities come into account.

The experience of the Quebec City assessment also shows that the effect of site amplification has more impact on the proposed SVI than it does in the current Canadian procedure. This allows for a better identification of buildings with seismic vulnerabilities that may relate to soil conditions rather than structural deficiencies.

5.9.2 Development of fragility and capacity curves with IDA

1. Number of accelograms used

It was shown in section 5.8 that the error in estimation of DM's and IM's can be reduced through increasing the number of accelograms used in the Incremental Dynamic Analysis of the structural models. Although almost all available significant real and synthetic accelograms for Eastern Canada has been used here, new studies in the future can develop new synthetic ground motion records. Moreover, future earthquakes in the region can provide us with new real accelograms. In this way, the number of accelograms used would be closer to the upper bound of the required number of accelograms stated in Chapter 3—20 as suggested by (Shome et al. 1998).

2. Bi-directional versus uni-directional analysis

At the time of the structural analysis for the CIW building, the bi-directional synthetic records become available. Therefore, for the second building, unlike the URMW building, bi-directional fragility curve were developed directly from the damage analysis stage. The combined fragility curves developed for the URMW building can be re-checked if the structural analyses are repeated using those bi-directional ground motion records to develop bi-directional curves. Considering the amount of time one needs to run the AEM models using an IDA approach, such a task was left as a future work.

3. Variation in the material properties

The values for the masonry and concrete material properties in the IDA of this research work are average ones which are chosen based on a literature review of buildings with masonry construction in Eastern Canada and especially in Quebec (Table 3.2 and Table 3.4). Considering the variation of such material properties in different constructions in the province, the structural analyses can be done for a range of properties (instead of single values done here) for the extreme possible low and high values. The results should then be integrated using computational algorithms (e.g., Monte Carlo Method) that rely on repeated random sampling to compute results. Knowing that the combination of such an approach with IDA would be extremely time consuming, an in advance validation of the gain in the obtained precision is necessary.

4. Number of building studied

As the fragility and capacity curves for each building class should aim to represent the average behaviour of that class, the Performance-based Seismic Vulnerability Evaluation methodology introduced here should be applied to evaluate more unreinforced masonry and RC frame with unreinforced masonry infill walls (with different height, dimensions, number of openings, etc.). The overall behaviour of all those models can then be used to produce a general fragility curve for each building class. Moreover, because of the time constrains in this research work, only two of the building classes in Table 1.5 were studied. This does not mean that, in the context of seismic vulnerability in Quebec, other building classes stated in that table are of less importance. As a part of a bigger project to increase public safety against seismic hazard in the province, the same methodology should be applied to develop the dynamic capacity and fragility curves for all building classes in Table 1.5.

5. Infill wall behaviour in RC frame buildings

The differences between the fragility curves for the CIW buildings in this study with those currently available in other references such as (NIBS 2003)—presented in section 5.4.2—show the real challenge over finding an optimized criteria to study the seismic behaviour of that building class. Although the application of the methodology proposed in this research work does not bring the large efforts in the engineering communities to assess the dynamic behaviour of such a building class to an end, results obtained from AE-based studies can be considered an important step forward. For this reason, it seems very useful to compare the analytical results from AE-based methods with small scale experimental tests to obtain a better idea regarding the analytical method precision.

APPENDIX I

CLASSIFICATION OF CITIES IN QUEBEC ACCORDING TO THEIR SEISMIC HAZARD LEVEL

Table-A 0.1 Spectral acceleration values of cities in Quebec that are in a high seismic hazard region according to the criteria of Table 2.1

Locality	Lat-N	Lon-W	Sa(0.2)	Sa(0.5)	Sa(1.0)	Sa(2.0)	PGA
La-Malbaie	47.65	-70.15	2z.3	1.2	0.6	0.19	1.1
RIIière-du-Loup	47.83	-69.53	1.1	0.63	0.29	0.098	0.67
St-Georges-de-Cacouna	47.92	-69.5	0.98	0.54	0.25	0.084	0.56
Montmagny	46.98	-70.55	0.89	0.48	0.23	0.076	0.49
Tadoussac	48.15	-69.72	0.84	0.46	0.22	0.073	0.46

Table-A 0.2 Spectral acceleration values of cities in Quebec that are in a moderate seismic hazard region according to the criteria of Table 2.1

Locality	Lat-N	Lon-W	Sa(0.2)	Sa(0.5)	Sa(1.0)	Sa(2.0)	PGA
Léry	45.35	-73.8	0.7	0.34	0.14	0.048	0.43
Montréal	45.5	-73.6	0.69	0.34	0.14	0.048	0.43
Matane	48.85	-67.53	0.68	0.38	0.17	0.052	0.44
Baie-Comeau	49.22	-68.15	0.66	0.37	0.16	0.05	0.44
Maniwaki	46.38	-75.97	0.66	0.3	0.14	0.04	0.42
Sorel	46.03	-73.12	0.65	0.32	0.13	0.044	0.41
St-Hubert-de-Témiscouata	47.82	-69.05	0.64	0.36	0.18	0.06	0.34
Lachute	45.65	-74.33	0.64	0.31	0.14	0.043	0.4
Chicoutimi (Bagotville)	48.35	-70.88	0.63	0.33	0.16	0.053	0.4
Mont-Joli	48.58	-68.18	0.62	0.33	0.15	0.048	0.39

Locality	Lat-N	Lon-W	Sa(0.2)	Sa(0.5)	Sa(1.0)	Sa(2.0)	PGA
Québec	46.8	-71.23	0.59	0.3	0.14	0.048	0.37
Drummondville	45.88	-72.48	0.5	0.25	0.1	0.037	0.32
Cowansville	45.2	-72.75	0.48	0.24	0.1	0.036	0.3
Port-Cartier	50.02	-66.87	0.46	0.26	0.11	0.038	0.29
Plessisville	46.22	-71.78	0.45	0.23	0.1	0.034	0.29
Sutton	45.1	-72.62	0.44	0.23	0.099	0.034	0.26
Victoriaville	46.05	-71.97	0.43	0.22	0.097	0.033	0.27
Brome	45.2	-72.57	0.42	0.22	0.097	0.034	0.25
Lac-Mégantic	45.58	-70.88	0.4	0.22	0.091	0.031	0.27
Richmond	45.67	-72.15	0.38	0.21	0.091	0.032	0.21
Sept-Iles	50.2	-66.38	0.37	0.22	0.092	0.033	0.21
Sherbrooke	45.42	-71.9	0.37	0.2	0.086	0.031	0.2
Thetford-Mines	46.08	-71.3	0.35	0.2	0.097	0.033	0.19
Ville-Marie	47.33	-79.43	0.33	0.16	0.075	0.022	0.21
Havre-St-Pierre	50.23	-63.6	0.33	0.17	0.07	0.023	0.22
St-Félicien	48.65	-72.45	0.31	0.18	0.086	0.029	0.2
La-Tuque	47.43	-72.78	0.29	0.18	0.091	0.03	0.16
Gaspé	48.83	-64.48	0.22	0.14	0.064	0.022	0.093
Val-d'Or	48.1	-77.78	0.22	0.12	0.063	0.018	0.12
Povungnituk	59.78	-77.32	0.22	0.088	0.041	0.011	0.15
Malartic	48.13	-78.13	0.21	0.12	0.059	0.017	0.11
Percé	48.53	-64.22	0.2	0.13	0.061	0.02	0.092
Rouyn	48.23	-79.02	0.2	0.11	0.056	0.016	0.11

Table-A 0.3 Spectral acceleration values of cities in Quebec that are in a low seismic hazard region according to the criteria of Table 2.1

Locality	**Lat-N**	**Lon-W**	**Sa(0.2)**	**Sa(0.5)**	**Sa(1.0)**	**Sa(2.0)**	**PGA**
Amos	48.57	-78.12	0.17	0.11	0.054	0.015	0.087
Gagnon	51.93	-68.17	0.12	0.09	0.045	0.013	0.059
Harrington-Harbour	50.5	-59.48	0.12	0.082	0.043	0.013	0.071
Kuujjuaq	58.1	-68.4	0.12	0.065	0.033	0.01	0.059
Nitchequon	53.21	-70.91	0.12	0.061	0.031	0.01	0.059
Schefferville	54.8	-66.83	0.12	0.059	0.031	0.01	0.059
Inukjuak	58.48	-78.1	0.12	0.056	0.023	0.006	0.059
Kuujjua-rapik	55.28	-77.75	0.12	0.056	0.023	0.006	0.059

APPENDIX II

VALIDATION OF THE APPLIED ELEMENT METHOD APPLICATION FOR NONLINEAR ANALYSIS OF CONCRETE AND MASONRY STRUCTURES

To validate the accuracy of the AEM to represent the nonlinear behaviour of masonry or concrete structures, results of some experimental tests have been compared with the analytical model outputs. As the first example, the experimental result of the monotonic loading on a concrete shear wall (Ghorbani-Renani et al. 2008) is compared with the output of the pushover analysis (Figure-A II.1).

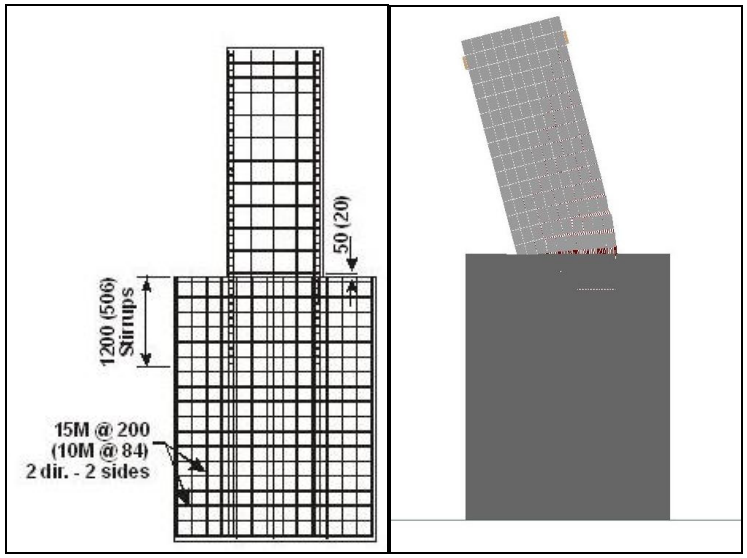

Figure-A 0.1 Plan view of the concrete wall under monotonic loading and the analytical model.
Taken from Ghorbani-Renani et al. (2008)

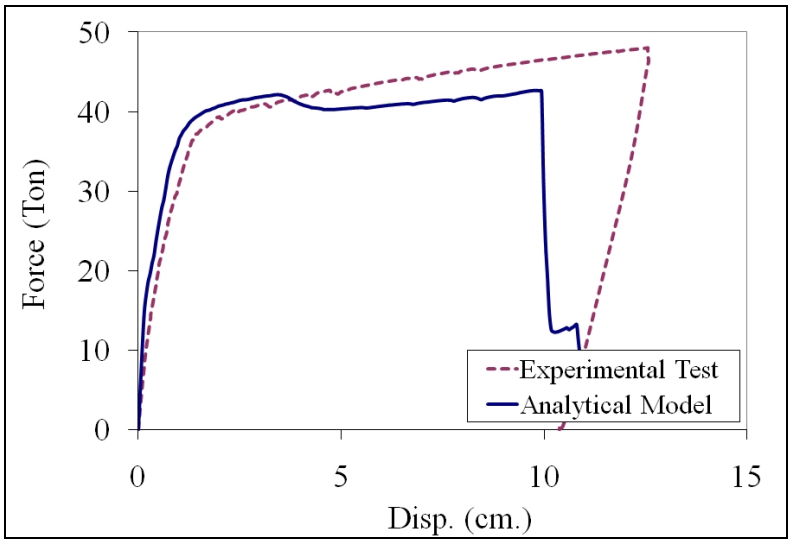

Figure-A 0.2 Load-deformation curve comparing the Pushover analysis and experimental test.

As seen in Figure-A II.2, the results from the analytical model coincide with the experimental test in the linear and nonlinear area. The divergence of the two lines in the collapse mode can be explained as a result of the reinforcement confinement in the analytical model which causes it to fail sooner than the experimental test.

The second verification is done by comparing the experimental test results of a concrete frame with masonry infill wall. This example is taken from the software verification documents of the Extreme Loading® for Structures (Applied Science International 2007). Figure-A II.3 shows the frame which is subjected to a lateral displacement control until reaching failure along with the analytical model.

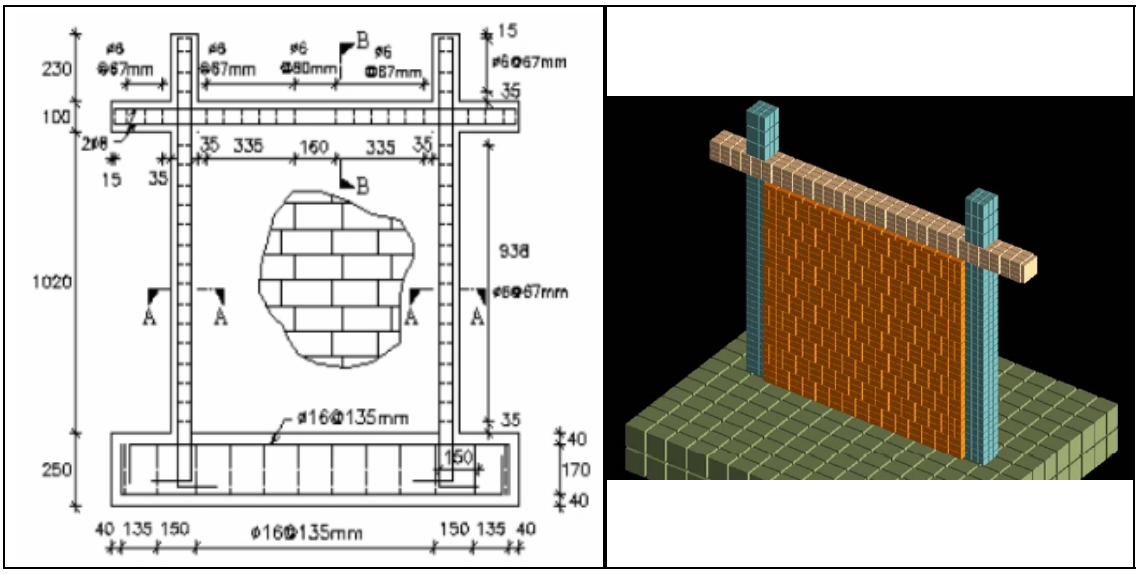

Figure-A 0.3 Plan view of the concrete frame with masonry infill wall and the analytical model.
Taken from Applied Science International (2007)

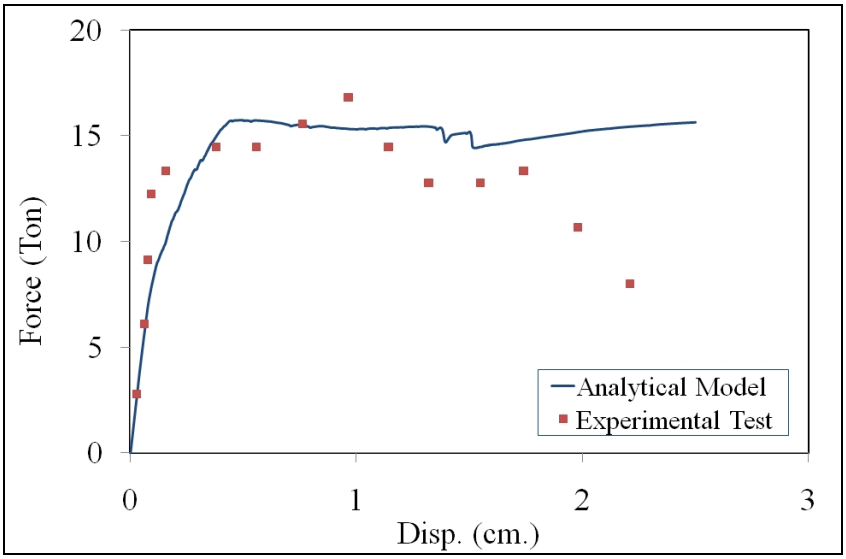

Figure-A 0.4 Load-deformation graph comparing the analytical and experimental test results.

Figure-A II.4 illustrates the analytical load-deflection results compared to the experimental ones. The analytical results show good agreement with the experiment test as the behaviour is well predicted in the elastic stage, post cracking stage, and in the post-yielding stage.

LIST OF BIBLIOGRAPHICAL REFERENCES

Abrams, D. P. 2001. « Performance-based engineering concepts for unreinforced masonry building structures ». *Progress in Structural Engineering and Materials*, vol. 30, n^{o} 2, p. 48-56.

Adams, J. and G. Atkinson. 2003. « Development of seismic hazard maps for the proposed 2005 edition of the National Building Code of Canada ». *Canadian Journal of Civil Enginering*, vol. 30, n^{o} 2, p. 255-271.

Adams, J., G. Rogers, S. Halchuk, T. C. McCormack and J. Cassidy. 2002. « The case for an advanced national earthquake monitoring system for Canada's cities at risk ». In *7th U.S. National Conference on Earthquake Engineering*. Boston, United States.

Adams J. and G. Atkinson. 2003. « Development of seismic hazard maps for the proposed 2005 edition of the National Building Code of Canada ». *Canadian. J. Civ. Eng.*, vol. 30, n^{o} 2, p. 255-271.

Applied Science International. 2007. *Extreme Loading® for Structures.* version 2.2 B192. Raleigh, NC.

Arrien, P. and M. Lemyre. 2003. *Étude de la capacité parasismique du bloc « D » du centre hospitalier Hôpital Saint-Sacrement (CHA)* Québec City, Canada.

ASCE. 1998. *Handbook for the Seismic Evaluation of Buildings - A Prestandard,* FEMA 310. Washington D.C.: American Society of Civil Engineers.

ASCE. 2000. *Pre-standard and Commentary for the Seismic Rehabilitation of Buildings,* FEMA-356. Reston, VA: Federal Emergency Management Agency.

ASCE. 2003. *Seismic Evaluation of Existing Buildings,* ASCE 31-03. Washington D.C.: American Society of Civil Engineers.

Asteris, P. G., A. D. Tzamtzis, P. P. Vouthouni and D. S. Sophianopoulos. 2005. « Earthquake Resistant Design and Rehabilitation of Masonry Historical Structures ». *Practice Periodical on Structural Design and Construction*, vol. 10, n^{o} 1, p. 49-55.

ATC. 1985. *Earthquake Damage Evaluation Data for California,* ATC 13. Redwood, CA: Applied Technology Council.

ATC. 1996. *Seismic Evaluation and Retrofit of Concrete Buildings,* ATC 40. Redwood, CA: Applied Technology Council.

ATC. 1998. *Rapid Visual Screening of Buildings for Potential Seismic Hazards.* FEMA 154 1st Edition. Redwood City, CA: Federal Emergency Management Agency.

ATC. 2002a. *Rapid Visual Screening of Buildings for Potential Seismic Hazards: A Handbook,* FEMA 154, 2nd Ed. Redwood City, CA: Federal Emergency Management Agency.

ATC. 2002b. *Rapid Visual Screening of Buildings for Potential Seismic Hazards: Supporting Documentation,* FEMA 155, 2nd Ed. Redwood, CA: Applied Technology Council prepared for the Federal Emergency Management Agency.

ATC. 2005. *Improvement of Nonlinear Static Seismic Analysis Procedures,* FEMA 440. Redwood, CA: Federal Emergency Management Agency.

ATC. 2009. *Guidelines for Seismic Performance Assessment of Buildings (50% draft),* ATC 58. Redwood, CA: Applied Technology Council.

Atkinson, G. 2009. « Earthquake Time Histories Compatible with the 2005 NBCC Uniform Hazard Spectrum ». *Canadian Journal of Civil Engineering*, vol. 36, n^{o} 6.

Atkinson, G. and I. Beresnev. 1998. « Compatible ground-motion time histories for new national seismic hazard maps ». *Canadian Journal of Civil Enginering*, vol. 25, p. 305-318.

Augusti, G. and M. Ciampoli. 2000. « Heritage buildings and seismic reliability ». *Progress in Structural Engineering and Materials*, vol. 2, n^{o} 2, p. 225-237.

Baker, J. W. and C. A. Cornell. 2006. « Spectral shape, epsilon and record selection ». *Earthquake Engineering and Structural Dynamics*, vol. 35, n^{o} 9, p. 1077-1095.

Beaulieu, J. 2006. « Essais sur maçonnerie pour la centrale hydroélectrique de Beauharnois. Qualitas-Concrete Laboratory ». In *Hydro-Quebec Workshop on URM*. Montreal, Canada.

Belmouden, Y. and P. Lestuzzi. 2007. *On The Seismic Vulnerability Assessment of Unreinforced Masonry Existing Buildings in Switzerland.* École Polytechnique Fédérale de Lausanne: Lausanne, Switzerland.

Biddah, A. M. S. (1997). *Seismic Behaviour of Existing and Rehabilitated Reinforced Concrete Frame Connections*. Hamilton, Canada: ETD Collection for McMaster University.

BSSC. 2003. *NEHRP recommended provisions for seismic regulations for new buildings and other structures. FEMa 450.* Building Seismic Safety Council: Washington, D.C.

Calderini, C. and S. Lagomarsino. 2008. « Continuum Model for In-Plane Anisotropic Inelastic Behavior of Masonry ». *Journal of Structural Engineering*, vol. 134, n^{o} 2, p. 209-220.

Canadian Standards Association. 2004. *S304.1-04 Masonry Design for Buildings*:

Carol, I., P. C. Prat and C. M. Lopez. 1997. « Normal/Shear Cracking Model: Application to Discrete Crack Analysis ». *Journal of Engineering Mechanics*, vol. 123, n° 8, p. 765-773.

Cervera, M. and M. Chiumenti. 2006. « Smeared crack approach: back to the original track ». *International Journal for Numerical and Analytical Methods in Geomechanics*, vol. 30, n° 12, p. 1173-1199.

Chopra, A. K. 2001. *Dynamics of Structures: Theory and Applications to Earthquake Engineering,* 2. New Jersey, USA: Prentice-Hall.

Chopra, A. K. and R. K. Goel. 2000. « Evaluation of NSP to Estimate Seismic Deformation: SDF Systems ». *Journal of Structural Engineering*, vol. 126, n° 4, p. 482-490.

Christovasilis, I. P., A. Filiatrault, M. C. Constantinou and A. Wanitkorkul. 2009. « Incremental dynamic analysis of woodframe buildings ». *Earthquake Engineering and Structural Dynamics*, vol. 38, n° 4, p. 477-496.

Coburn, A. and R. Spence. 2002. *Earthquake Protection,* 2nd Chichester: John Wiley and Sons.

Cohen, G. L., R. E. Klingner, J. John R. Hayes and S. C. Sweeney. 2004. « Seismic Evaluation of Low-Rise Reinforced Masonry Buildings with Flexible Diaphragms: II. Analytical Modeling». *Earthquake Spectra*, vol. 20, n° 3, p. 803-824.

Colliat, J., B., , L. Davenne and A. Ibrahimbegovic. 2002. « Modelling of nonlinear behaviour of masonry structures: phenomenological approach ». In *Proceedings of the sixth conference on Computational structures technology*, 153. Civil-Comp press.

D'Ayala, D., R. Spence, R. Oliveira and A. Pomonis. 1997. « Earthquake loss estimation for Europe's historic town centers ». *Earthquake Spectra*, vol. 13, n° 4, p. 773-793.

D'Ayala, D. and E. Speranza. 2001. « Seismic vulnerability of Historical Centres: the case study of Nocera Umbra, Italy ». In *Two thousand years and more in the history of structures and architecture conference*. Paris, France.

D'Ayala, D. and E. Speranza. 2002. « An integrated procedure for the assessment of seismic vulnerability of historic buildings ». In *Proceeding of the 12th European Conference on Earthquake Engineering*. London, UK.

Decanini, L. D., A. De Sortis, A. Goretti, L. Liberatore, F. Mollaioli and P. Bazzurro. 2004. « Performance of reinforced concrete buildings during the 2002 Molise, Italy, earthquake ». *Earthquake Spectra*, vol. 20, n° 1, S221-S255.

Faccioli, E., V. Pessina, G. M. Calvi and B. Borzi. 1999. « A study on damage scenarios for residential buildings in Catania city ». *Journal of Seismology*, vol. 3, n^{o} 3, p. 327-343.

Fah, D., F. Kind, K. Lang and D. Giardini. 2001. « Earthquake scenarios for the city of Basel ». *Soil Dynamics and Earthquake Engineering* vol. 21, n^{o} 5, p. 405-413.

Freeman, S. A., J. P. Nicoletti and J. V. Tyrell. 1975. « Evaluations of Existing Buildings for Seismic Risk - A Case Study of Puget Sound Naval Shipyard, Bremerton, Washington ». In *Proceeding of the U.S. National Conference on Earthquake Engineering*. Berkeley, U.S.A., p. 113-122.

Gauthier, M. 1976. *Rapport d'étude de la charpente, Édifice E - Restauration et Rénovation des édifices de la Colline parlementaire.* Quebec, Canada.

Ghorbani-Renani, I., N. Velev, R. Tremlay, D. Palermo, B. Massicotte and P. Léger. 2008. « Modeling and Testing The Influence of Scaling Effects on The Inelastic of Scaling Effects on The Inelastic Response of Shear Walls». *ACI Structural Journal*, vol. 106, n^{o} 3, p. 358-367.

GNDT. 1993. *Rischio Sismico di Edifici Pubblici, Parte I: Aspetti Metodologici.* Gruppo Nazionale Difesa dai Terremoti.

Halchuk, S., J. Adams and F. Anglin. 2007. « Revised Deaggregation Of Seismic Hazard For Selected Canadian Cities ». In *Ninth Canadian Conference on Earthquake Engineering*. Ottawa, Canada, p. 420-432.

Haldar, A. and S. Mahadevan. 2000. *Probability, Reliability and Statistical Methods in Engineering Design,* New York: John Wiley and Sons, Inc. 320.

Hancock, J., J. Bommer and P. Stafford. 2008. « Numbers of scaled and matched accelerograms required for inelastic dynamic analyses ». *Earthquake Engineering and Structural Dynamics*, vol. 37, n^{o} 14, p. 1585-1607.

Heidebrecht, A. C. 2003. « Overview of seismic provisions of the proposed 2005 edition of the National Building Code of Canada ». *Canadian Journal of Civil Enginering*, vol. 30, n^{o} 2, p. 241-254.

Ibarra, L. F. and H. Krawinkler. 2005. *Global Collapse of Frame Structures under Seismic Excitations.* John A. Blume Earthquake Engineering Center:

Ismail, N., H. Mahmood, H. Derakhshan, W. Clark and J. M. Ingham. 2009. « Case Study and Development of Seismic Retrofit Solution for a Heritage URM Building ». In *11th Canadian Masonry Symposium* Toronto, Canada, C5-5.

Karbassi, A. and M.-J. Nollet. 2008. « Development of an index assignment procedure compatible with the regional seismicity in the province of Quebec for the rapid visual screening of existing buildings ». *Canadian Journal of Civil Engineering*, vol. 35, p. 925-937.

Krawinkler, H., R. Medina and B. Alavi. 2003. « Seismic drift and ductility demands and their dependence on ground motions ». *Engineering Structures*, vol. 25, n^{o} 5, p. 637-653.

Krawinkler, H. and E. Miranda. 2004. « Performance-Based Earthquake Engineering ». In *Earthquake Engineering: From Engineering Seismology to Performance-Based Engineering*. Y. Bozorgnia and V. V. Bertero, p. 9-1 - 9-59. CRC Press.

Kunnath, S. K. and E. Kalkan. 2005. « IDA Capacity Curves: The Need for Alternative Intensity Factors ». In *ASCE Structures Congress*, p. 187.

Lagaros, N. D. 2009. « Multicomponent incremental dynamic analysis considering variable incident angle ». *Structure and Infrastructure Engineering: Maintenance, Management, Life-Cycle Design and Performance*.

Lang, K. 2002. « Seismic vulnerability of existing buildings ». Ph.D. Thesis, Zurich, Swiss Federal Institute of technology, 200 p.

LeBoeuf, D. and M.-J. Nollet. 2006. *Microzonage et vulnérabilité sismique de la ville de Québec 2005-2006, for the City of Québec.* Quebec.

Lefebvre, K. 2004. « Caractérisation structurale et évaluation de la vulnérabilité sismique des bâtiments historiques en maçonnerie du Vieux-Montréal (M.Sc. Thesis) ». Masters of Science, Constructional Engineering, Monreal, Ecole de Technologie Superieure, 208 p.

Lefebvre, K. and M.-J. Nollet. 2009. « Parametric Evaluation of the Response of In-filled RC Frames Built in Quebec before 1960 Under Seismic Load ». In *11th Canadian Masonry Symposium*. Toronto, Canada.

Mayorca, P. and K. Megura. 2003. « Modeling Masonry Structures using the Applied Element Method ». *Monthly Journal of Institute of Industrial Science, University of Tokyo*, vol. 55, n^{o} 6, p. 581-584.

McCormack, T. C. and F. N. Rad. 1997. « An Earthquake Loss Estimation Methodology for Buildings Based on ATC-13 and ATC-21 ». *Journal of Earthquake Spectra*, vol. 13, n^{o} 4, p. 605-621.

Meguro, K. and H. R. Tagel-Din. 2000. « Applied element method for structural analysis: Theory and application for linear materials. ». *Proceedings of JSCE (Japan Society of Civil Engineers)*, vol. 647, p. 32-45.

Meguro, K. and H. R. Tagel-Din. 2002. « Applied Element Method Used for Large Displacement Structural Analysis ». *J Nat Disaster Sci*, vol. 24, n° 1, p. 25-34.

Newmark, N. M. and W. J. Hall. 1982. *Earthquake Spectra and Design,* Oakland: Earthquake Engineering Research Institute (EERI), Oakland, CA.

NIBS. 1999. *Earthquake Loss Estimation Methodology Technical Manual, HAZUS99 Service Release 1 (SR1).* National Institute of Building Sciences: Washington, D.C.

NIBS. 2003. *Earthquake Loss Estimation Methodology, HAZUS-MH MR1 Technical and User's Manual, developed by the National Institute of Building Sciences for the Federal Emergency Management Agency.* Washington, D.C.

Nollet, M.-J., O. Chaallal and K. Lefebvre. 2005. « Seismic vulnerability study of historical buildings in Old Montreal: overview and perspectives ». In *Proceeding of the Conference on Structural Studies, Repairs and Maintenance of Heritage Architecture IX*. Malta, Italy, p. 227-236.

Nollet, M.-J., A. Karbassi, K. Lefebvre and O. Chaallal. 2009. « Développement de courbes de fragilité des bâtiments existants par la méthode des éléments appliqués ». In *9e Colloque National en Calcul des Structures*. Giens, France.

NRC-IRC. 1992. *Manual for Screening of Buildings for Seismic Investigation,* Ottawa: Institute for Research in Construction- National Research Council Canada.

NRCC. 1990. *National Building Code of Canada 1990.* National Research Council of Canada: Ottawa, Ont.

NRCC. 2005. *National Building Code of Canada 2005,* NBCC 2005. Ottawa, NRCC 47666:

Onur, T. 2001. « Seismic Risk Assessment in Southwestern British Columbia ». Ph.D. Thesis, Civil Engineering, Vancouver, University of British Columbia, 224 p.

Porter, K. A., A. S. Kiremidjian, J. Legrue and S. A. King. 2000. « A Building Damage Estimation Method for Business Recovery ». In *12th World Conference on Earthquake Engineering*. New Zealand.

Powell, G. H. 2006. « Static Pushover Methods - Explanation, Comparison and Implementation ». In *Proceeding of the 8th U.S. National Conference on Earthquake Engineering*. San Francisco, California, USA, Paper No. 1608.

Rodrigue, P. A. 2006. *Typologie Structurale et Sélection Sismique des Bâtiments du Vieux Montréal.* École de technologie supérieure: Montréal.

Rossetto, T. and A. Elnashai. 2003. « Derivation of vulnerability functions for European-type RC structures based on observational data ». *Engineering Structures*, vol. 25, n° 10, p. 1241-1263.

Rossetto, T. and A. Elnashai. 2005. « A new analytical procedure for the derivation of displacement-based vulnerability curves for populations of RC structures ». *Engineering Structures*, vol. 27, n° 3 p. 397-409.

Sandi, H. 1982. « Seismic vulnerability and seismic intensity ». In *Proceeding of the 7th European Conf. on Earthquake Engineering, Athens*. Athens, p. 431-438.

Shaw, D., C. H. Yeh, W. Y. Jean, C. H. Loh and Y. L. Kuo. 2007. « A Probabilistic Seismic Risk Analysis of Building Losses in Taipei: An Application of Haz-Taiwan with its Pre-Processor and Post-Processor ». *Journal of the Chinese Institute of Engineers*, vol. 30, n° 2, p. 289-297.

Shome, N., C. A. Cornell, P. Bazzurro and J. E. Carballo. 1998. « Earthquakes, Records, and Nonlinear Responses ». *Earthquake Spectra*, vol. 14, n° 3, p. 469-500.

Tagel-Din, H. and K. Meguro. 2000. « Applied Element Method for Dynamic Large Deformation Analysis of Structures ». *Structural Eng./Earthquake Eng., International Journal of the Japan Society of Civil Engineers (JSCE)*, vol. 17, n° 2, p. 215-224.

Tantala, M. W., G. J. P. Nordenson and G. Deodatis. 2000. *Earthquake loss estimation study for the NewYork city area.* MCEER: Buffalo.

Turenne, R. 2009. *Mise à jour de la procédure de sélection des bâtiments en vue de leur évaluation sismique du CNRC en conformité avec les nouvelles exigences du CNBC 2005. Rapport de maîtrise,* École de technologie superieure: Montréal.

USGS/EERI. 2010. *The MW 7.0 Haiti Earthquake of January 12, 2010 Advance Reconnaissance Team Report.*

Valluzzi, M. R., G. Cardani, A. Saisi, L. Binda and C. Modena. 2005. « Study of the seismic vulnerability of complex masonry buildings ». In *Proceeding of the Conference on Structural Studies, Repairs and Maintenance of Heritage Architecture IX*. Malta, Italy, p. 301-310.

Vamvatsikos, D. and C. A. Cornell. 2002. « Incremental dynamic analysis ». *Earthquake Engineering and Structural Dynamics*, vol. 31, n° 3, p. 491-514.

Ventura, C. E., W. D. Liam-Finn, T. Onur, A. Blanquera and M. Rezai. 2005. « Regional seismic risk in British Columbia-classification of buildings and development of damage probability functions ». *Canadian Journal of Civil Engineering*, vol. 32, n° 2, p. 372-387.

White, T., C. E. Ventura, G. Taylor and K. Elwood. 2005. « Performance-Based Seismic Risk Assessment of Buildings in British Columbia ». In *Proceeding of the 33rd Annual General Conference of the Canadian Society for Civil Engineering*. Toronto, Canada.